PREPARATION AND PROPERTIES OF REVERSIBLE POLYMERS AND SELF-ASSEMBLY OF CARBON NANOTUBES

PREPARATION AND PROPERTIES OF REVERSIBLE POLYMERS AND SELF-ASSEMBLY OF CARBON NANOTUBES

By

James D. Mayo, B.Sc.H.

A Thesis

Submitted to the School of Graduate Studies

in Partial Fulfillment of the Requirements

for the Degree

Doctor of Philosophy

McMaster University

DOCTOR OF PHILOSOPHY (2013) McMaster University
(Chemistry) Hamilton, Ontario

TITLE: PREPARATION AND PROPERTIES OF REVERSIBLE POLYMERS AND SELF-ASSEMBLY OF CARBON NANOTUBES

AUTHOR: James D. Mayo, B.Sc.H. (University of Toronto)

SUPERVISOR: Professor Alex Adronov

NUMBER OF PAGES: xxiv, 167

ABSTRACT

A series of linear reversible polymers based on Diels Alder (DA) chemistry, were prepared and characterized. Four pairs of bismaleimide and bisfuran monomers were synthesized and then combined to produce thermally reversible polymers. Reversibility was demonstrated through multiple heating and cooling cycles, which resulted in low viscosity liquids, and then hard films respectively. Reversibility was verified using ^{1}H NMR spectroscopy, as well as differential scanning calorimetry (DSC). Variation of the spacer chemistry in the monomers was found to profoundly influence the physical properties of the resulting polymers. The rate of hardening varied significantly among the four polymers, ranging from seconds to hours. The rate and degree of polymerization were also influenced by the spacer group chemistry, as was the rheology of the molten and solid materials produced. Adhesive strength of the polymers was found to be surprisingly high, and this was quantified by measuring the tensile adhesive strength. A fifth monomer pair, consisting of a tripodal maleimide and furan, was then synthesized and characterized. Somewhat surprisingly, the incorporation of cross-linking into the polymer network did not significantly alter the mechanical properties as compared with the linear polymers. Combinations of linear and multi-podal monomers were then made and characterized, but did not result in any significant improvements relative to the linear polymers alone.

In an earlier study, phase separation of polystyrene (PS) and poly(methyl methacrylate) (PMMA) blends was used as a means to pattern PS- or PMMA-functionalized single-walled carbon nanotubes (SWNTs) in thin films. Dilute solutions (5 wt% in THF) of 1:1 PS/PMMA blends containing the functionalized nanotubes were spin cast and annealed at 180°C for 12 h. Characterization of the annealed films by scanning Raman spectroscopy, which utilized the

unique Raman fingerprint of carbon nanotubes, enabled accurate mapping of the functionalized SWNTs within the films relative to the two phase-separated polymers. It was found that the migration of the nanotubes in the films could be controlled using the appropriate functionality on the nanotubes, thus the PS-functionalized nanotubes were found to migrate to the PS domains, while the PMMA-functionalized nanotubes migrated to the PMMA domains.

In an attempt to demonstrate the concept of nanotube solubilization using reversible polymers, one of the linear reversible polymers was bound to furan-functionalized carbon nanotubes. Solutions (DCM) containing an excess of the maleimide-furan polymer relative to the furan functionality on the nanotubes were mixed at room temperature for 1 week, and resulted in significant solubilization of the nanotubes. Similar mixtures, containing the maleimide and furan monomers, did not afford any solubility to the substituted nanotubes. Heating of the former solution resulted in a collapse of the DA polymer, and precipitation of the dissolved nanotubes, illustrating the reversible nature of the polymers, and their influence on carbon nanotube solubilization.

ACKNOWLEDGEMENTS

This work would not have been possible without the financial assistance and support of the Xerox Research Centre of Canada (XRCC). XRCC has always fostered exploration and learning, and there is no better example of this than their support of continuing education. A number of my colleagues have completed their graduate studies while at XRCC, and that has been inspirational to me. I offer my thanks to the many people in the Centre who have provided technical help, or words of advice and encouragement along the way. Jim Duff and Stephan Drappel hired me at XRCC many years ago, and have been the source of countless invaluable discussions, both personal and professional.

If this endeavor would not have begun without the support of XRCC, it surely would not have been completed without the help of Alex Adronov. Alex is a superb teacher, and has instilled in me a much better understanding of the language of chemistry. I travelled out to the University many times for individual or group meetings, and I always came away feeling energized and much more positive about things than when I arrived. I am indebted to Alex and his group for their patience and understanding, and for always making me feel a part of their team.

One cannot maintain a full time job and complete graduate studies without the support of their family. In the time it has taken me to complete this degree, my son Matthew has grown nearly two feet. During this pivotal time in his life, both he and my wife Melinda have had to accommodate my odd schedules, and times of frustration and quiet refuge. Their enthusiasm and encouragement throughout this venture have been invaluable. My love and thanks to you both.

Finally, to my parents and family, thank you for a lifetime of love and support.

PREFACE

This thesis is comprised of previously published work as follows:

In Chapter 2, "Phase Separation of Polymer-Functionalized SWNTs within a PMMA/Polystyrene Blend" by Mayo, J.D., Behal, S., and Adronov, A. has been reproduced with permission from the Journal of Polymer Science. James Mayo is the lead author who wrote the paper, conducted the experiments and interpreted the data under the supervision of Alex Adronov.


for Lori
Master of Science

Table of Contents

List of Abbreviations

ABF	Arylbenzofuranone
AcOH	Acetic acid
AFM	Atomic Force Microscopy
ASTM	American Society for Testing and Materials
ATRP	Atom transfer radical polymerization
CNT	Carbon nanotubes
CPD	Cyclopentadiene
DA	Diels Alder
DABBF	Diarylbibenzofuranone
DCM	Dichloromethane
DCPD	Dicyclopentadiene
DMA	Dynamic Mechanical Analysis
DMF	Dimethylformamide
DMSO	Dimethyl sulfoxide
DP	Degree of polymerization
DSC	Differential Scanning Calorimetry
DSI	Depth-sensing Indentation
EBiB	Ethyl-2-bromoisobutyrate
Et_2O	Diethyl ether
EtOH	Ethanol
FTIR	Fourier Transform Infrared Spectroscopy

GISAXS	Grazing Incidence Small Angle X-Ray Scattering
GPC	Gel Permeation Chromatography
HEEDTA	Hydroxyethyl ethylenediaminetriacetic acid
HRMS	High-resolution Mass Spectroscopy
LCST	Lower Critical Solution Temperature
LED	Light Emitting Diode
MeOH	Methanol
NHC	N-heterocyclic carbenes
NMR	Nuclear Magnetic Resonance Spectroscopy
P2VP	Poly(2-vinyl pyridine)
PEG	Poly(ethylene glycol)
PF-SWNT	Polymer-functionalized single-walled nanotubes
PMDETA	N,N,N’N’,N”-pentamethyl diethylenetriamine
PMMA	Poly(methyl methacrylate)
PNIPAM	Poly(N-isopropylacrylamide)
PPG	Poly(propylene glycol)
PS	Polystyrene
ROMP	Ring-opening metathesis polymerization
SEM	Scanning Electron Microscopy
SPM	Scanning Probe Microscopy
SWNT	Single-walled nanotubes
TBAB	Tetrabutylammonium bromide
TDCB	Tapered double-cantilever beam

TEM	Transmission Electron Microscopy
TEMPO	2,2,6,6-tetramethylpiperidinoxyl
TGA	Thermogravimetric Analysis
THF	Tetrahydrofuran
TMS	Tetramethylsilane
TOPO	Tri-n-octyl phosphine oxide
UPI	Ureido-pyrimidinones
UV-Vis	Ultraviolet-visible spectroscopy
XRD	X-Ray Diffraction

List of Figures

List of Schemes

List of Tables

Chapter 1
Literature Review of Self-Assembly of Carbon Nanotubes and Reversible Polymers

1.1 Self-assembly of Carbon Nanotubes

1.1.1 Functionalization of Carbon Nanotubes

It has been more than twenty years since Iijima published his seminal paper on carbon nanotubes.[1] Since that time, nanotubes have garnered tremendous scientific interest in both industrial and academic settings. Their unique combination of electrical, mechanical and thermal properties make them equally suited for applications in molecular electronics[2] or as high performance polymer nanocomposites.[3] Electrically, they can act as both a conductor, capable of ballistic electron transport,[4,5] or as a semi-conductor, with band gaps being inversely proportional to their diameter.[6] Applications in electrical devices such as field effect transistors,[7-9] chemical sensors,[10] and light emitting diodes (LED)[11] have all been envisioned and studied as a result of their exceptional electron transport properties. Mechanically, single-walled carbon nanotubes possess a tensile strength as high as ~1 TPa, more than an order of magnitude greater than steel. This incredible strength, coupled with very low densities (1.3-2.5 g/cm^3) and exceptionally high aspect ratios (>1000), make them ideally suited as nanocomposite reinforcing agents.[12-14] Our interest in carbon nanotubes was to explore the potential for self-assembly of these macromolecules within polymer films or devices.

One of the principal shortcomings of carbon nanotubes is their decided lack of solubility in common organic solvents. Whether they are to be incorporated into electronic devices, or fabricated into ultra-strong fibres, solubilization or homogeneous dispersion is required to take

full advantage of their properties. Ironically, the graphite-like structure that contributes to their unique properties also creates strong intermolecular forces, resulting in bundles of tubes that are very difficult to disperse. Dissolution first requires breakdown and wetting of these bundles, whether by mechanical energy or ultrasonic radiation. Ionic or steric stabilization of the separated tubes is then required to prevent re-aggregation. Surfactants and polymers are then used to impart sterically controlled stabilization to the separated tubes, and this has been the focus of much of the research done to date.[15-17]

Both covalent[15,18-21] and non-covalent[22-27] functionalization have been explored, and numerous approaches have been examined within each class. For covalently bound systems, two different methodologies, "grafting to" and "grafting from", have been used to decorate the surface of nanotubes. In the former case, prefabricated polymers are coupled to the nanotube surface via reactive moieties incorporated onto the polymer chain. Separate synthesis of the polymer then ensures better polymerization control, and narrower polydispersities. However, the entangled chains encounter steric hindrance as they approach the nanotube surface, resulting in lower graft densities. In the latter case, polymers are synthesized directly from the surface of the nanotubes, via initiators grafted to the surface. The relatively small initiator molecules can easily populate the surface of the tubes, enabling high polymer graft densities, and greater solubilities. However, control of both molecular weight and polymer architecture is more difficult in this scenario. We have chosen the former technique, employing the [3 + 2] Huisgen cycloaddition reaction to graft azide-terminated polymers to alkyne anchor sites that were installed on the nanotube surface (Scheme 1.1).[28] We then turned our attention to the incorporation of these polymer-functionalized nanotubes into thin polymer films.

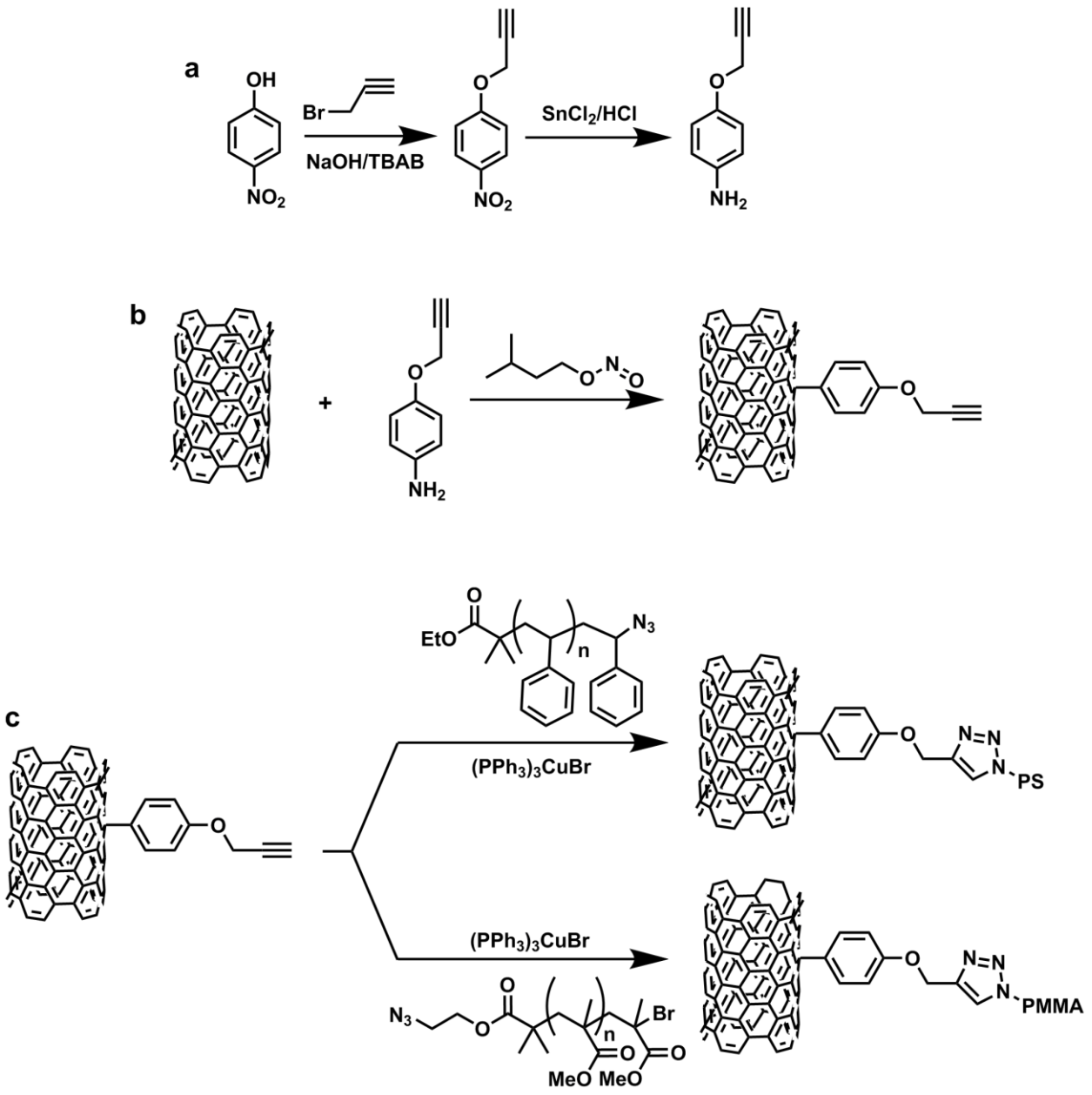

Scheme 1.1. Polymer functionalization of carbon nanotubes:a) Preparation of p-aminophenyl propargyl ether; b) Installation of alkyne anchoring site on carbon nanotube surface; c) [3+2] Huisgen cycloaddition reaction between alkyne anchoring site and azide-terminated polymers.

1.1.2 Incorporation of Carbon Nanotubes into Polymer Films

Self-assembly within thin polymer films has been investigated extensively, targeting both mechanical and electronic applications that rely on highly ordered polymer arrays patterned on a micro or nanometer scale.[29,30] The system of polystyrene (PS) and poly(methylmethacrylate) (PMMA) has received much attention, owing to the marked difference in polarities of the two materials and their high degree of phase separation.[31-33] In our investigation, polymer-functionalized carbon nanotubes were added to PS-PMMA blend solutions and then spin cast and annealed to form the distinctive self-assembled patterns shown in Figure 1.1.[34] Characterization of the resulting annealed films using scanning Raman Spectroscopy leveraged the unique Raman fingerprint of carbon nanotubes,[34-36] and served to illustrate selective migration of the nanotubes within the thin films. Both PS- and PMMA-functionalized nanotubes were incorporated into the films, and were found to migrate to their respective domains, illustrating the potential for self-assembly of carbon nanotubes.

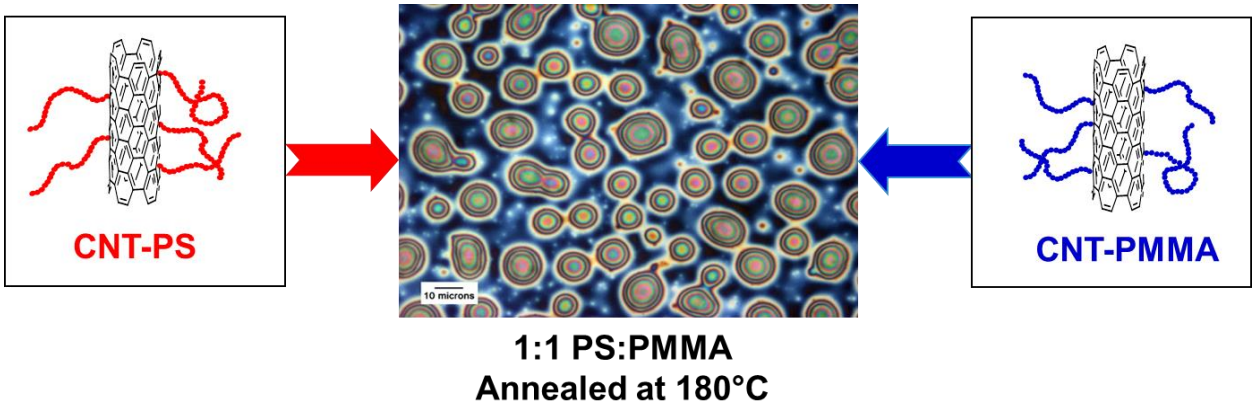

Figure 1.1. Incorporation of functionalized carbon nanotubes into PS/PMMA films.

1.2 Reversible Polymers

Following our investigation of the self-assembly of carbon nanotubes, we turned our attention to the field of reversible polymers. Initially, this comprised the synthesis and characterization of both linear and cross-linked polymers without the use of reinforcing agents, such as carbon nanotubes. However, our success with the self-assembly of CNTs led us to attempt to functionalize them using reversible polymers. The many attributes of these materials are well documented, but the ability to self-heal would offer a unique feature to nanotube-reinforced structures and films.

The field of reversible polymers has grown considerably over the past two decades. Numerous investigators have explored the use of both covalent and non-covalent bonding as a means to impart reversibility to polymer networks.[37-43] The ability to repeatedly interchange between the monomeric and polymeric forms instills a unique set of properties in these materials that has given them tremendous recognition in both academic and industrial settings.[44-52] Perhaps the most alluring of these properties is the ability to undergo self-healing, and this has been the focus of much of the research related to reversible polymers.[40-43,53-56] However, the low viscosities attainable in the molten state also greatly facilitate materials processing, an essential requirement for many industrial applications, and it is this latter attribute that was of interest to us.

Polymer processing in the form of blending or extrusion relies heavily on the rheological characteristics of the materials being processed.[57] Low molecular weight thermoplastics generally require only mild conditions to yield conformable solids that can be easily processed using conventional methods, and in many instances, these polymers offer sufficient mechanical integrity for their intended application. However, many applications require higher molecular weights and more complex architectures, and these materials can be exceedingly difficult to process.[58] Cross-

linking creates a strong three dimensional polymer network, and is a very effective means to improve the robustness of many types of polymers, but can also prevent reshaping or remolding of the final material. Furthermore, at the end of their life cycle, permanently cross-linked thermoset polymers cannot be recycled, making them unattractive from an environmental perspective.[56,59,60] While the former issue can be addressed by introducing cross-linking after processing or fabrication has been completed, the lack of recyclability remains a significant setback for thermosetting polymers.[59,60] Incorporation of reversible bonds in these three dimensional networks would not only offer more options in processing, but would also enable end of life recycling of the product.

1.3 Self-healing Polymers

While there are significant benefits to be gained in the realm of materials processing, the majority of interest in reversible polymers has been in their potential as a solution for thermal and mechanical breakdown of both structural and thin films, so-called self-healing polymers.[37,40-43,55] Formation and propagation of micro-cracks within a polymer matrix ultimately lead to failure of the material. Reparation using traditional adhesives occurs only on a macro scale, and does not treat the fracture at its onset. Reversible polymers enable reparation on a nano-scale within the crack well before critical levels of propagation can occur. The inherent low viscosity of the monomeric materials enables flow and realignment of the reactive sites across the damaged area, allowing formation of covalent bonds across the micro-crack with or without the use of healing agents or additives. This in turn enables much higher healing efficiencies than have been realized with traditional epoxies or surface treatments, and also allows the materials to undergo multiple healing events.[40,61,62] The basic concept for reversible polymers, depicted in Figure 1.2, has been

explored by numerous investigators using both covalent and non-covalent bonding motifs, and can be divided into three categories. In the simplest form, ditopic monomers are coupled sequentially to form linear polymeric chains (Figure 1.2a). Multi-podal monomers can also be used, resulting in more complex, cross-linked architectures (Figure 1.2b). The third approach involves existing polymer chains having reactive pendant groups that can generate reversible cross-links within the polymer system. (Figure 1.2c) In all cases, the bonds can be decoupled with the application of a stimulus such as heat or light, thus they can be used either to generate a reversible base polymer network, or to impart reversible cross-linking to existing polymer chains. Reversible bonding can also be integrated into dendrimeric structures, opening up a broad range of applications specific to these unique materials. One of the significant advantages to arise from this form of bonding is that in all of these cases, materials that can be readily processed in the neat state are viable, as the melt viscosities of the molten monomers can be much lower than might be expected using comparable conventional polymers. Materials that enjoy both the durability of thermosetting polymers and the processing and recyclability characteristics of a thermoplastic can therefore be produced. Additionally, thin films and bulk polymeric devices can be prepared with minimal or no use of solvents, offering both financial and environmental incentives with their use.

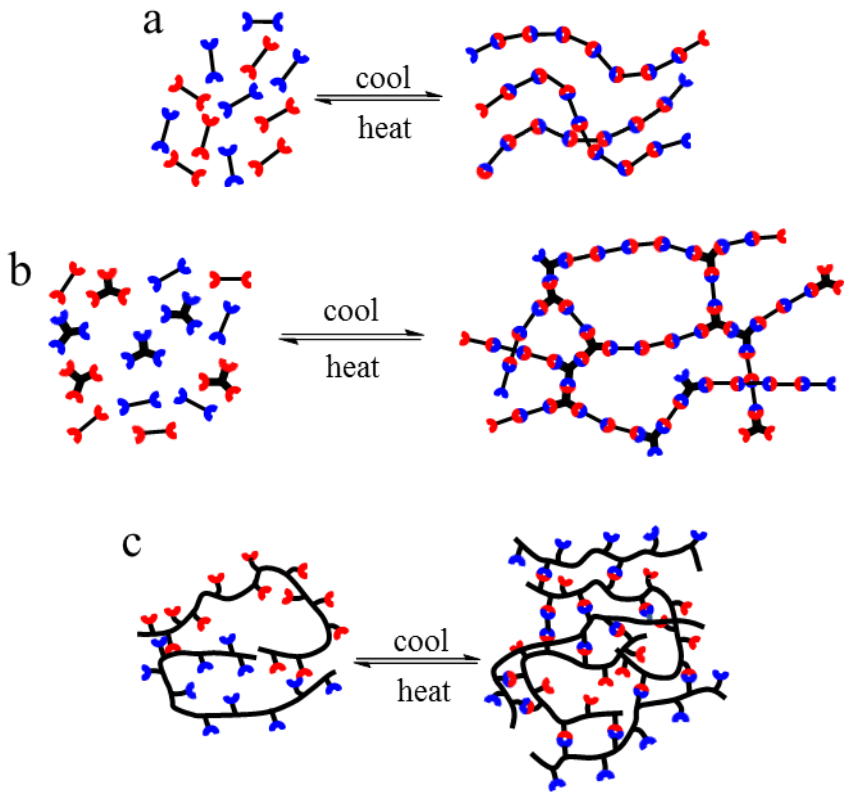

Figure 1.2. Schematic representation of reversible polymer formation: a) linear ditopic monomeric components; b) multi-podal monomeric components; c) decorated polymer backbone.

1.3.1 Methods for Self-healing

1.3.1.1 Autonomic Healing

In the study of self-healing materials, two approaches have been pursued, distinguished by the need for user intervention upon material failure. The use of healing agents embedded within structural materials enables completely autonomic healing, and has been explored for more than a decade.[37,43,53,63] In one of the first instances of reduction to practice of this concept, Dry et al. incorporated cyanoacrylates into hollow glass fibres that were being used to reinforce both

polymers and construction materials such as cement.[64,65] Fracture of the bulk material resulted in spontaneous release of the cyanoacrylate healing agent due to rupture of the reinforcing fibres. Several issues were encountered in this preliminary work. Most notably, the reactivity of the cyanoacrylates prevented diffusion of the healing agent to the damage site, limiting the healing efficiency of the system. Secondly, the high viscosity of the cyanoacrylates hindered loading of the liquid curing agent into the fibres. Despite these challenges, the concept of autonomic self-healing was successfully demonstrated in polymeric solids using cyanoacrylates and other healing agents.

In 2001, Sottos and co-workers exploited this same principle, using ring-opening metathesis polymerization (ROMP) to induce instantaneous crack repair without user intervention.[53] Microcapsules composed of a urea-formaldehyde shell and containing a monomeric healing agent were dispersed throughout the polymer. Formation of a crack resulted in rupture of the capsules, and release of the monomer into the polymer matrix. Suitable catalysts or initiators, dispersed throughout the bulk polymer, would then initiate polymerization across the newly formed crack. A schematic depiction of this process is shown in Figure 1.3. In this scenario, the monomer and catalyst system must rapidly polymerize upon contact with one another, while remaining inert for long periods of time in the presence of a wide range of functional groups. With these criteria in mind, the materials of choice for the ROMP reaction were the monomer dicylclopentadiene (DCPD), and the monomer-soluble Grubbs' catalyst bis(tricyclohexylphosphine)benzylidene ruthenium (IV) dichloride (Figure 1.4). Polymeric samples containing these components were prepared, and the initial fracture toughness of a molded strip was measured using a tapered double-cantilever beam (TDCB). A fresh sample was then pre-scored with a razor blade and the resulting crack was carefully propagated along its

length. Healing was conducted at room temperature by contacting the two newly exposed surfaces to one another with minimal force. The fracture test was then repeated and healing efficiency determined as a function of fracture toughness before and after healing. Values of approximately 75% of the original fracture load were observed, as compared with close to 60% for samples repaired using a conventional epoxy resin, thus confirming the validity of this technique.

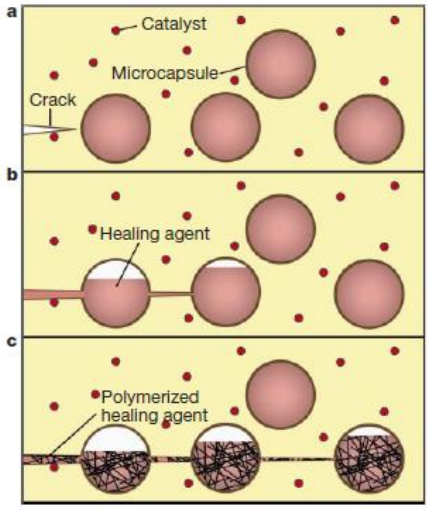

Figure 1.3. Autonomic self-healing polymer systems: a) Inititation of crack in polymer matrix; b) propagation of the crack, resulting in fracture of microcapsules; c) interaction of healing agent with catalyst, initiating polymerization and crack healing. (Reprinted by permission from Macmillan Publishers Ltd: Nature, 409, 794 copyright 2001.)

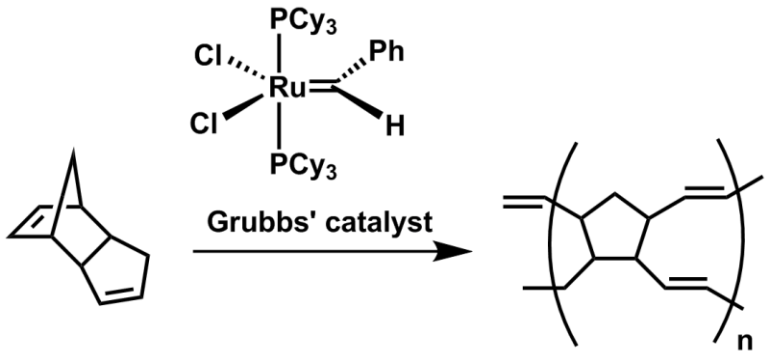

Figure 1.4. Ring-opening metathesis polymerization (ROMP) using Grubbs' catalyst.

1.3.1.2 Alternative Core-shell Chemistries

Stability and cost issues relating to the Grubbs' catalyst have prompted investigations using a number of other materials options, while using the same principle of healing.[41] Environmentally stable organotin catalysts have been encapsulated and incorporated into several different polymer complexes, so as to promote the polycondensation of hydroxyl-terminated siloxanes upon their release.[66,67] This offers a much more environmentally stable system, and also allows for widespread distribution of the polymeric healing agent throughout the polymer matrix, rather than being restricted to being contained within the microcapsules. Solvents have also been used as healing agents in both PMMA and polycarbonate systems.[68-70] Liberation of the solvent in the fracture area resulted in healing by increased diffusion, which simply allowed greater entanglement of the polymer chains. This concept has seen limited success, although its simplicity makes it a very attractive option. Alternative approaches have been considered, and significant progress continues to be made in this field, as investigators address the many challenges of the concept, including encapsulation and mobility of the repair agent, kinetics of the reparation chemistry, and the overall healing efficiency of these autonomic systems.[37,53,63,67,71-73] Nevertheless, while truly autonomic healing of damaged polymers has been demonstrated via

several different mechanisms, the additional components incorporated into the polymer matrix would elevate the cost and complexity of the device, and in some cases could compromise performance.

1.3.1.3 Reversible Polymers via Radical Coupling

Imato et al. have also developed dynamic materials that exhibit autonomic coupling at room temperature.[74] Reversibility stems from the room temperature equilibrium that exists between arylbenzofuranone (ABF) and its dimer diarylbibenzofuranone (DABBF) (Figure 1.5a).[75,76] Cross-linked polymer gels were prepared using a poly(propylene glycol) (PPG) backbone having pendant DABBF units that serve as reversible cross-linking agents (Figure 1.5b). The self-healing characteristics of the cross-linked gels were demonstrated with the complete fracture of a solid polymer monolith, followed by re-attachment of the two fragments using minimal pressure. Tensile tests before and after fracture revealed a time-dependence for healing, ultimately leading to a 98% recovery of the original mechanical strength after 24 h. Notably, recovery of mechanical strength remained high even when the separated pieces were kept apart for up to 5 days, demonstrating the air stability of the radical species generated upon dissociation of the dimer. Addition of an excess of the dimer DABBF to the cross-linked polymer shown in Figure 1.5b afforded a THF-soluble fraction, which was identified as PPG using ^{1}H NMR spectroscopy. This was considered as evidence for the breakdown of the cross-links via exchange with the newly added free dimer, and the reinforcement of the PPG chains by cross-linking was in turn attributed to the ABF-DABBF equilibrium. A control sample, in which the cross-linking agent was comprised of irreversible covalent bonds, did not yield any soluble material under these conditions, nor did it display any self-healing characteristics, further

confirming the hypothesis. However, it should be noted that mechanical testing was conducted in the absence of light so as to avoid the effect of extraneous radical species, thus it is not clear what the intrinsic stability of the ABF radicals would be in daylight. Nonetheless, the ease and efficiency with which these materials were healed is impressive, as no alignment aids or pressure was required to completely restore the initial mechanical integrity of the polymers.

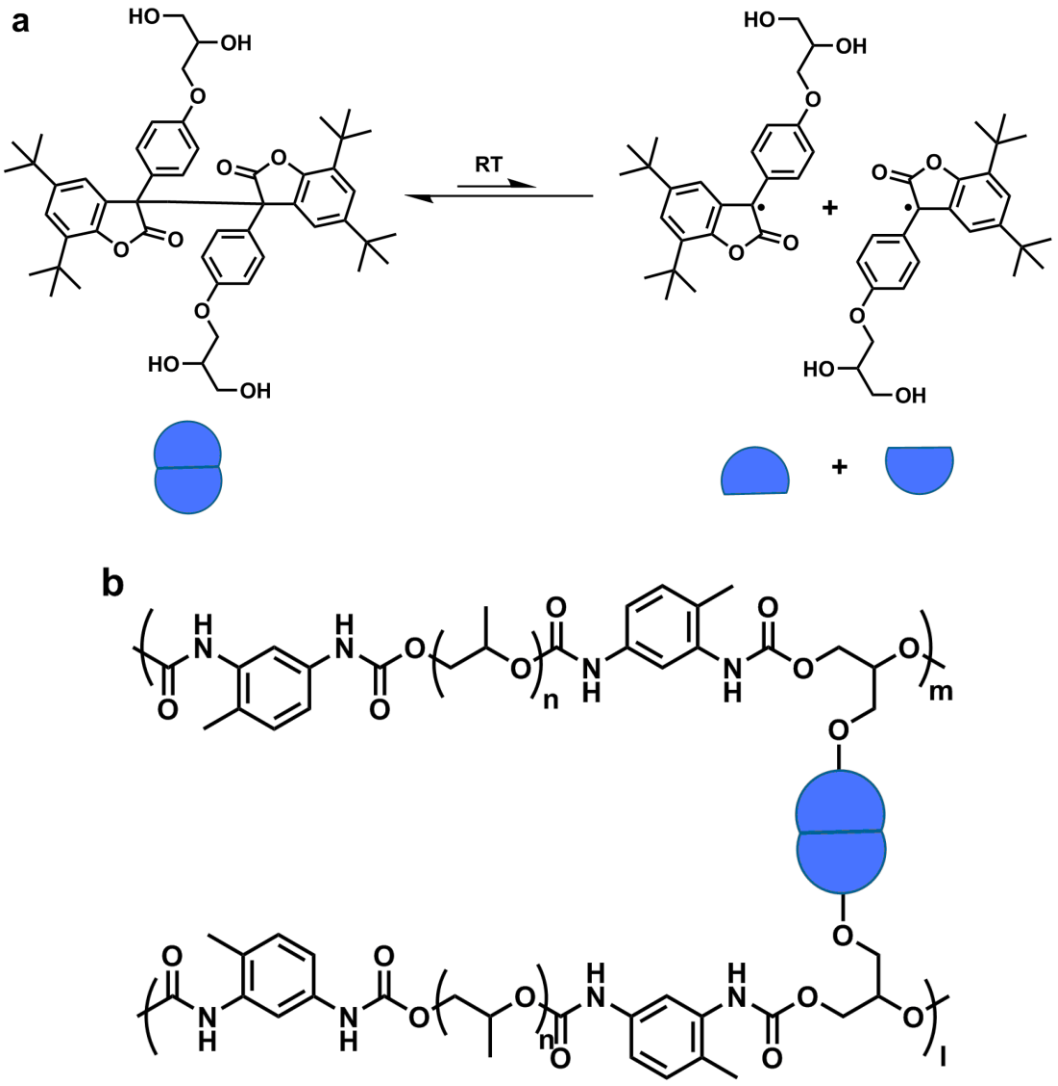

Figure 1.5. Reversible polymers via radical coupling: a) equilibrium of DABBF at room temperature; b) PPG chain having reversible DABBF cross-linking unit.

1.3.2 Non-autonomic Healing

The second approach to self-healing relies on reversible bonding systems to serve as the formative polymer bonds or cross-links within films or structural materials. In this case, material repair does require user intervention, usually in the form of applied heat or light. However, no additives or cross-linking agents are necessary, offering a distinct advantage over the autonomic processes just described. As was the case with the autonomic systems, a wide variety of strategies have been used to develop and understand self-healing materials.

1.3.2.1 Hydrogen Bonded Systems

Meijer and co-workers were among the first to develop tough supramolecular materials based on reversible bonding.[77,78] Innovative design of small molecules having multiple hydrogen bonding sites enabled the use of this relatively weak bond to collectively form a strong link between adjacent monomer units. Specifically, self-complementary ureido-pyrimidinones (UPy), capable of quadruple hydrogen bonding, were synthesized (Figure 1.6a). Covalent tethering of these UPy adducts converted them to ditopic monomers having two terminal, multi-point hydrogen bonding sites that could effectively serve as non-covalent, reversible bonds or cross-links (Figure 1.6b). Application of heat would weaken the hydrogen bonds and thereby reduce the molten viscosity, making processing much more practical. Cooling of the processed liquid would then restore the hydrogen bonds, resulting in the formation of robust solids. A wide variety of polymers having thermodynamically controlled architectures have been prepared and characterized using this concept, offering the potential for use in a variety of applications.[79-84]

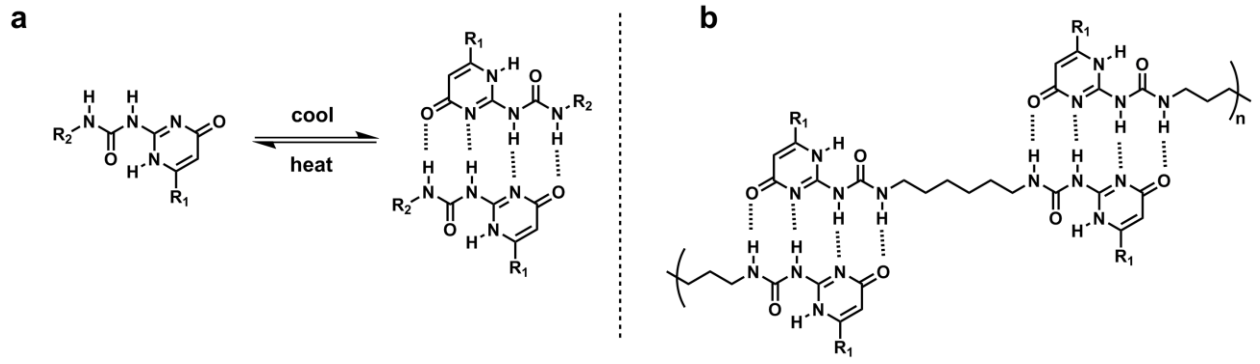

Figure 1.6. Formation of supramolecular networks using multi-point hydrogen bonded systems: a) reversibility of a ureido-pyrimidinone; b) formation of a reversible polymer using a bis(ureido-pyrimidinone).[78]

1.3.2.2 Metal-ligand Co-ordination Polymers

Kinetically labile metal-ligand coordination bonds have also been used to form supramolecular networks, resulting in a class of reversible polymers that can leverage both the physical characteristics of a polymer and the functional properties of a metal. Reversibility is governed by the magnitude of the metal-ligand binding constant, such that kinetically inert bonds lead to essentially irreversible co-ordination bonded systems, while more labile bonds afford dynamic materials that exist in an equilibrium state.[85] In the latter case, ditopic monomers can be combined with a suitable metal ion to afford stimulus-responsive reversible polymers (Figure 1.7). In this capacity, efforts have largely been directed toward complexes formed between N-heterocycles and a wide array of transition metals. The multi-dentate ligands bipyridine and terpyridine are particularly well-suited for formation of metal-ligand complexes, and each of these has received significant attention.[85-94] Rowan and co-workers have linked bis(terpyridine) monomers using a variety of metal atoms to yield self-assembled, linear supramolecular polymers.[86] Two different spacer groups were used in the monomers, and these were found to

significantly affect the properties of the resulting polymers. The choice of a poly(tetrahydrofuran) core led to film-forming polymeric metal complexes consisting of soft polyether segments and hard ionic segments. Conversely, metal complexes formed from monomers having the more flexible penta(ethylene glycol) core did not exhibit polymeric properties, and could not be processed into mechanically robust films. This was attributed to the propensity of the more flexible monomers to form macrocyclic species, rather than linear polymers, and indeed, these macrocycles showed little improvement in mechanical integrity over the monomers themselves. The choice of metal ion was also found to affect material properties, as the stronger binding metal ions Co(II) and Fe(II) led to more thermally stable polymers than the more labile Cd(II) and Zn(II). A wide variety of material properties can therefore be achieved using this approach, using the influence of both spacer chemistry and metal ion on the thermal and mechanical properties of the resulting supramolecular polymers.

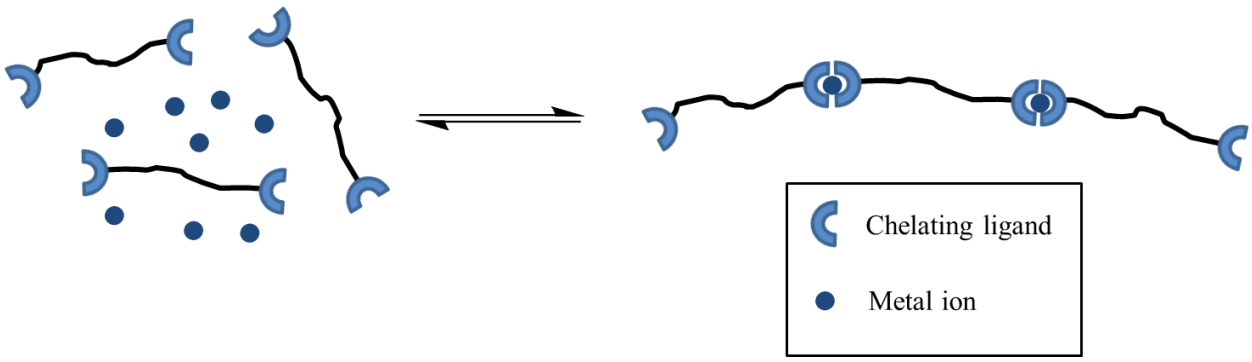

Figure 1.7. Schematic representation of ditopic metal-ligand monomer-polymer equilibrium.

Schubert and co-workers have explored this same concept in a novel manner, as they combined a second non-covalent bonding motif into the polymer backbone. Poly(ε-caprolactone) spacers were functionalized with a terpyridine adduct on one end and a UPy group on the other end, such that the introduction of either Fe(II) or Zn(II) metal ions resulted in formation of supramolecular polymers with alternating metal-ligand and hydrogen bonding linkages throughout the linear chains (Figure 1.8).[89] Polymer formation was easily detected, as it was accompanied by a pronounced color change in solution to deep purple. Polymerizations were conducted at concentrations greater than 2.1 mg/mL so as to deter the formation of macrocycles, and indeed, solution viscometry studies confirmed the formation of high molecular weight polymers at these higher concentrations. Reversibility was demonstrated by the addition of the strong complexing agent hydroxyethyl ethylenediaminetriacetic acid (HEEDTA), which triggered the collapse of the metal-ligand polymer, as this small molecule effectively consumed the metal ions by overwhelming the terpyridine-metal bonds. This transformation was also easily observed, as the intense purple color originally generated by the polymer disappeared upon addition of the complexing agent. Further confirmation of reversible behavior was made using UV-Vis spectroscopy, as the bands of the free terpyridine moieties were clearly distinguishable after decomplexation of the polymer. Restoration of the polymer could be achieved with the addition of $FeCl_2$, which was also accompanied by a reversion of the solution to its original deep purple color.

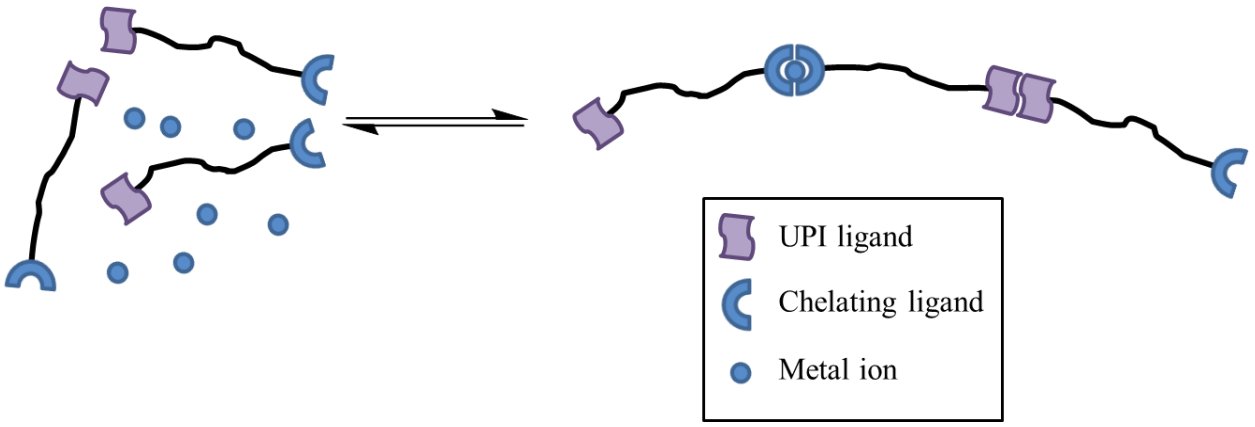

Figure 1.8. Schematic representation of metal-ligand/H-bonding monomer-polymer equilibrium.

The Schubert group further explored the use of dual switching mechanisms, as they installed a metal-chelating endgroup on a thermally responsive core.[87] Specifically, terpyridine-terminated poly(N-isopropylacrylamide) (PNIPAM) was self-coupled using either Fe(II) or Zn(II) metal ions. The resulting supramolecular polymers offered unique properties, as either of the monomer functionalities could be addressed as desired. Heating of the PNIPAM spacer above its lower critical solution temperature (LCST) led to clouding of the solution, as the hydrogen bonds between the polymer and water molecules were disrupted at the higher temperature, leading to a reduction in polymer solubility.[95] Alternatively, addition of a competing chelating agent, for example HEEDTA, resulted in the collapse of the metal-complex, signified by an easily discernible color change, as well as a shift of several key diagnostic proton peaks in the ^{1}H NMR spectrum. Interestingly, the choice of metal ion offered a means for control of not only the binding energy of the metal-ligand bond but the cloud point of the PNIPAM moiety, providing the potential for a wide variety of material properties and applications.

1.3.2.3 Covalently Bound Reversible Systems

While many different forms of bonding can impart reversibility, there would be certain advantages to using covalent bonds as the linking chemistry in reversible polymers. Hydrogen bonded polymers can indeed be very robust, but the electromagnetic attraction that provides their strength still exists in the molten state, making melt viscosities directly related to the number and strength of the hydrogen bonds at each linkage site. As a result, multi-point hydrogen bonded systems might be expected to have sizable melt viscosities.[81] By comparison, the attractive forces in a covalent system would be greatly reduced in the molten state, thus the viscosity of such systems can potentially be very low, making them very attractive in terms of materials processing.

1.3.2.4 Reversible Carbene Chemistry

Bielawski and co-workers have used covalent bonding as a thermally reversible co-ordinating link to generate polymeric materials, leveraging the reversible equilibrium that exists between imidazole based carbenes and their dimers (Figure 1.9a).[96,97] A systematic study, in which the N-substituents on the heterocyclic ring were varied, led to an optimal balance of the monomer-polymer equilibrium. From this study, a biphenyl spaced carbene dimer having two N-ethyl substituents was chosen for investigation of the reversibility of these materials (Figure 1.9b). Reversibility was demonstrated in dilute toluene-*d8* solutions using ^{1}H NMR spectroscopy, as the relative intensities of monomer and polymer peaks could be controlled with heating and cooling cycles. These homopolymers were found to be somewhat impractical as they were unstable in the presence of air and moisture, and physical properties of the resulting polymers were therefore not measured. However, the viability of forming reversible polymers using this chemistry was successfully demonstrated. More recently, new classes of reversible polymers were prepared and

characterized based on N-heterocyclic carbene (NHC) chemistry.[98,99] Reaction of the bis(NHC)s with bis(isothiocyanates) and bis(azides) afforded copolymers that were not only thermally reversible and stable, but conductive as well. An example of a polymer comprised of a bis(NHC) and bis(isothiocyanate) is shown in Figure 1.9c. In this case, control of the equilibrium required the addition of bis(NHC) for polymer formation and bis(isothiocyanate) for reversion to monomers, thus it was not a simple thermal equilibrium, as described in many of the examples above. However, further investigation based on this same principle led to the coupling of Group X metals with bis(NHC)s, which resulted in reversible, semiconducting polymers (Figure 1.9d). These new materials offered the unique combination of thermal reversibility and conjugation in both the monomeric and polymeric states, making them interesting candidates for development of dynamic materials in the broad field of organic electronics.

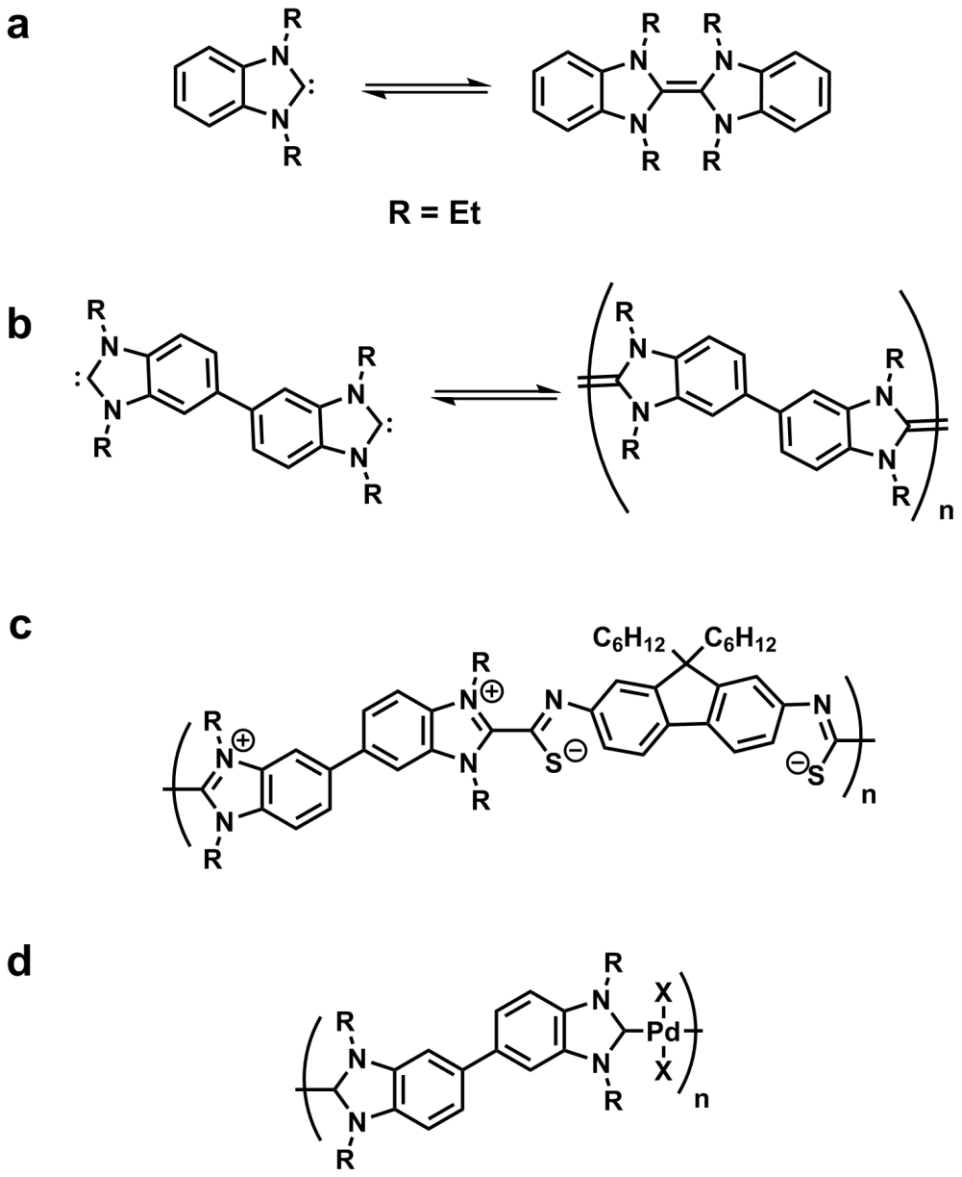

Figure 1.9. Reversible polymers via carbene chemistry: a) equilibrium between N-substituted carbene and its dimer; b) coupling of a ditopic carbene to form a reversible polymer; c) reversible polymer formed by combination of a ditopic carbene and isothiocyanate; d) reversible polymer formed by combination of a ditopic carbene and Pd-ligand dimer.[97]

1.3.2.5 Reversible Polymers via Transesterification

Liebler and co-workers have also used reversible covalent links to provide high performance materials that were both processable and reparable.[100] Polymer networks were constructed by coupling the diglycidyl ether of bisphenol A with a mixture of di- and tri-carboxylic acids (Figure 1.10a). Reversibility was thermally induced by means of a $Zn(OAc)_2$ catalyzed transesterification reaction between the free –OH and ester groups within the base polymer network. Interestingly, the application of heat merely served to rearrange the existing bonding organization within the material and afford a more malleable version of the cross-linked solid (Figure 1.10b). The newly formed ester bonds prevented complete depolymerization, generating somewhat softer solids that could be easily reshaped and reprocessed. However, in keeping with other reversible systems, cooling of the softened polymer restored the mechanical integrity to its original level. Examples of material shaping using a simple heat gun illustrated the dynamic nature of the reversibility. Using only this crudely regulated heat source, the internal structure and viscosity of an inflexible, cross-linked system could be altered in a controlled manner, allowing formation and processing of the solid polymer while averting structural failure or total solubility. Cooling of the reshaped material then restored its dimensional stability such that it behaved as a hard epoxy resin. Resins having modulus values on the order of 1.8 GPa were prepared, showing the potential for preparation of industrially relevant materials having the unique ability to undergo reshaping and recycling using only thermal energy.

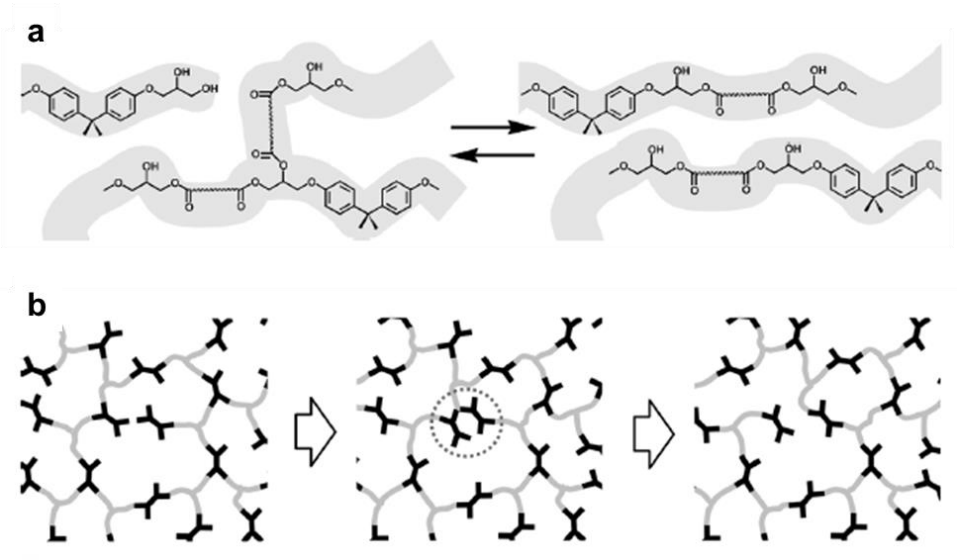

Figure 1.10. Reversible polymers via transesterification: a) schematic depiction of transesterification, showing the preservation of the total number of linkages; b) reversibility of the transesterification process based on hydroxy-ester networks. (From Science, 2011, 334, 965. Reprinted with permission from AAAS.)

1.3.2.6 Diels Alder Chemistry in Reversible Systems

While each of the above methodologies stands on its own merits, the most thoroughly examined approach for self-healing polymers involves the well-known Diels Alder (DA) reaction, a cycloaddition that occurs via a concerted mechanism between an alkene and a conjugated diene. Formation of two new sigma bonds in the product alkene ring system provides the driving force for the coupling reaction, while the application of heat restores the original component parts via the retro-DA reaction.[101] Both the forward and reverse reactions can therefore be driven by temperature alone, while not generating any small molecule by-products, making this an ideal candidate for a reversible polymer system. In terms of starting materials, the conjugated double bonds in the diene must be aligned in a cis configuration, so as to produce a ring structure when

coupled with the dienophile. Dienes in the trans conformation will not simply hinder the reaction, but prevent it altogether, and for this reason, cyclic dienes are often used in DA reactions.[38,61,62,102] Steric crowding must also be avoided, placing a further limitation on both the diene and dienophile. Boutelle et al. used dynamic combinatorial chemistry to study the effects of electron donating and withdrawing substituents on maleimide and furan ring systems.[103] A systematic study, in which the position and nature of the substituents on each of the reagents was varied, was undertaken. Enthalpy and free energy were determined for a series of DA reactions, clearly illustrating the impact of the substituents on the speed and reversibility of the reaction. As expected, electron rich dienes and electron poor dienophiles were found to be most favorable for Diels Alder coupling. Interestingly, the substituent effect was found to be significantly greater for furans than for maleimides, as noted by a wide range of free energies observed with different furans.[103] Catalysts can also be used to accelerate the coupling reaction, but are not required with appropriate electronic and steric design of the two starting materials. In practical terms, incorporation of catalytic materials would be undesirable, as they could add significant cost and complexity to the final material.[101,103,104]

Products of a DA reaction may consist of two different stereoisomers, depending on the orientation of the diene and dienophile relative to one another (Figure 1.11). Detailed studies have been conducted to determine the factors driving formation of either the endo or exo conformer,[28,30,31] although in general, this does not play a significant role in self-healing polymers. Nevertheless, both electronic and steric effects have been shown to influence the stereoselectivity of the reaction.

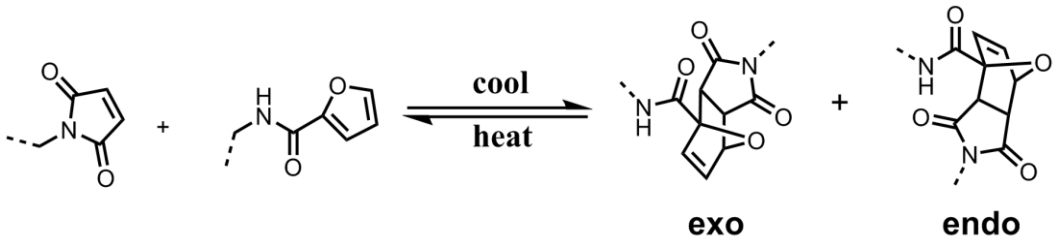

Figure 1.11. Thermally induced DA and retro DA reaction.

1.3.2.7 Furan-maleimide Systems

One of the first reports of the use of the DA reaction for reversible cross-linking was made by Stevens et al. in 1979. Pendant maleimide groups were installed on commercially available polystyrene, and the resulting polymer was cross-linked in 1,2-dichloroethane using difurfuryl adipate as the coupling agent (Figure 1.12). The effects of cross-linking were observed by way of gelation of the solution, which occurred within 15 minutes at 80°C. Confirmation of the DA reaction was made using IR spectroscopy, noted by a distinct broadening in the carbonyl absorptions at 1705 cm^{-1} and 1765 cm^{-1}. The cross-linked products were not isolated, thus no rheological data was reported. However, this study did serve to demonstrate the viability of DA chemistry as a potential route to reversible polymer cross-linking.

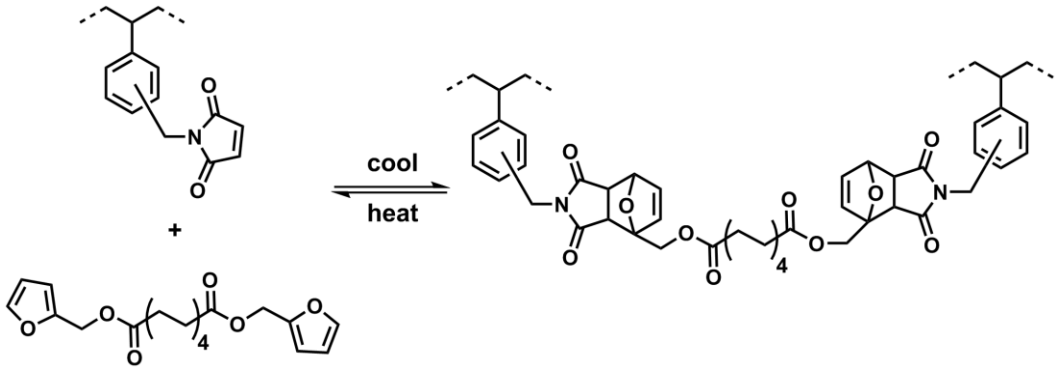

Figure 1.12. Reversible cross-linking of maleimide-substituted polystyrene.

More than ten years later, interest in this system was piqued by Wudl and co-workers, who prepared reversible, cross-linked polymers using multi-valent maleimides and furans.[61] In their investigation, a tetrapodal furan and tripodal maleimide were coupled via DA cycloaddition to form tough, cross-linked polymers that could be reversibly melted and solidified (Figure 1.13). Solutions of the two monomers in DCM were placed in glass molds and heated gently under reduced pressure to effect removal of the solvent and to trigger polymerization. After breaking the glass molds, tensile and compression strength and moduli were measured on the resulting monoliths, and found to compare favourably to typical epoxy resins. The practicality of this phenomenon was then demonstrated by repeated restoration of a fractured polymer via multiple heating and cooling cycles. A novel method of inducing and repairing cracks in the materials was used to quantify healing efficiency. By ensuring close alignment of the two newly exposed surfaces during the repair, the polymers were able to recover more than 80% of their original strength. Reversibility of the chemistry was verified using ^{13}C NMR spectroscopy, comparing diagnostic peaks in the furan rings to those of the vinyl protons in the newly formed norbornyl ring system. Temperature modulated DSC was also used to distinguish reversible and irreversible thermal events, and again showed evidence for the retro-DA reaction. A degree of polymerization of only 60 – 70% was achieved over a period of 5 days at room temperature, although this increased to 95 ± 5% within 3 hours when the temperature was increased to 75°C.

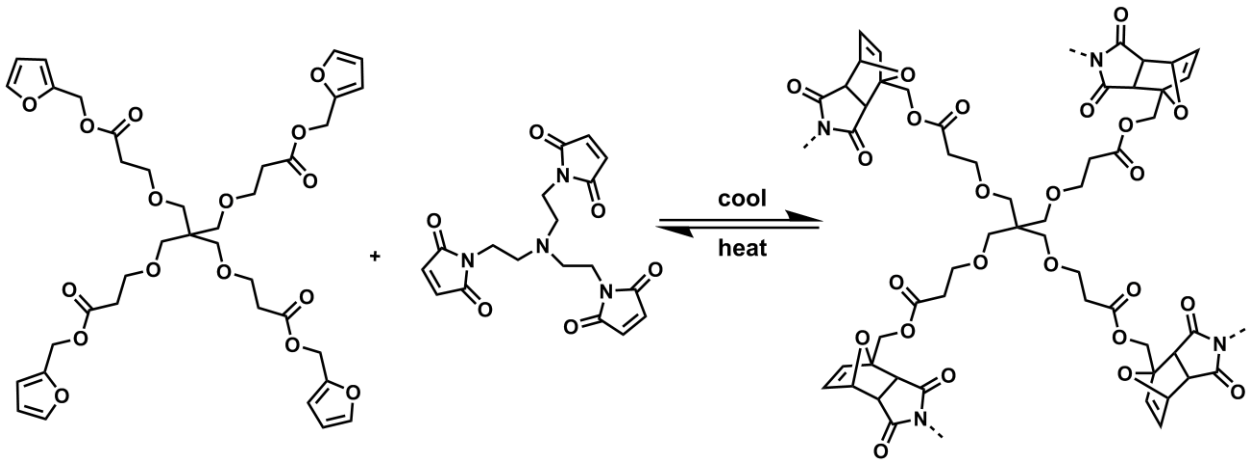

Figure 1.13. Preparation of cross-linked reversible polymer by Diels Alder chemistry.

Further exploration by this group using linear bismaleimides expanded their library of remendable polymeric materials (Figure 1.14).[62] The use of linear bismaleimides provided the advantage of increased solubility in the tetrapodal furan monomer, allowing for polymerizations to be conducted in the neat state. This was a significant development, as the elimination of solvent during synthesis and processing bears considerable financial and environmental advantages. Furthermore, DA coupling of ditopic monomers at lower concentrations increases the tendency for formation of macrocyclic oligomers, rather than linear polymers, and this would compromise the mechanical integrity of the final materials.[89,105] Despite this advantage, mechanical properties of the polymers were found to be somewhat inferior to the highly cross-linked networks prepared earlier,[61] although this was believed to be dependent on the chemistry of the spacer group used in the bismaleimides. A clear distinction could be observed in polymer physical properties when a short, branched alkyl chain was used as compared with a flexible ethylenedioxy spacer in the bismaleimide. In the former case, Young's modulus and compression strength were found to be only slightly lower than the cross-linked materials made in their earlier studies, within the realm of commercial epoxy resins. However, when the more flexible

ethylenedioxy spacer was used, a much more malleable resin was produced. Despite this finding, it was noted that the rheological characteristics of this material were still significantly better than the values reported for silicon-based DA polymers.[49,62] It was also pointed out that these materials exhibited identical healing efficiency characteristics to those prepared earlier, as the cracked polymers could be repaired multiple times.

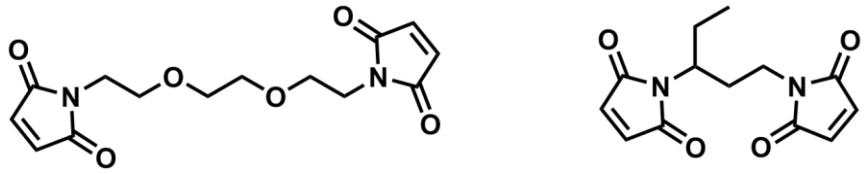

Figure 1.14. Linear bismaleimides coupled with the tetrapodal furan shown in Figure 1.13.

1.3.2.8 Dicyclopentadiene Systems

The DA reaction has been given significant attention in self-healing polymer studies, owing to the thermal equilibrium that exists between monomer and polymer, and to the relative ease of synthesis of the starting materials. However, synthesis of both a diene and dienophile would add cost and complexity to a commercially viable system, and this would be detrimental from both environmental and financial perspectives. Furthermore, homogeneity of the monomer mixtures is dependent on their respective solubilities in one another, which may place limitations on the choice of monomers to be combined, and this in turn would limit the design space of the polymers that might be investigated. Wudl and co-workers addressed these issues by developing a system based on cyclopentadiene (CPD), a single component capable of acting as both diene and dienophile.[102] Two different macrocyclic monomers were prepared, linked by a fused dicyclopentadiene (DCPD) ring system. These two monomers were differentiated by the diol tethering unit joining the CPDs, but could both be opened into linear α,ω-bis(cyclopentadienes)

upon heating. The liberated CPD moieties were then available for intermolecular DA coupling and formation of extended polymer chains when cooled back to room temperature. Additionally, the norbornene double bond in the coupled DCPD could be re-introduced as a dienophile, potentially leading to highly cross-linked materials based on trimeric architectures (Figure 1.15). Indeed, heating and cooling of these monomers resulted in hard, transparent, colorless materials, capable of undergoing multiple repair cycles. Interestingly, the longer diol unit, having an added ether linkage, afforded a stronger, stiffer and more brittle material than its alkyl counterpart, and this was attributed to the propensity for macrocyclic oligomer formation by the shorter monomer. Although neither of the materials was as strong as the DA polymers developed earlier by this group, this novel strategy affords the opportunity to prepare materials with tunable mechanical properties that are able to undergo multiple repair cycles.

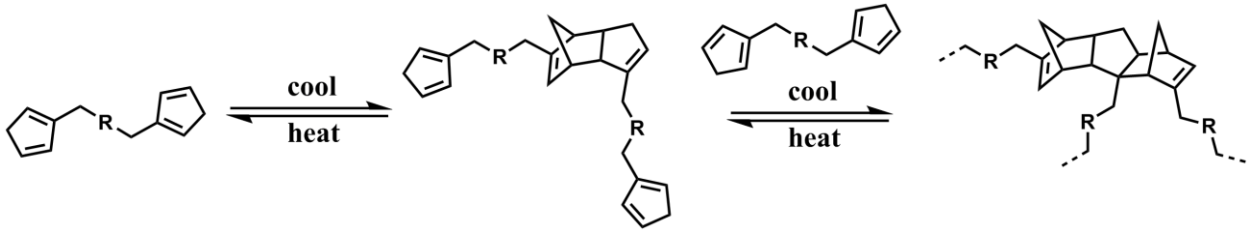

Figure 1.15. Reversible mendomers based on dicyclopentadiene monomers.

1.3.2.9 Reversible Epoxy Resins

Much of the work in the field of self-healing polymers cites the qualities of toughness, flexibility and strength possessed by epoxy resins as the metric for desired rheological properties. Although the curing of an epoxy resin is an irreversible process, Tian et al introduced a measure of reversibility to this system by preparing a base molecule containing two epoxide groups and a single furan group.[106] Coupling with a bismaleimide afforded reversible DA adducts within a

cross-linked epoxy network. Thermal reversibility was confirmed by ^{1}H NMR spectroscopy and Differential Scanning Calorimetry (DSC) by cycling the DA and retro-DA reactions up to four times. The resulting resins exhibited mechanical properties similar to commercial thermosetting epoxies, while maintaining the processable melt viscosity of a thermoplastic resin. Furthermore, cured films prepared with these reversible epoxy resins could undergo crack repair, although in this case, the remendability was only demonstrated on a visual basis. Nevertheless, incorporation of reversible DA chemistry into curable epoxy networks has been shown to be a highly effective means for leveraging the advantages of both of these concepts.

1.3.2.10 Reversible Dendrimers

Dendrimers are a unique class of macromolecules that have been studied extensively for several decades.[107-109] Their highly ordered, branched architectures engender physical characteristics that clearly distinguish them from conventional linear and branched polymers. Most notably, their exceptionally low polydispersities and low melt viscosities make them ideally suited for applications in the biomedical and numerous other fields of science.[110-112] A wide array of chemistries and synthetic methodologies have been conceived and developed, enabling the production of multi-generation dendrimers with highly specific functionalities and performance characteristics. The multi-step nature of dendrimer synthesis limits the synthetic options, and only highly efficient reactions are used in their production. To this end, the group of "click" reactions, identified by Sharpless in 2001,[113] are commonly chosen. The DA reaction falls into this class, as it can be executed in the neat state, and typically affords high yields while exhibiting atom economy. McElhanon and co-workers have exploited these attributes, as they coupled a bismaleimide central linker to furan-bearing dendrons in producing multi-generation, reversible

dendrimers (Figure 1.16).[114] Reversibility between dendrimer formation and collapse was confirmed using gel permeation chromatography (GPC), as the sharp peaks characteristic of dendrimers were used to distinguish each generation as it was formed or disassembled. To date, the potential for reversibility has not been heavily exploited in dendrimer research, and the DA reaction has largely been used only in a synthetic capacity. Nevertheless, it has emerged as a viable means to afford thermal reversibility to these exciting materials.

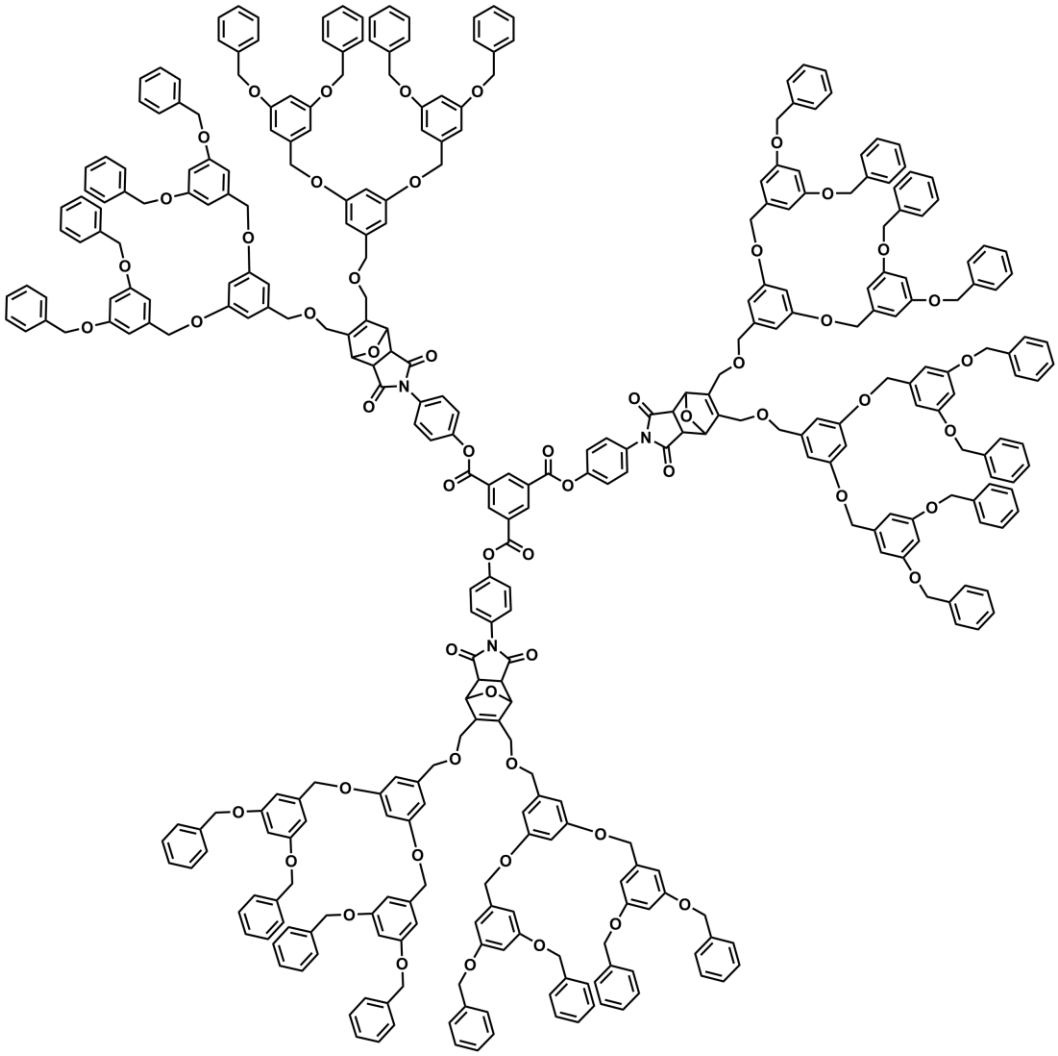

Figure 1.16. G-3 dendrimer containing cleavable DA linkage. [114]

1.3.2.11 Decoration of Existing Polymer Backbones

Decoration of polymer backbones with functional groups has been explored extensively in many different fields of polymer chemistry. A wide variety of pendant functional groups can be installed on linear polymer backbones such that permanent cross-links can be formed after processing has been completed references.[115-117] The report by Stevens et al. described above imparts reversibility to this concept by coupling ditopic furan monomers to pendant maleimide adducts bound to a polystyrene backbone.[118] Zhang et al inverted this method by generating pendant furan moieties on 1,4-polyketones, and then coupling them with ditopic maleimides.[56] Synthetic transformations were achieved using the relatively mild conditions of a Paal-Knorr reaction, in which 1,4-dicarbonyl groups in the polyketones were coupled with a primary amine. Specifically, furfurylamine was condensed with the dicarbonyl units in low molecular weight polyketones to afford pyrrolediyl units having pendant furan groups. (Scheme 1.2) A bisphenyl based bismaleimide was then used as a cross-linking agent to afford a thermally healable epoxy resin. Reversibility was demonstrated using FTIR spectroscopy, noted by the changing intensity of the diagnostic C-O-C absorption peak at 1182 cm^{-1}, as the mixture was heated (150°C) and cooled (50°C). The ability to cycle the DA-retroDA-DA reactions was then demonstrated in the solid state, and repeated four times to show the reworkability of the system. Cycling of the DA reaction was also demonstrated using dynamic mechanical analysis (DMA), which was used to quantify the mechanical strength of molded bars made with the polyketone-furans. Dynamic mechanical properties were found to be dependent on the maleimide/furan molar ratio, reflected in the increased glass transition temperatures observed at higher maleimide contents. This was considered to be a direct result of the degree of cross-linking. Mechanical strength and modulus of these reversible polymers were found to be on the order of typical thermosetting resins, about

40 – 100 MPa and 4 GPa, respectively. Healing efficiencies of 100% were reported, although in this case healing was measured by grinding the entire sample of solidified resin into a powder and re-molding a fresh sample for a repeat mechanical analysis measurement. Nonetheless, this represents a working example of the use of a reversible coupling reaction to enable processing of a highly cross-linked material.

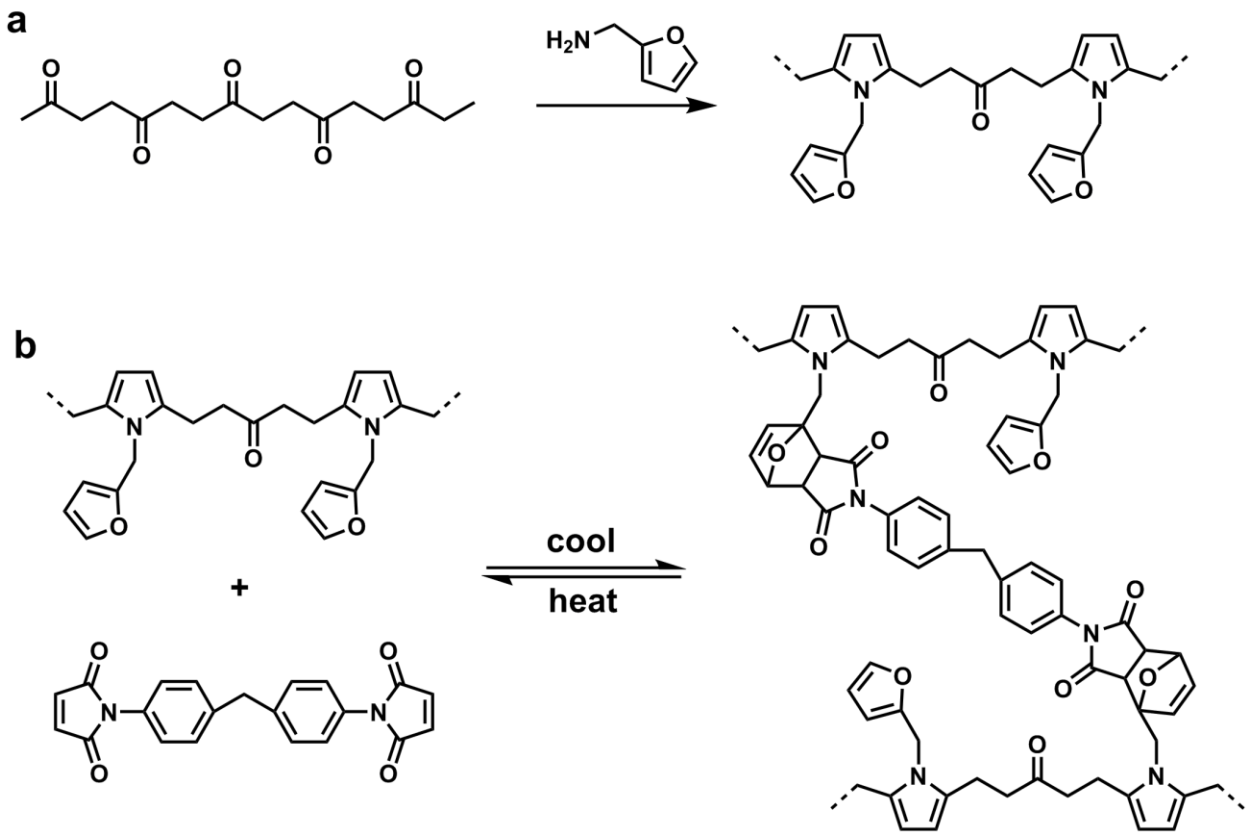

Scheme 1.2. Reversible cross-linking using pendant furan moieties: a) Paal-Knorr reaction between 1,4-polyketones and furfurylamine; b) reversible cross-linking of polyketone-furan with bis-maleimide.

1.3.3 Characterization of Reversible Polymers

Many characterization techniques have been used in the study of reversible DA polymers.[119] The properties of both the monomers and polymers are of importance, in terms of chemical makeup in the former case, and physical properties in the latter. Conventional methods such as NMR and IR spectroscopy are excellent tools for structure elucidation, but can also be used to confirm the occurrence and reversibility of polymerization. Confirmation of reversibility is of central importance in the study of reversible polymers, and these techniques are well-suited for this purpose, as they are able to clearly distinguish monomer from polymer. Thermal methods such as DSC are also important tools in this regard, as they account for thermal events that occur as the equilibrium shifts from monomer to polymer. The healing efficiency of reversible polymers is a critical parameter for many of the studies conducted in this field, and it can be determined in a number of ways, although the essence of the analysis is simply the measurement of resistance to fracture of a material before and after healing. This requires a means to subject the material to controlled fracture, followed by exact realignment of the two fractured pieces with minimal force used to assist in their repair. Resistance to mechanical failure before and after the imposed fracture can then be compared, and this is often accomplished using DMA. Very little has been reported with respect to the molecular weights of reversible DA polymers, as the majority of the reports are based on cross-linked materials. Complications also arise when linear polymers are being considered, as they have the potential for formation of macrocyclic chains that would significantly confound the determination of molecular weight.

1.3.3.1 Spectroscopic Methods

NMR spectroscopy has been used extensively for both structure elucidation and reversibility confirmation by way of the diagnostic peaks distinguishing the maleimide/furan monomers from the fused ring system produced by the polymerization.[38,103,104,106] In ^{1}H NMR, significant changes can be observed in the downfield portion of the spectrum as polymerization occurs. The vinyl protons on the furan ring produce signals at 7.2, 6.6, and 7.8 ppm for the 1, 2, and 3 substituents respectively. A sharp singlet can also be observed at 7.0 ppm, ascribed to the two vinyl maleimide protons (Figure 1.17a). As the two rings merge in the DA reaction, several new signals arise, although these are largely obscured by existing peaks. The new norbornyl ring system that has been formed gives rise to a doublet of doublets, centred at 6.6 ppm (Figure 1.17b). While formation of this new multiplet is plainly visible, quantification of peak area is difficult, due to the overlap with the existing peak in that vicinity. A particularly useful diagnostic signal appears at 5.2 ppm, assigned to the norbornyl bridgehead proton. This peak is generally in an unobscured region of the spectrum, and therefore affords an opportunity to not only confirm the occurrence of polymerization, but also to quantify the degree of polymerization (DP). Comparing the signals for the bridgehead and furan protons, DP can be calculated using the formula $i_{5.2}/(i_{5.2} + i_{7.8})\times 100\%$, where i_x is the integral of the NMR peak at x ppm. In Figure 1.17c, the restoration of the spectrum from Figure 1.17a can be observed as the monomers are decoupled via the retro-DA reaction. Researchers have used solid state ^{13}C NMR spectroscopy in a similar capacity, as they were able to highlight the appearance and disappearance of signals attributed to the furan ring as the material alternated between its monomeric and polymeric forms.[61,62] While this did serve to demonstrate the reversibility of the reaction, it was not quantitative, thus was not used in establishing DP. Similarly, IR spectroscopy can be used to distinguish between monomer and

polymer, although this is also mostly done in a qualitative sense.[39,120] UV/Vis spectroscopy has been used both qualitatively and quantitatively, as the absorption maximum can be monitored during the transformation from monomer to polymer. In this manner, Imai et al determined the degree of cross-linking between maleimide- and furan-modified poly(2-methyl-2-oxazoline)s by monitoring the absorbance of neat polymer films at 296 nm.[120]

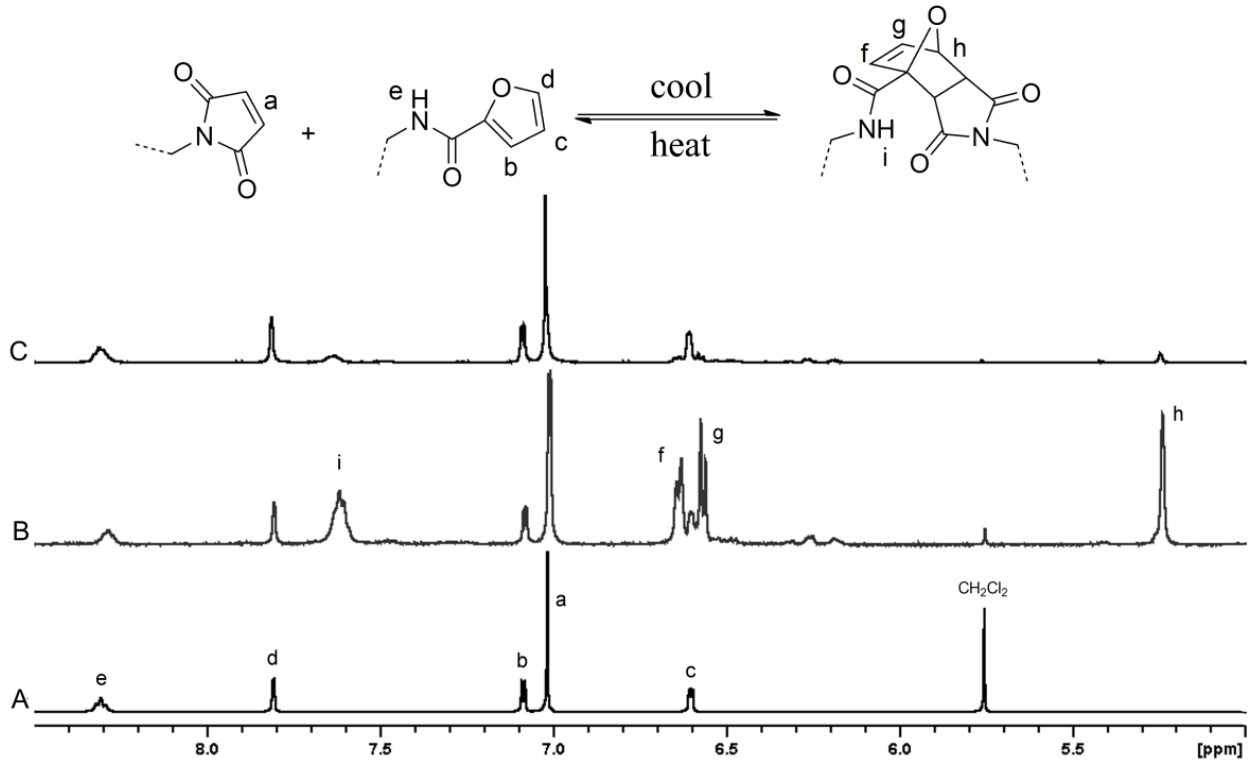

Figure 1.17. DA and retro-DA reactions confirmed by ^{1}H NMR spectroscopy: A) bismaleimide (M) + bisfuran (F); B) maleimide-furan polymer (MF); C) restoration of the two monomers M and F.

1.3.3.2 Differential Scanning Calorimetry

Differential Scanning Calorimetry (DSC) provides an excellent means to verify the reversibility of a DA polymerization.[121-123] Based on the scenario depicted in Figure 1.2a, two distinct small molecules would be present prior to any heating taking place, thus two transitions would be expected during the first heating cycle. Cooling of the molten monomers would then initiate the DA reaction, leading to polymer formation. An endothermic transition may be expected in this cycle, although this may not necessarily be the case, due to the potentially slow polymerization times relative to the cooling cycle time. Of greater interest is the change that occurs during the second heating cycle of the sample. Multiple transitions can be observed, as the material being heated is now polymeric in nature. Depending on the nature of the polymer, a glass transition or melting peak may be observed as the mobility of the polymer chains is increased. Further heating of the sample results in collapse of the polymer to its monomeric components via the retro-DA reaction, and this can be seen as a broad endothermic peak centered at approximately 130°C. The changing nature of these DSC curves can be observed multiple times as the material is cycled from monomer to polymer repeatedly.

1.3.3.3 Dynamic Mechanical Analysis

The most commonly used method for measuring the physical properties of viscoelastic materials is dynamic mechanical analysis (DMA).[124] In principle, the technique constitutes an accurate measurement of the deformation (strain) of a material in response to an applied force (stress). Alternatively, stress can be measured in response to an applied strain, but in either case, the method relies on the assumption that purely elastic materials deform instantaneously under an applied stimulus, while purely viscous materials exhibit a delay in their response. Application of

the stimulus in an oscillatory manner can therefore provide information about both the viscous and elastic rheological components of a material, and this is what distinguishes DMA from other conventional mechanical testing methods.[124] Depending on the nature of the material, the stress (or strain) can be applied in the form of tension, compression, bending, or shear, but in all cases, a relationship between stress and strain can be derived that can teach a great deal about the nature of the material's physical characteristics. In the simplest model, the slope of the line in the resulting stress-strain curve is related to the stiffness, or modulus, of the material. However, more detailed analysis of both the storage (elastic) and loss (viscous) components of the modulus can reveal information about the ability of the material to absorb or dissipate mechanical energy, revealing whether it exhibits solid-like or liquid-like behavior. This can be accomplished by varying the frequency, time, or temperature of the measurement, thus determining the influence of these variables on the properties of the material. Despite the advantages of applying a dynamic stimulus, testing can also be done in static mode, wherein the sample is placed under constant stress or strain, and this affords additional information about the 'creep' or 'relaxation' behavior of the material, respectively. For self-healing materials, the three-point bending flexural test is perhaps the most commonly used technique.[125] Flexural strength and modulus can be determined by measuring the resistance to bending or fracture of a test specimen, as shown schematically in Figure 1.18. Again, this can be done in static or dynamic mode, but in either case, healing efficiency can be calculated as the resistance of the material to cracking before and after it has been compromised.

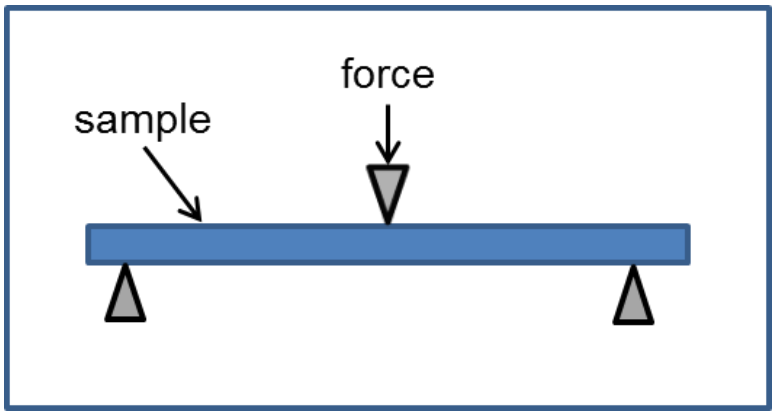

Figure 1.18. Schematic depiction of three-point bending flexural test.

1.3.3.4 Nanoindentation

The inherent brittleness of the polymers prepared in this study precluded the ability to prepare samples for conventional DMA analysis, thus rheology of the films was determined using nanoindentation. The field of nanoindentation has grown considerably over the past decade, and is now commonly used to determine the rheological characteristics of a wide variety of materials.[126-129] The basis of this method arose from macro-indentation testing, in which a hard tip of known geometry is pressed into a solid material.[130,131] Visual determination of the exact area made by the resulting indentat then allows for calculation of the hardness of the material simply expressed as the load divided by the contact area. This remains an effective tool for materials characterization, however, the increasing prevalence of nanostructured materials has given rise to a need for more localized indentation measurements, such that micro- and nano-scale domains can be studied independently. As a result, the size of indentation tips has become smaller by orders of magnitude, comparable in size to the tip used in an atomic force microscope (AFM). Traditional optical methods are therefore no longer sufficient for the determination of indent dimensions on this scale. Instead, modern instrumentation is based on depth sensing indentation (DSI), in which the load and displacement of the indenter tip are measured very

accurately as the load is applied to the sample. Typically, this is achieved by means of an electromagnetic coil or a piezoelectric transducer element, which controls the force and position of the indenter tip. The resulting dynamic measurements enable precise monitoring of the rate of change of both load and displacement, allowing for calculation of the modulus of the material.[129] As a result of the high level of accuracy and precision of these instruments, other factors, such as the compliance of the instrument hardware, and the environmental conditions during the test, must be given careful consideration. The size and shape of the nanoindenter tip also becomes of critical importance, as it must be able to generate reproducible penetration shapes and depths when dealing in such small dimensions. To this end, the Berkovich tip is the most widely used in nanoindentation measurements. It is similar to the four-sided Vickers tip commonly used for macro-indentations, but has only three facets, thus ensuring the tip always comes to a sharp point. Due to its small size, the exact area of the tip must be determined by a series of calibration indents made into a known substance such as quartz or sapphire. The accuracy of the resulting area function is critical in enabling calculation of the hardness of the material, as the maximum load over the area of penetration (Equation 1-1).[132]

$$H = \frac{P_{max}}{A} \qquad (1\text{-}1)$$

In all nanoindenters, the principle of operation remains the same as described for macro-indentation above, as the tip is driven into the sample to produce an indentation. However, both penetration and withdrawal are achieved under very well controlled conditions of rate and load. Continuous monitoring of load and displacement data then generates a load-unload curve, as shown in Figure 1.19. After reaching the selected maximum load (P_{max}), the tip is extracted until returning to zero load. A plot of load vs displacement of the tip during indentation can be recorded, and the stiffness (S) and reduced modulus (E_r) of the material calculated from the

unloading curve (Figure 1.19). Specifically, the slope of the unloading curve at maximum load (dP/dh) represents the contact stiffness of the material, and this can be used to derive E_r using equation 1-2 below.[132]

$$S = \frac{dP}{dh} = \frac{2\sqrt{A}}{\sqrt{\pi}} E_r \qquad (1\text{-}2)$$

In a rigid solid, very little elastic recovery is experienced, and the impression left in the sample is equal to the maximum area of contact, which can be used to calculate the hardness of the material. However, elastic recovery is experienced to some degree in all materials, and the indent remaining will be somewhat smaller than the maximum area of contact. This results in a non-linear unloading curve (Figure 1.19), which means that only the initial portion of this curve can be used to determine the elastic modulus of the material. To this end, a power law equation is used to describe the unloading portion of the curve, with the differential of this equation affording the initial unloading slope (Equation 1-3).[132]

$$P = A(h - h_f)^m \qquad (1\text{-}3)$$

where $(h - h_f)$ is the difference between the maximum depth of penetration and the final depth after tip withdrawal, while A and m are constants. On this basis, nanoindentation experiments can be used to determine both the resistance to penetration of a material (hardness), and its resistance to distortion or stiffness (reduced modulus), which together provide a measure of overall mechanical integrity.

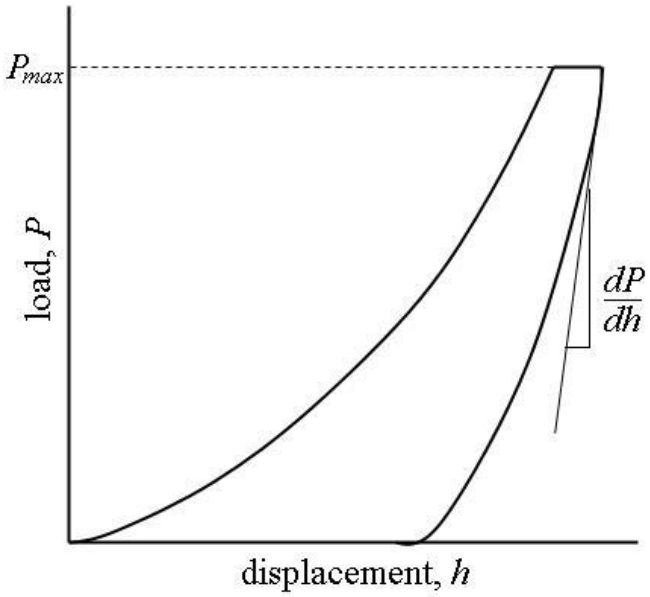

Figure 1.19. Typical load-displacement curve derived from a nanoindentation experiment.

1.3.3.5 Nanoindentation Instrumentation

Several different manufacturers offer instruments capable of performing nanoindentation. In its essence, a nanoindenter must be capable of very accurately controlling the position and force applied to an indenter tip while measuring its resulting displacement into a solid material. Measurement of applied load and displacement can be accomplished in several different ways, and that is what sets each of the available instruments apart. Transducers can be actuated by electromagnetic or electrostatic forces, or using springs, such as a cantilevered beam. Each of these methods has advantages and disadvantages, with the choice of instrument depending on the materials being studied and the information being sought. In our research, we used a Hysitron Triboscan®, available from Hysitron Inc in Minneapolis, MN. Two orthogonal three-plate transducer assemblies are used to at once control the applied force and measure the resulting displacement of the indenter tip (Figure 1.20). A bias voltage, applied to the bottom plate of the horizontal capacitor assembly, creates an electrostatic attraction between the bottom and center plates, resulting in a downward deflection of the center plate, to which the indenter tip is attached. This same mechanism can be used to dynamically control the vertical plate assemblies, driving the tip in the x-y plane, if necessary. In this capacity, the TriboIndenter® can also be used to perform Scanning Probe Microscopy (SPM) imaging, enabling topographical mapping of the surface before and after nanoindentation.

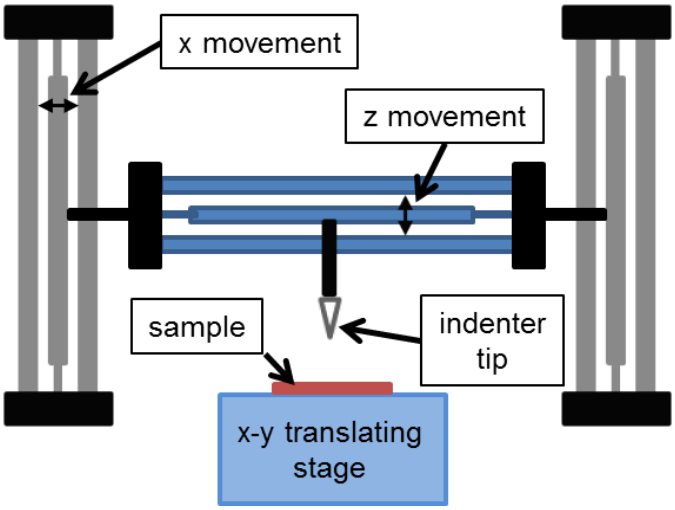

Figure 1.20. Schematic representation of the Hysitron Triboindenter®.

1.4 References

(1) Iijima, S. *Nature* **1991**, *354*, 56.

(2) Collins, P. G.; Avouris, P. *Scientific American* **2000**, *283*, 62.

(3) Harris, P. J. F. *Int. Mater. Rev.* **2004**, *49*, 31.

(4) Berger, C.; Poncharal, P.; Yi, Y.; de Heer, W. *Journal of Nanoscience and Nanotechnology* **2003**, *3*, 171.

(5) Poncharal, P.; Berger, C.; Yi, Y.; Wang, Z. L.; de Heer, W. A. *J. Phys. Chem. B* **2002**, *106*, 12104.

(6) Ajayan, P. M. *Chem. Rev.* **1999**, *99*, 1787.

(7) Freitag, M.; Martin, Y.; Misewich, J. A.; Martel, R.; Avouris, P. H. *Nano Lett.* **2003**, *3*, 1067.

(8) Tans, S. J.; Verschueren, A. R. M.; Dekker, C. *Nature* **1998**, *393*, 49.

(9) Weitz, R. T.; Zschieschang, U.; Effenberger, F.; Klauk, H.; Burghard, M.; Kern, K. *Nano Lett.* **2007**, *7*, 22.

(10) Kong, J.; Franklin, N. R.; Zhou, C. W.; Chapline, M. G.; Peng, S.; Cho, K. J.; Dai, H. J. *Science* **2000**, *287*, 622.

(11) Li, J.; Hu, L.; Wang, L.; Zhou, Y.; Gruner, G.; Marks, T. J. *Nano Lett.* **2006**, *6*, 2472.

(12) Coleman, J. N.; Khan, U.; Blau, W. J.; Gun'ko, Y. K. *Carbon* **2006**, *44*, 1624.

(13) Dalton, A. B.; Collins, S.; Munoz, E.; Razal, J. M.; Ebron, V. H.; Ferraris, J. P.; Coleman, J. N.; Kim, B. G.; Baughman, R. H. *Nature* **2003**, *423*, 703.

(14) Lau, K. T.; Lu, M.; Liao, K. *Composites Part a-Applied Science and Manufacturing* **2006**, *37*, 1837.

(15) Dyke, C. A.; Tour, J. M. *J. Phys. Chem. A* **2004**, *108*, 11151.

(16) Dyke, C. A.; Tour, J. M. *Chemistry-a European Journal* **2004**, *10*, 813.

(17) Ma, P. C.; Siddiqui, N. A.; Marom, G.; Kim, J. K. *Composites Part a-Applied Science and Manufacturing* **2010**, *41*, 1345.

(18) Clave, G.; Campidelli, S. *Chemical Science* **2011**, *2*, 1887.

(19) Kakade, B. A.; Pillai, V. K. *Appl. Surf. Sci.* **2008**, *254*, 4936.

(20) Martinez-Rubi, Y.; Guan, J.; Lin, S.; Scriver, C.; Sturgeon, R. E.; Simard, B. *Chem. Commun.* **2007**, 5146.

(21) Xiao, Q.; Wang, P. H.; Si, Z. C. *Progress in Chemistry* **2007**, *19*, 101.

(22) Bahun, G. J.; Wang, C.; Adronov, A. *Journal of Polymer Science Part a-Polymer Chemistry* **2006**, *44*, 1941.

(23) Hu, C. Y.; Xu, Y. J.; Duo, S. W.; Zhang, R. F.; Li, M. S. *J. Chin. Chem. Soc.* **2009**, *56*, 234.

(24) Lemek, T.; Mazurkiewicz, J.; Stobinski, L.; Lin, H. M.; Tomasik, P. *Journal of Nanoscience and Nanotechnology* **2007**, *7*, 3081.

(25) Ma, A. S.; Lu, J.; Yang, S. H.; Ng, K. M. *J. Cluster Sci.* **2006**, *17*, 599.

(26) Meuer, S.; Braun, L.; Zentel, R. *Macromol. Chem. Phys.* **2009**, *210*, 1528.

(27) Ogunro, O. O.; Wang, X. Q. *New J. Chem.* **2010**, *34*, 1084.

(28) Li, H. M.; Cheng, F. O.; Duft, A. M.; Adronov, A. *J. Am. Chem. Soc.* **2005**, *127*, 14518.

(29) Bogwe, R. *Assembly Automation* **2008**, *28*, 211.

(30) Huie, J. C. *Smart Materials & Structures* **2003**, *12*, 264.

(31) Ahn, D. U.; Wang, Z.; Campbell, I. P.; Stoykovich, M. P.; Ding, Y. F. *Polymer* **2012**, *53*, 4187.

(32) Kim, Y.; Park, S.; Seo, Y. S.; Lee, N.; Seo, Y.; Han, S. J. *J. Korean Phys. Soc.* **2009**, *54*, 749.

(33) Li, X.; Han, Y. C.; An, L. J. *Appl. Surf. Sci.* **2004**, *230*, 115.

(34) Mayo, J. D.; Behal, S.; Adronov, A. *Journal of Polymer Science Part a-Polymer Chemistry* **2009**, *47*, 450.

(35) Costa, S.; Borowiak-Palen, E.; Kruszynska, M.; Bachmatiuk, A.; Kalenczuk, R. J. *Materials Science-Poland* **2008**, *26*, 433.

(36) Keszler, A. M.; Nemes, L.; Ahmad, S. R.; Fang, X. *Journal of Optoelectronics and Advanced Materials* **2004**, *6*, 1269.

(37) Bergman, S. D.; Wudl, F. *J. Mater. Chem.* **2008**, *18*, 41.

(38) Gousse, C.; Gandini, A.; Hodge, P. *Macromolecules* **1998**, *31*, 314.

(39) Laita, H.; Boufi, S.; Gandini, A. *Eur. Polym. J.* **1997**, *33*, 1203.

(40) Liu, Y. L.; Chuo, T. W. *Polymer Chemistry* **2013**, *4*, 2194.

(41) Murphy, E. B.; Wudl, F. *Prog. Polym. Sci.*, *35*, 223.

(42) Wool, R. P. *Soft Matter* **2008**, *4*, 400.

(43) Wu, D. Y.; Meure, S.; Solomon, D. *Prog. Polym. Sci.* **2008**, *33*, 479.

(44) Bosman, A. W.; Folmer, B. J. B.; Hirschberg, J.; Keizer, H. M.; Sijbesma, R. P.; Meijer, E. W. *Abstr. Pap. Am. Chem. S.* **2002**, *223*, D22.

(45) Cordier, P.; Tournilhac, F.; Soulie-Ziakovic, C.; Leibler, L. *Nature* **2008**, *451*, 977.

(46) Gotsmann, B.; Duerig, U.; Frommer, J.; Hawker, C. J. *Adv. Funct. Mater.* **2006**, *16*, 1499.

(47) Liu, Y. L.; Hsieh, C. Y.; Chen, Y. W. *Polymer* **2006**, *47*, 2581.

(48) Luo, X. F.; Lauber, K. E.; Mather, P. T. *Polymer* **2010**, *51*, 1169.

(49) McElhanon, J. R.; Russick, E. M.; Wheeler, D. R.; Loy, D. A.; Aubert, J. H. *J. Appl. Polym. Sci.* **2002**, *85*, 1496.

(50) van Gemert, G. M. L.; Peeters, J. W.; Sontjens, S. H. M.; Janssen, H. M.; Bosman, A. W. *Macromol. Chem. Phys.* **2012**, *213*, 234.

(51) Paine, A. J., Hamer, G.K., Tripp, C.P., Bareman, J.P., Mayer, F.M., Sacripante, G.G., Xerox Corporation, 5,844,020, December 1, 1998.

(52) Meinhardt, M. B., King, C.R., Xerox Corporation, 6,042,227, March 28, 2000.

(53) White, S. R.; Sottos, N. R.; Geubelle, P. H.; Moore, J. S.; Kessler, M. R.; Sriram, S. R.; Brown, E. N.; Viswanathan, S. *Nature* **2001**, *409*, 794.

(54) Wietor, J.-L.; Sijbesma, R. P. *Angewandte Chemie-International Edition* **2008**, *47*, 8161.

(55) Yuan, Y. C.; Yin, T.; Rong, M. Z.; Zhang, M. Q. *Express Polym. Lett.* **2008**, *2*, 238.

(56) Zhang, Y.; Broekhuis, A. A.; Picchioni, F. *Macromolecules* **2009**, *42*, 1906.

(57) Rochman, A.; Frick, A.; Martin, P. *Polym. Eng. Sci.* **2012**, *52*, 2114.

(58) Madbouly, S. A.; Ougizawa, T. *Journal of Macromolecular Science-Physics* **2004**, *B43*, 471.

(59) DeRosa, R.; Telfeyan, E.; Mayes, J. S. *J. Thermoplast. Compos. Mater.* **2005**, *18*, 219.

(60) Pickering, S. J. *Composites Part a-Applied Science and Manufacturing* **2006**, *37*, 1206.

(61) Chen, X. X.; Dam, M. A.; Ono, K.; Mal, A.; Shen, H. B.; Nutt, S. R.; Sheran, K.; Wudl, F. *Science* **2002**, *295*, 1698.

(62) Chen, X. X.; Wudl, F.; Mal, A. K.; Shen, H. B.; Nutt, S. R. *Macromolecules* **2003**, *36*, 1802.

(63) Dry, C.; Sottos, N. R. *Passive Smart Self-repair in Polymer Matrix Composite-materials*, 1993; Vol. 1916.

(64) Dry, C. *Compos. Struct.* **1996**, *35*, 263.

(65) Dry, C. *Improvement in reinforcing bond strength in reinforced concrete with self repairing chemical adhesives*, 1997; Vol. 3043.

(66) Cho, S. H.; Andersson, H. M.; White, S. R.; Sottos, N. R.; Braun, P. V. *Adv. Mater.* **2006**, *18*, 997.

(67) Cho, S. H.; White, S. R.; Braun, P. V. *Chem. Mater.* **2012**, *24*, 4209.

(68) Caruso, M. M.; Delafuente, D. A.; Ho, V.; Sottos, N. R.; Moore, J. S.; White, S. R. *Macromolecules* **2007**, *40*, 8830.

(69) Lin, C. B.; Lee, S. B.; Liu, K. S. *Polym. Eng. Sci.* **1990**, *30*, 1399.

(70) Wu, T.; Lee, S. *Journal of Polymer Science Part B-Polymer Physics* **1994**, *32*, 2055.

(71) Chen, Y. L.; Kushner, A. M.; Williams, G. A.; Guan, Z. B. *Nature Chemistry* **2012**, *4*, 467.

(72) Plaisted, T. A.; Nemat-Nasser, S. *Acta Mater.* **2007**, *55*, 5684.

(73) White, S. R.; Caruso, M. M.; Moore, J. S. *MRS Bull.* **2008**, *33*, 766.

(74) Imato, K.; Nishihara, M.; Kanehara, T.; Amamoto, Y.; Takahara, A.; Otsuka, H. *Angewandte Chemie-International Edition* **2012**, *51*, 1138.

(75) Bejan, E. V.; Font-Sanchis, E.; Scaiano, J. C. *Org. Lett.* **2001**, *3*, 4059.

(76) Scaiano, J. C.; Martin, A.; Yap, G. P. A.; Ingold, K. U. *Org. Lett.* **2000**, *2*, 899.

(77) Beijer, F. H.; Sijbesma, R. P.; Kooijman, H.; Spek, A. L.; Meijer, E. W. *J. Am. Chem. Soc.* **1998**, *120*, 6761.

(78) Lange, R. F. M.; Van Gurp, M.; Meijer, E. W. *Journal of Polymer Science Part a-Polymer Chemistry* **1999**, *37*, 3657.

(79) Altintas, O.; Schulze-Suenninghausen, D.; Luy, B.; Barner-Kowollik, C. *Acs Macro Letters* **2013**, *2*, 211.

(80) Bosman, A. W.; Brunsveld, L.; Folmer, B. J. B.; Sijbesma, R. P.; Meijer, E. W. *Macromolecular Symposia* **2003**, *201*, 143.

(81) Brunsveld, L.; Folmer, B. J. B.; Meijer, E. W.; Sijbesma, R. P. *Chem. Rev.* **2001**, *101*, 4071.

(82) Khor, S. P.; Varley, R. J.; Shen, S. Z.; Yuan, Q. *J. Appl. Polym. Sci.* **2013**, *128*, 3743.

(83) Ni, Y. P.; Becquart, F.; Chen, J. D.; Taha, M. *Macromolecules* **2013**, *46*, 1066.

(84) Zaltariov, M. F.; Cazacu, M.; Shova, S.; Vlad, A.; Stoica, I.; Hamciuc, E. *Journal of Polymer Science Part a-Polymer Chemistry* **2012**, *50*, 3775.

(85) Chiper, M.; Hoogenboom, R.; Schubert, U. S. *Macromol. Rapid Commun.* **2009**, *30*, 565.

(86) Beck, J. B.; Ineman, J. M.; Rowan, S. J. *Macromolecules* **2005**, *38*, 5060.

(87) Chiper, M.; Fournier, D.; Hoogenboom, R.; Schubert, U. S. *Macromol. Rapid Commun.* **2008**, *29*, 1640.

(88) Han, F. S.; Higuchi, M.; Kurth, D. G. *Adv. Mater.* **2007**, *19*, 3928.

(89) Hofmeier, H.; Hoogenboom, R.; Wouters, M. E. L.; Schubert, U. S. *J. Am. Chem. Soc.* **2005**, *127*, 2913.

(90) Hornig, S.; Manners, I.; Newkome, G. R.; Schubert, U. S. *Macromol. Rapid Commun.* **2010**, *31*, 771.

(91) Kumpfer, J. R.; Jin, J. Z.; Rowan, S. J. *J. Mater. Chem.* **2010**, *20*, 145.

(92) Schubert, U. S.; Eschbaumer, C. *Angewandte Chemie-International Edition* **2002**, *41*, 2893.

(93) Schubert, U. S.; Weidl, C. H.; Lehn, J. M. *Des. Monomers Polym.* **1999**, *2*, 1.

(94) Shunmugam, R.; Gabriel, G. J.; Aamer, K. A.; Tew, G. N. *Macromol. Rapid Commun.* **2010**, *31*, 784.

(95) Esteve, A.; Bail, A.; Landa, G.; Dkhissi, A.; Brut, M.; Rouhani, M. D.; Sudor, J.; Gue, A. M. *Chem. Phys.* **2007**, *340*, 12.

(96) Coady, D. J.; Bielawski, C. W. *Macromolecules* **2006**, *39*, 8895.

(97) Kamplain, J. W.; Bielawski, C. W. *Chem. Commun.* **2006**, 1727.

(98) Neilson, B. M.; Tennyson, A. G.; Bielawski, C. W. *J. Phys. Org. Chem.* **2012**, *25*, 531.

(99) Norris, B. C.; Bielawski, C. W. *Macromolecules* **2010**, *43*, 3591.

(100) Montarnal, D.; Capelot, M.; Tournilhac, F.; Leibler, L. *Science*, *334*, 965.

(101) Kwart, H., King, K. *Chem. Rev.* **1968**, *68*, 415.

(102) Murphy, E. B.; Bolanos, E.; Schaffner-Hamann, C.; Wudl, F.; Nutt, S. R.; Auad, M. L. *Macromolecules* **2008**, *41*, 5203.

(103) Boutelle, R. C.; Northrop, B. H. *J. Org. Chem.***2011**, *76*, 7994.

(104) Canadell, J.; Fischer, H.; De With, G.; Van Benthem, R. *Journal of Polymer Science Part a-Polymer Chemistry* **2010**, *48*, 3456.

(105) ten Cate, A. T.; Kooijman, H.; Spek, A. L.; Sijbesma, R. P.; Meijer, E. W. *J. Am. Chem. Soc.* **2004**, *126*, 3801.

(106) Tian, Q.; Yuan, Y. C.; Rong, M. Z.; Zhang, M. Q. *J. Mater. Chem.* **2009**, *19*, 1289.

(107) Bosman, A. W.; Janssen, H. M.; Meijer, E. W. *Chem. Rev.* **1999**, *99*, 1665.

(108) Grayson, S. M.; Frechet, J. M. J. *Chem. Rev.* **2001**, *101*, 3819.

(109) Zeng, F. W.; Zimmerman, S. C. *Chem. Rev.* **1997**, *97*, 1681.

(110) Benhabbour, S. R.; Parrott, M. C.; Gratton, S. E. A.; Adronov, A. *Macromolecules* **2007**, *40*, 5678.

(111) Parrott, M. C.; Marchington, E. B.; Valliant, J. F.; Adronov, A. *J. Am. Chem. Soc.* **2005**, *127*, 12081.

(112) Sevenson, S.; Tomalia, D. A. *Advanced Drug Delivery Reviews* **2012**, *64*, 102.

(113) Kolb, H. C.; Finn, M. G.; Sharpless, K. B. *Angewandte Chemie-International Edition* **2001**, *40*, 2004.

(114) Szalai, M. L.; McGrath, D. V.; Wheeler, D. R.; Zifer, T.; McElhanon, J. R. *Macromolecules* **2007**, *40*, 818.

(115) Antony, P.; De, S. K.; van Duin, M. *Rubber Chem. Technol.* **2001**, *74*, 376.

(116) Chen, J. N.; Yang, G. C.; Zhang, H. Q.; Chen, Z. X. *Reactive & Functional Polymers* **2006**, *66*, 1434.

(117) Hou, H. Y.; Di Vona, M. L.; Knauth, P. *J. Membrane Sci.* **2012**, *423*, 113.

(118) Stevens, M. P.; Jenkins, A. D. *Journal of Polymer Science Part a-Polymer Chemistry* **1979**, *17*, 3675.

(119) Nielsen, C.; Weizman, O.; Nemat-Nasser, S. In *Behavior and Mechanics of Multifunctional Materials and Composites 2010*; Ounaies, Z., Li, J., Eds. 2010; Vol. 7644.

(120) Imai, Y.; Itoh, H.; Naka, K.; Chujo, Y. *Macromolecules* **2000**, *33*, 4343.

(121) Pyda, M.; Wunderlich, B. *Journal of Polymer Science Part B-Polymer Physics* **2000**, *38*, 622.

(122) Ribeiro, M.; Grolier, J. P. E. *J. Therm. Anal. Calorim.* **1999**, *57*, 253.

(123) Song, M. *J. Therm. Anal. Calorim.* **2001**, *63*, 699.

(124) Menard, K. P. *Dynamic Mechanical Analysis, A Practical Introduction*; CRC Press LLC: USA, 1999.

(125) ASTM-D790; Materials, A. S. f. T. a., Ed.; American Society for Testing and Materials: 1996, p 1.

(126) Nai, M. H.; Lim, C. T.; Zeng, K. Y.; Tan, V. B. C. In *Science and Technology of Nanomaterials - ICMAT 2003* 2005; Vol. 23, p 363.

(127) Naimi-Jamal, M. R.; Kaupp, G. *Macromolecular Symposia* **2008**, *274*, 72.

(128) Oliver, W. C.; Pharr, G. M. *MRS Bull.*, *35*, 897.

(129) Pharr, G. M.; Oliver, W. C. *MRS Bull.* **1992**, *17*, 28.

(130) Bucaille, J. L.; Stauss, S.; Felder, E.; Michler, J. *Acta Mater.* **2003**, *51*, 1663.

(131) Tabor, D. *The hardness of metals*; Oxford University Press, 1951.

(132) Oliver, W. C.; Pharr, G. M. *J. Mater. Res.* **1992**, *7*, 1564.

Chapter 2
Phase Separation of Polymer-Functionalized SWNTs within a PMMA/Polystyrene Blend

2.1 Abstract

Phase separation of polystyrene (PS) and poly(methyl methacrylate) (PMMA) blends was used as a means to segregate PS- or PMMA-functionalized single-walled carbon nanotubes (SWNTs) in thin films. Dilute solutions (5 wt% in THF) of 1:1 PS/PMMA blends containing the functionalized nanotubes were spin cast and annealed at 180°C for 12 h. Two different polymer molecular weights were used (Mn = 8,000 or Mn = 22,000), and were of approximately equivalent molecular weight to those attached to the surface of the nanotubes. Nanotube functionalization was accomplished using the Cu(I)-catalyzed [3 + 2] Huisgen cycloaddition, in which alkyne-decorated nanotubes were coupled with azide-terminated polymers, resulting in polymer-SWNT conjugates that were soluble in THF. Characterization of the annealed films by scanning Raman spectroscopy, which utilized the unique Raman fingerprint of carbon nanotubes, enabled accurate mapping of the functionalized SWNTs within the films relative to the two phase-separated polymers. It was found that nanotube localization within the phase separated polymer films was influenced by the type of polymer attached to the nanotube surface, as well as its molecular weight.

This chapter has been reproduced with permission from the Journal of Polymer Science: "Phase Separation of Polymer-Functionalized SWNTs within a PMMA/Polystyrene Blend", Mayo, J.D., Behal, S., and Adronov, A., Journal of Polymer Science Part a – Polymer Chemistry, **2009**, *47*, 450.

2.2 Introduction

2.2.1 Carbon Nanotubes

The unique combination of electrical, mechanical and thermal properties of carbon nanotubes makes them ideally suited for numerous applications in molecular electronics[1] and high performance polymer nanocomposites.[2] Electronically, they can behave as both a conductor, capable of ballistic electron transport,[3,4] or as a semi-conductor, with band gaps being inversely proportional to their diameter.[5] Applications in electronic devices such as field effect transistors,[6-8] chemical sensors,[9] and light emitting diodes (LEDs)[10] have all been envisioned and studied as a result of their exceptional electron transport properties. Mechanically, single-walled carbon nanotubes (SWNTs) possess tensile strengths as high as ~1 TPa, an order of magnitude greater than steel. This exceptional strength, together with their very low densities (1.3-2.5 g/cm^3) and high aspect ratios (>1000), make them ideally suited as nanocomposite reinforcing agents.[11-13]

2.2.1.1 Self-assembly of Carbon Nanotubes

Whether they are to be incorporated into electronic devices, or used in the fabrication of ultra-strong fibers, highly ordered patterning of carbon nanotubes on a micro or nanometer scale is desirable. A number of methods to align nanotubes in defined patterns by controlled growth[14-16] or self-assembly[17-20] have been reported. Along these lines, the use of polymer self-assembly to organize nano-scale structures on substrates has also received recent attention. Lin et al. generated thin films having poly(2-vinylpyridine) (P2VP) domains in a PS matrix using PS-b-P2VP. CdSe nanoparticles stabilized with tri-n-octylphosphine oxide (TOPO) were introduced prior to spin casting, and after annealing could be observed entirely within the P2VP domains

using TEM and grazing incidence small angle X-ray scattering measurements (GISAXS).[21] Buriak and co-workers have also used polymer self-assembly to pattern inorganic nanoparticles on silicon surfaces.[22,23] In light of this work on self-assembly of nano-scale structures, we sought to determine whether or not polymer phase separation would be a viable route toward organization of functionalized carbon nanotubes. In particular, we were interested in using PS/PMMA blends, which are well known to undergo phase separation in thin films when annealed at temperatures above the glass transition temperature (Tg) of both polymers.[24-27] It was speculated that addition of single-walled carbon nanotubes (SWNTs) that are covalently functionalized with one of the two components of the PS/PMMA blend would, upon annealing, result in nanotube migration to the polymer phase that is similar to what is bound to its surface. If successful, this concept may potentially lead to the preparation of surfaces that are patterned with nanotube-rich domains of controllable size and morphology, through a single-step self-assembly process.

2.2.1.2 Functionalization of Carbon Nanotubes

Functionalization of carbon nanotubes has been explored extensively, owing to their decided lack of solubility in common organic solvents. Both covalent and supramolecular functionalization methods with a variety of small molecules have been reported.[28-30] Polymer functionalization has also received significant attention, with examples of both "grafting from" and "grafting to" methods being successfully applied.[31-35] We have demonstrated the use of click chemistry for the functionalization of carbon nanotubes in the past,[36] whereby the introduction of alkyne functionalities on the SWNT surface enabled coupling to azide-terminated polystyrenes in an efficient manner. The resulting functionalized nanotubes were found to be soluble in THF and

other solvents, on the order of 100 – 200 mg/L. In the present work, we have adopted this strategy for the preparation of both polystyrene (PS) and poly(methyl methacrylate) (PMMA) decorated nanotubes. Both PS and PMMA functionalized carbon nanotubes were then incorporated into the PS/PMMA blend solutions prior to spin casting and annealing. Characterization of the annealed films was performed by scanning Raman microscopy, which utilized the unique Raman fingerprint of carbon nanotubes to locate their position within the phase-separated polymer domains.[37,38]

2.3 Experimental

2.3.1 General

Styrene (99$^+$%) and methyl methacrylate (99%), obtained from Aldrich Chemical Company, were passed through a basic Al_2O_3 chromatographic column, and then distilled from CaH_2. CuBr (Aldrich, 99.99%) was stirred in H_2SO_4 (1 N), filtered and then washed (3X) with glacial AcOH, EtOH, and then Et_2O. The resulting white powder was dried at 100ºC under vacuum for 30 minutes, and then stored in a vacuum dessicator. p-Xylene (Aldrich, 99$^+$%) was shaken with concentrated H_2SO_4, washed (3X) with de-ionized water, dried over $MgSO_4$, and then distilled from sodium/benzophenone. Carbon nanotubes (SWNT), purified grade, were obtained from Carbon Nanotechnologies Inc. and used as received. All other reagents were obtained from Aldrich Chemical and used as received. ^{1}H NMR spectra were obtained on a Bruker Avance 300 MHz Spectrometer using deuterated chloroform ($CDCl_3$) as solvent and TMS as internal reference. Infrared Spectroscopy was run on a Nicolet Magna-IR 500 Series II Spectrometer. Films were prepared using a Model # G3-8 Spin Coater, from Specialty Coating

Systems. Raman spectra and maps were obtained using a Renishaw InVia Raman Microscope equipped with 514 and 785 nm lasers and a high-resolution mapping stage.

2.3.2 Synthesis

*Preparation of 2-azidoethyl-2-bromo-2-methylpropanoate (**2**)*

In a 250 mL round bottom flask, equipped with a stir bar and condenser, 2-bromoisobutyryl bromide (19.5 g, 85 mmol), triethylamine (10.3 g, 102 mmol) and THF (125 mL) were added and then chilled in an ice bath to 3-4°C. 2-azidoethanol (7.4 g, 85 mmol) in THF (30 mL) was then added dropwise. The creamy beige suspension was removed from the ice bath, and stirred at room temperature for 2 h. $NaHCO_3$ (4.2 g, 50 mmol) was then added, causing a thick, light yellow precipitate to form. After filtering the solid away, the filtrate was transferred to a 250 mL separatory funnel and extracted with diethyl ether (3 x 50 mL). The organic layers were combined and washed with de-ionized water (3 x 50 mL), dried over $MgSO_4$, and the solvent removed by rotary evaporation. The crude product was purified by column chromatography (90:10 hexanes/EtOAc), to yield the pure product as a light yellow oil (13.1 g, 65%). ^{1}H NMR (300 MHz, $CDCl_3$): δ = 1.97 (s, 6H), 3.53 (t, 2H, J = 5.0 Hz), 4.35 (t, 2H, J = 5.0 Hz). ^{13}C NMR (50 MHz, $CDCl_3$): δ = 37.42, 56.39, 62.07, 71.42, 178.17. MS Calc.: $[M]^+$ m/z = 235, 237. Found EI MS: $[M + H]^+$ = 236, 238.

*Preparation of PS-Br (**4a**)*

A 250 mL Schlenk tube, equipped with a stir bar, was charged with styrene (20.8 g, 200.0 mmol), 2-ethylbromoisobutyrate (975 mg, 5 mmol), N,N,N',N',N"-pentamethyldiethylenetriamine (PMDETA; 867 mg, 5 mmol), and p-xylene (20 mL). The tube

was swirled to ensure complete dissolution, and then degassed by three freeze-pump-thaw cycles. After purging with Ar for 5 min, CuBr (717 mg, 5 mmol) was added to the frozen mixture by quickly removing and then replacing the septum. After a 5 min Ar purge, the tube was submerged in an oil bath (110ºC), and the reaction mixture was stirred under a constant flow of Ar. The solution turned green within 5 min of heating. Time zero was noted as the point of complete melting of the frozen mixture. After 16 h of heating, the green solution was removed from the oil bath and cooled slightly. THF (30 mL) was added, and the resulting solution was added dropwise to methanol (300 mL), causing a white precipitate to form. The precipitate was filtered and washed with methanol (3 x 100 mL), and dried under vacuum. The product was dissolved in THF (200 mL), passed through a neutral alumina column, and then concentrated by rotary evaporation of THF under vacuum. The product was re-precipitated by adding the concentrated solution in THF dropwise to MeOH (500 mL). Filtration, followed by vacuum oven drying (35ºC) afforded the product as a white powder (75% yield). ^{1}H NMR (300 MHz, $CDCl_3$): δ = 1.2-1.6 (br), 1.65-2.2 (br), 6.35-6.8 (br), 6.85-7.2 (br). GPC: M_n = 5,800, PDI = 1.14.

*Preparation of azido-terminated PS (**4b**)*

Into a 100 mL round bottom flask was added polystyrene (**4a**, 5.8 g, 1 mmol), sodium azide (0.65 g, 10 mmol) and DMF (50 mL). The solution was stirred for 24 h at room temperature under Ar, and then added dropwise to de-ionized water (250 mL). The resulting light yellow precipitate was filtered and washed with H_2O (3 x 50 mL), MeOH (3 x 50 mL), and then oven dried at 50°C (91% yield). ^{1}H NMR (300 MHz, $CDCl_3$): δ = 1.2-1.6 (br), 1.7-2.2 (br), 6.3-6.8 (br), 6.85-7.2 (br). GPC: M_n = 5,800, PDI = 1.14.

*Preparation of PS-Br (**4c**)*

PS-Br **4c** was prepared from styrene (20.8 g, 200.0 mmol), 2-ethylbromoisobutyrate (195 mg, 1 mmol), PMDETA (173 mg, 1 mmol), CuBr (143 mg, 1 mmol) and p-xylene (20 mL) according to the method used for **4a** (75% yield). ^{1}H NMR (300 MHz, $CDCl_3$): δ = 1.2-1.6 (br), 1.65-2.2 (br), 6.3-6.7 (br), 6.85-7.2 (br). GPC: M_n = 27,700, PDI = 1.28.

*Preparation of azido-terminated PS (**4d**)*

The process used to prepare **4b** was repeated, using **4c** as starting material. Due to the higher molecular weight of polymer **4c**, a 100-fold excess of sodium azide was used. The product was isolated in 95% yield. ^{1}H NMR (300 MHz, $CDCl_3$): δ = 1.2-1.6 (br), 1.65-2.2 (br), 6.25-6.8 (br), 6.85-7.2 (br). GPC: M_n = 27,700, PDI = 1.28.

*Preparation of PMMA (**5a**)*

A 250 mL Schlenk tube was charged with MMA (10.0 g, 100.0 mmol), 2-ethylbromoisobutyrate (390 mg, 2 mmol), PMDETA (347 mg, 2 mmol), and p-xylene (20 mL). The tube was swirled to ensure complete dissolution, and then degassed by three freeze-pump-thaw cycles. After purging with Ar for 5 minutes, CuBr (287 mg, 2 mmol) was added to the frozen mixture by quickly removing and then replacing the septum. After a 5 min Ar purge, the tube was submerged in an oil bath (90ºC) under a constant flow of Ar. The solution turned green within 5 min of heating. Time zero was noted as the point of complete melting of the frozen mixture. After 16 h of heating, the green solution was removed from the oil bath and cooled slightly. THF (30 mL) was added, and the resulting solution was added dropwise to methanol (300 mL), causing a white precipitate to form. The precipitate was filtered and washed with

methanol (3 x 100 mL), and dried under vacuum. The product was dissolved in THF (200 mL), passed through a neutral alumina column, and then concentrated by rotary evaporation of THF under vacuum. The product was re-precipitated by adding the concentrated solution in THF dropwise to MeOH (500 mL). Filtration, followed by vacuum oven drying (35ºC), afforded the product as a white powder (45% yield). ^{1}H NMR (300 MHz, $CDCl_3$): δ = 0.84 (s), 1.02 (s), 1.7-2.1 (br), 3.60 (s). GPC: M_n = 11,600, PDI = 1.28.

*Preparation of azido-terminated PMMA (**5b**)*

PMMA-N_3 **5b** was prepared from MMA (20.0 g, 200 mmol), initiator **2** (2.36 g, 10 mmol), PMDETA (1.73 g, 10 mmol), CuBr (1.43 g, 10 mmol), and p-xylene (20 mL) according to the method used for **5a**. The polymerization was run for 16 h at a temperature of 80°C. The product was isolated in 39% yield. ^{1}H NMR (300 MHz, $CDCl_3$): δ = 0.84 (s), 1.02 (s), 1.7-2.1 (br), 3.60 (s). GPC: M_n = 10,300, PDI = 1.31.

*Preparation of PMMA (**5c**)*

PMMA-Br **5c** was prepared from MMA (20.0 g, 200.0 mmol), 2-ethylbromoisobutyrate (156 mg, 0.8 mmol), PMDETA (139 mg, 0.8 mmol), CuBr (115 mg, 0.8 mmol), and p-xylene (20 mL) according to the method used for **5a**. The polymerization was run for 6 h at a temperature of 90°C. The product was isolated in 76% yield. ^{1}H NMR (300 MHz, $CDCl_3$): δ = 0.84 (s), 1.02 (s), 1.7-2.1 (br), 3.60 (s). GPC: M_n = 22,600, PDI = 1.28.

*Preparation of azido-terminated PMMA (**5d**)*

PMMA-N_3 **5d** was prepared from MMA (20.0 g, 200 mmol), initiator **2** (472 mg, 2 mmol), PMDETA (347 mg, 2 mmol), CuBr (287 mg, 2 mmol), and p-xylene (20 mL) according to the method used for **5a**. The polymerization was run for 18 h at a temperature of 50°C. The product was isolated in 26% yield. ^{1}H NMR (300 MHz, $CDCl_3$): δ = 0.84 (s), 1.02 (s), 1.7-2.1 (br), 3.60 (s). GPC: M_n = 17,100, PDI = 1.23.

2.3.3 Coupling of Polymer to Nanotubes

In a typical experiment, alkyne decorated nanotubes (10 mg) were sonicated in DMF (7 mL) for 5 min in a 50 mL Schlenk tube. PS-N_3 or PMMA-N_3 (500 mg), was then dissolved in DMF (8 mL), and the solution added into the Schlenk tube, which was then subjected to three cycles of freeze-pump-thaw. After purging with Ar for 5 min, $(PPh_3)_3CuBr$ (372 mg, 0.4 mmol) was added quickly to the frozen mixture, and another Ar purge (5 min) was done. The Schlenk tube was then submerged in an oil bath at 60°C for 24 h. The suspension was cooled to room temperature and THF (30 mL) was added. The suspension was then filtered through a 0.2 μm PTFE membrane, and the solid washed successively with THF, de-ionized water, MeOH, and DCM (3 x 30 mL each). The solid was then dried in a vacuum oven at 50°C.

2.3.4 Film Preparation

Two concentrated (25 wt%) stock solutions of a 1:1 weight ratio of either low **(4a + 5a)** or high **(4c + 5c)** molecular weight PS and PMMA were prepared. These solutions were diluted to 5 wt % with either PS-SWNT or PMMA-SWNT solutions in THF, matching the molecular weight of the nanotube-bound polymer with that of the free polymer mixture. The concentration of the

nanotubes in the coating solutions was approximately 0.04 wt%. Silicon wafers were cleaned by dropping water, acetone and then THF onto a spinning wafer. Two drops of polymer solution were then placed on the wafer, and it was immediately spun at 2000 RPM for 60 seconds. The wafer was then placed on a hot stage and heated to 80ºC for 12 h, followed by annealing at 180ºC for 12 h.

2.4 Results and Discussion

2.4.1 Synthetic Procedures

Use of the Huisgen cycloaddition reaction to couple azido-functionalized polystyrenes with alkyne-decorated nanotubes was completed in three separate steps. Coupling of the alkyne functionality to the carbon nanotube was effected via diazotization of p-aminophenyl propargyl ether **1** in the presence of pristine single-walled carbon nanotubes.[36] The propargyl ether itself was prepared according to literature procedures (Scheme 2.1).[39] Briefly, substitution of propargyl bromide on p-nitrophenyl ether by phase transfer catalysis afforded p-nitrophenyl propargyl ether. Purification by re-precipitation from 1,4-dioxane afforded pure product, which was then reduced to the aminophenyl derivative using $SnCl_2$.[39]

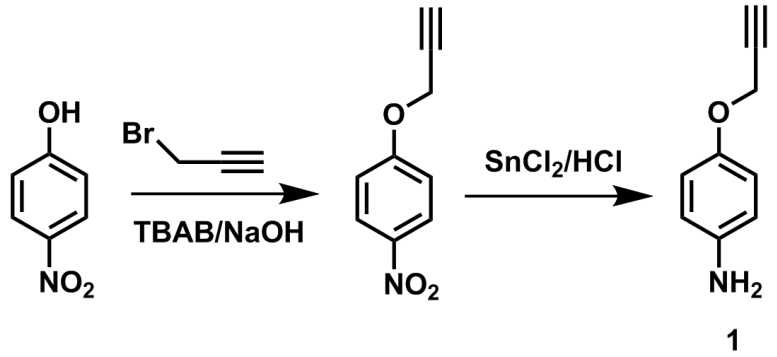

Scheme 2.1. Preparation of p-aminophenyl propargyl ether.

Azido-functionalized polystyrene (PS-N_3) samples having two different molecular weights (Table 2.1) were prepared by Atom Transfer Radical Polymerization (ATRP) of styrene using ethyl-2-bromoisobutyrate (EBiB) as initiator, followed by substitution of the terminal bromide with sodium azide.[40] In the case of PMMA, substitution of the azide functionality on the bromo-terminated polymer was found inefficient. Instead, an azido-functionalized initiator **2** was prepared for PMMA polymerizations, analogous to the initiator previously reported by Haddleton and co-workers.[41] Preparation of initiator **2** involved esterification of 2-bromoisobutyryl bromide with azidoethanol, to afford the product as a light yellow oil (Scheme 2.2). Azido-terminated PMMA samples (PMMA-N_3) were then prepared using conditions similar to those used for ATRP of styrene.

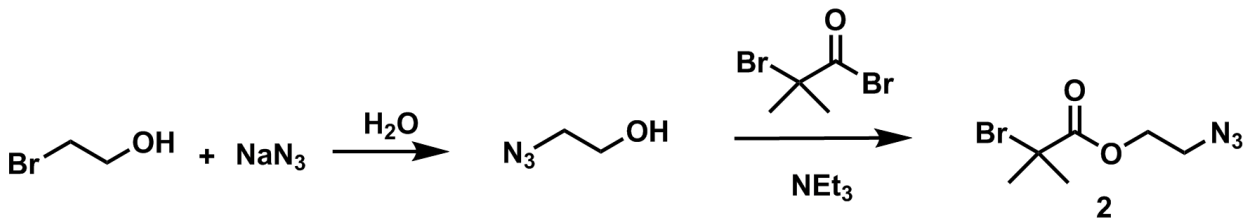

Scheme 2.2. Preparation of azido-functionalized initiator.

After polymerization, retention of the azido functional group at the PMMA chain end was confirmed by IR spectroscopy, where a clear signal was observed at 2106 cm^{-1} for the polymer prepared using the azido-functionalized initiator only (data not shown). No peak was observed in this area when the analogous bromo-terminated initator was used to prepare PMMA under identical conditions.

Having prepared the two sets of polymers, we turned our attention to coupling each of the azido-functionalized polymers to the alkyne-decorated nanotubes by Huisgen cycloaddition, using

$(PPh_3)_3CuBr$ as catalyst. This was accomplished using our previously reported methods and produced SWNT-polymer samples that exhibited solubility in THF consistent with the published results.[36]

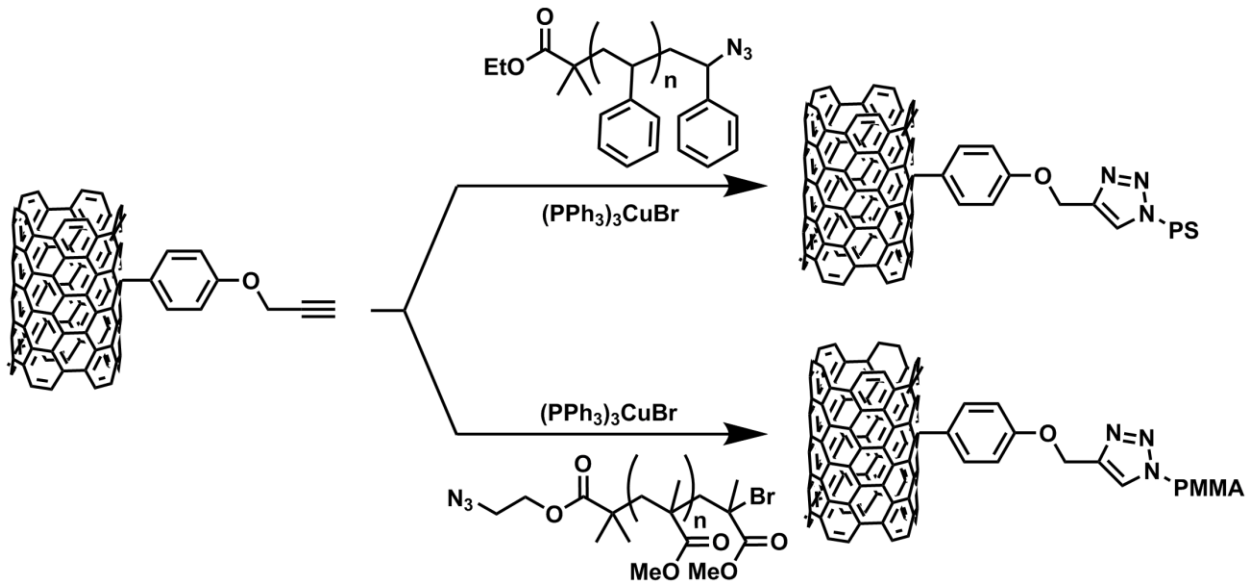

Scheme 2.3. Huisgen coupling for functionalization of SWNTs with PS and PMMA.

Since the azido-functionalized PS samples **(4b + 4d)** were prepared directly from their bromo-terminated analogs **(4a + 4c)**, these latter polymers could be used as the bulk material for film preparation, allowing exact matching of PS molecular weights in the film with those attached to the SWNTs. In the case of PMMA however, the bromo-terminated analog required for film preparation was made separately using ethyl-2-bromoisobutyrate as initiator. Therefore, the molecular weights of PMMA within the bulk films were not exactly matched to those attached to SWNTs, but reasonable agreement was achieved (Table 2.1).

Table 2.1. Polymer samples used for SWNT functionalization and phase separation studies.

Compound	Polymer	Mn	Mw	PDI
4a	PS-Br	5,800	6,600	1.14
4b*	PS-N_3	5,800	6,600	1.14
4c	PS-Br	27,700	35,400	1.28
4d*	PS-N_3	27,700	35,400	1.28
5a	PMMA-Br	11,600	14,800	1.28
5b	PMMA-N_3	10,300	13,500	1.31
5c	PMMA-Br	22,600	28,800	1.28
5d	PMMA-N_3	17,100	21,100	1.23

* Prepared from the corresponding Br-terminated polymer.

2.4.2 PS/PMMA Film Preparation

To prepare phase-separated films, 5 wt% solutions containing equal weights of PS-Br and PMMA-Br (**4a** and **5a** or **4c** and **5c**, respectively) in THF were spin cast on silicon wafers at 2000 rpm, followed by a two step annealing process (12 h at 80°C followed by 12 h at 180ºC). This resulted in phase separation of the two polymers and formation of spherical PS domains within a continuous phase of PMMA (Figure 2.1A). Visual inspection of the films after selective dissolution of the PMMA phase using an acetic acid wash confirmed the makeup of the two phases in the film.[42] Conditions for film formation and annealing were selected so as to afford PS domains on the order of 5-10 μm in size, allowing for rapid characterization using optical microscopy.

The effect of introducing either PS- or PMMA-functionalized SWNTs on the composition of the annealed films was then investigated. Two concentrated (25 wt%) stock solutions of a 1:1 weight ratio of either low (**4a** + **5a**) or high (**4c** + **5c**) molecular weight PS and PMMA were prepared. These solutions were diluted with either PS-SWNT or PMMA-SWNT solutions in

THF, matching the molecular weight of the nanotube-bound polymer with that of the free polymer mixture. Final polymer concentrations of these solutions were maintained at 5 wt%, while the concentration of the nanotubes was approximately 0.04 wt%. The resulting four solutions, which differed in both type of polymer attached to nanotubes (PS or PMMA), and the molecular weight of the polymers (low or high) were spin coated and annealed on Si substrates according to the method described above. At the SWNT concentrations used, no discernible differences were noted between annealed films containing carbon nanotubes and those without, thus the presence of nanotubes did not appear to influence the overall morphology of the films.

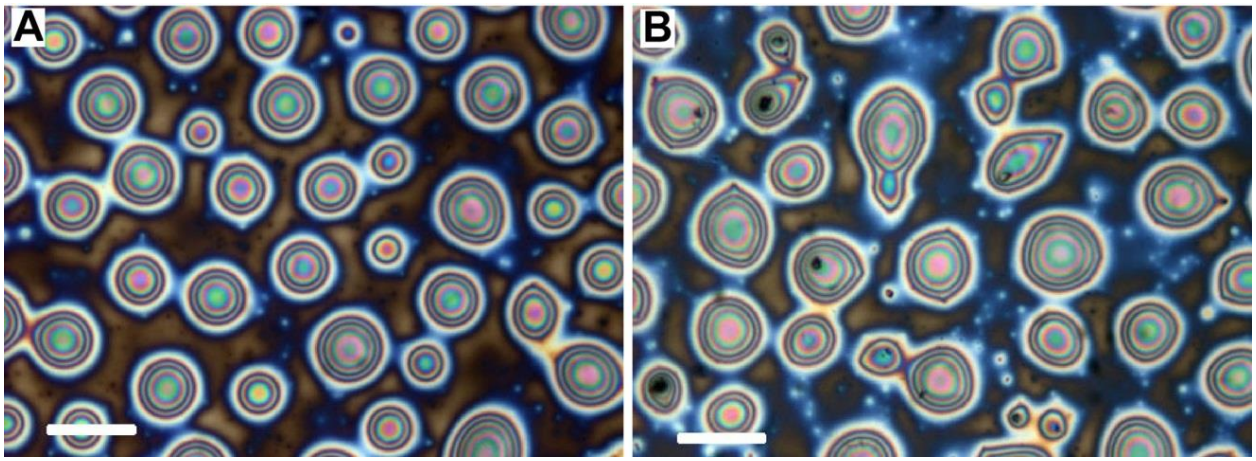

Figure 2.1. Optical micrographs of phase separated films of PS-PMMA (50/50 wt%) after annealing for 18 h: (A) without addition of SWNTs; (B) with addition of SWNTs. Scale bars correspond to 20 μm.

2.4.3 Self-assembly of Carbon Nanotubes

Having accomplished film preparation and phase separation in the presence of SWNTs, it was necessary to determine whether or not the SWNTs migrated to the polymer phase that

corresponded with the nanotube-bound polymer. Initial attempts using TEM and AFM analyses proved unsuccessful, as the nanotubes could not be detected due to their low concentration within the films. Raman Spectroscopy, which is a commonly used characterization tool for carbon nanotubes, proved more useful in this regard, as it is not limited to probing surface topology and small sample areas. Using a Raman spectrometer equipped with an X-Y translation stage, compositional maps of the phase-separated polymer films were acquired, with and without polymer-functionalized SWNTs (PF-SWNTs). In the cases where PF-SWNTs were incorporated, the location of the nanotubes was determined using a principal component analysis, where the spectrum acquired from individual pixels of the map were matched to the spectrum of the PS- and PMMA-functionalized SWNTs. A Raman map of the high molecular weight phase separated polymers containing PS-functionalized SWNTs is depicted in Figure 2.2a. Locations of spectral signals corresponding to the presence of SWNTs within this sample are overlaid and color-coded green, showing the spatial distribution of nanotubes within the phase-separated film. The insets in Figure 2.2 (b-d) show a close-up view of a single PS domain, mapped to highlight the location of each of the three components, SWNTs (b, green), PS (c, yellow), and PMMA (d, blue). The spectra attributed to each of these components are also shown, demonstrating the clear discrimination of the three components. Complete Raman maps for the four samples consisting of PS- and PMMA-functionalized SWNTs within films of both high and low polymer molecular weight are provided in the supporting information (Figure 2.3). Analysis of these maps involved manual counting of the number of spots that reside fully within the PS domains, fully within the PMMA continuous phase, or at the PS-PMMA interface. In all cases, the majority of PF-SWNTs ended up at the interface of the two polymer phases (Table 2.2). This result may indicate that the PF-SWNTs favored the PS-PMMA interface within the phase-separated films or that complete

migration toward the compatible phase was hindered by the large size of the nanotubes and could not be completed within the annealing time investigated (12 h). Alternatively, this observation may simply be the result of the relatively large interfacial surface area, making it statistically probable that the majority of nanotubes resided at the interface. When considering the nanotube spots that resided fully within either the PS or PMMA domains, three of the four cases showed a significantly higher percentage of nanotube-rich regions within the polymer phase that matched the polymer appended to the SWNT surface (Table 2.2). Thus, when considering the percentage of spots located fully within one domain or the other, there was a clear tendency for the polymer-functionalized SWNTs to migrate to their respective domain. Interestingly, the two samples bearing low MW polymers had a significantly higher number of matches than did their high MW counterparts. This could be due to greater graft density of the lower MW polymers, resulting in more complete coverage of the nanotube surface. Alternatively, this result may indicate that longer annealing times are necessary to achieve the same level of nanotube migration when higher molecular weight polymers are used. More detailed studies are required to determine whether molecular weight and annealing times play a significant role in the migration patterns of the functionalized nanotubes.

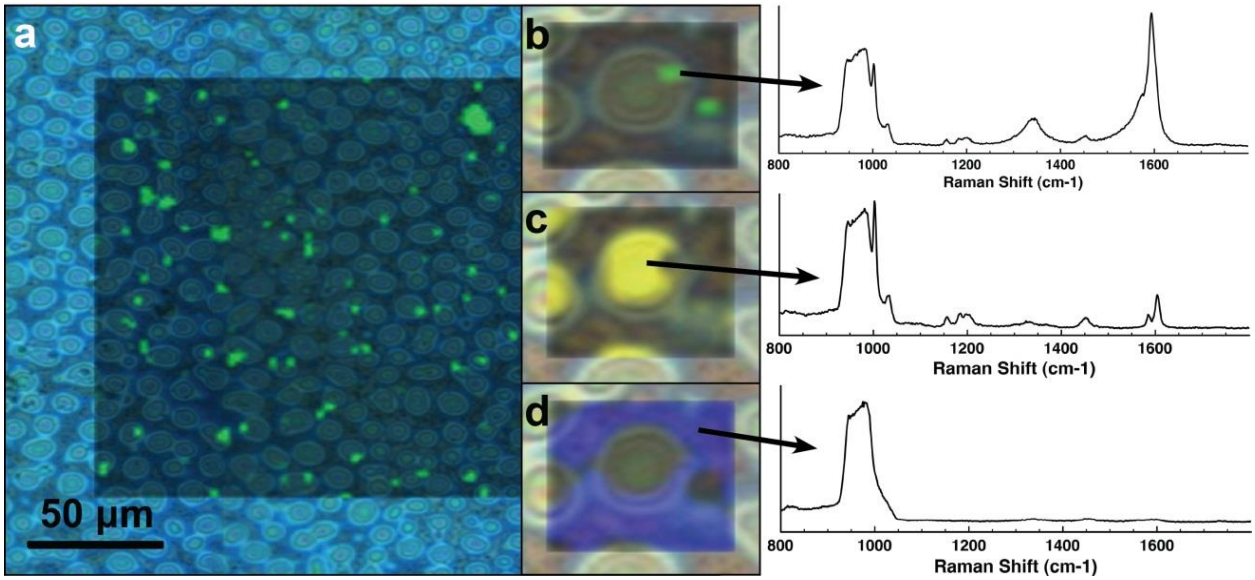

Figure 2.2. Large area Raman map of the high molecular weight polymer sample with PS-functionalized SWNTs: (a) where locations of Raman signals corresponding to SWNTs are highlighted in green. Insets show close-up views of a spot from the same sample that has been mapped to highlight signals from the three components: SWNTs (b), PS (c), and PMMA (d). At right are the Raman spectra that correspond to each of the three components.

Table 2.2. Manual analysis of Raman correlation maps.

Sample	Total # of spots	Fully in respective domain (%)	PS-PMMA interface (%)	Fully in opposite domain (%)
PS – low MW	157	36	50	12
PS – high MW	77	16	63	15
PMMA – low MW	45	41	37	10
PMMA – high MW	141	26	56	11

2.5 Conclusions

Self-assembly of PF-SWNTs within phase-separated polymer films has been demonstrated using both PS- and PMMA-functionalized SWNTs. The PF-SWNTs were incorporated into PS-PMMA solutions, which were cast as thin films and annealed at high temperature to induce phase separation of the two incompatible polymers. Scanning Raman Spectroscopy was used to determine the location of the PF-SWNTs within the phase-separated films. In each case, the majority of the nanotube-rich spots were found at the interface between the two phase-separated polymers. However, consideration of the spots residing completely in one phase or the other revealed a significant number within their respective polymer domains. Thus, PS-SWNTs were found consistently within the PS domains, and PMMA-SWNTs were found in the PMMA continuous phase. Further investigation of the effects of both polymer molecular weight and annealing times are currently being considered.

2.5.1 Acknowledgements

Financial support for this work was provided by the Natural Science and Engineering Council of Canada (NSERC) and the Xerox Research Centre of Canada (XRCC). We also thank Richard Bormett for help with Raman mapping.

2.6 Supporting Information

Phase Separation of Polymer-Functionalized SWNTs within a PMMA/Polystyrene Blend

James D. Mayo[a], Sonia Behal[b], and Alex Adronov[b]*

a- Xerox Research Centre of Canada, Mississauga, Ontario

b- Department of Chemistry and the Brockhouse Institute for Materials Research (BIMR), McMaster University, Hamilton, Ontario

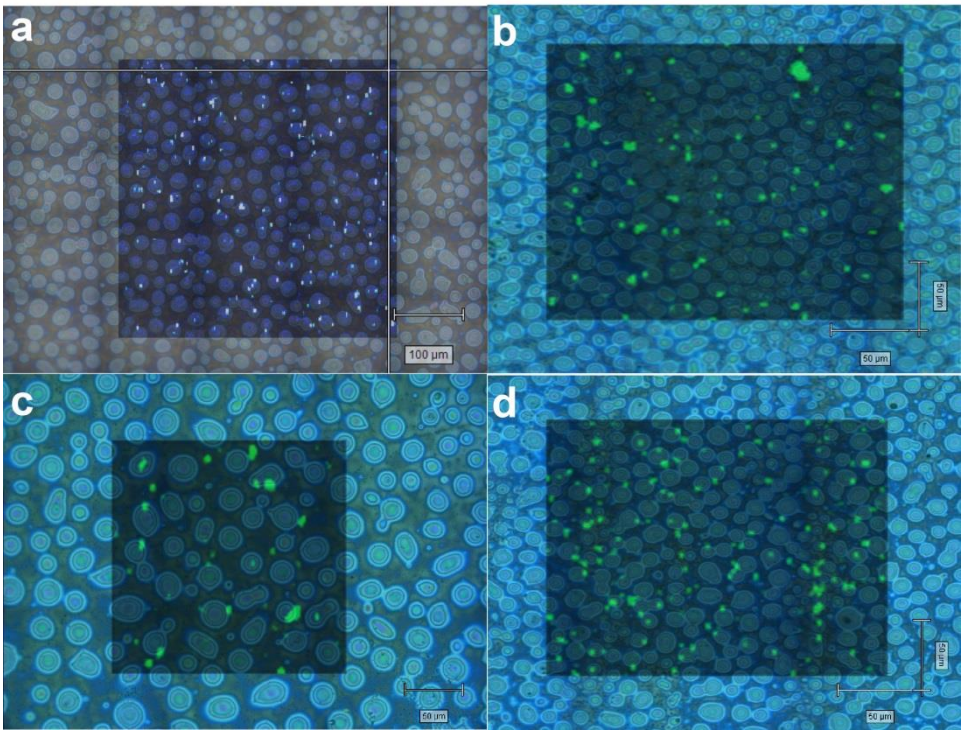

Figure 2.3. Scanning Raman images of annealed polymer/nanotube films: a) PS-SWNT (low MW PS); b) PS-SWNT (high MW PS); c) PMMA-SWNT (low MW PMMA); d) PMMA-SWNT (high MW PMMA).

2.7 References

(1) Collins, P. G.; Avouris, P. *Scientific American* **2000**, *283*, 62.

(2) Harris, P. J. F. *Int. Mater. Rev.* **2004**, *49*, 31.

(3) Berger, C.; Poncharal, P.; Yi, Y.; de Heer, W. *Journal of Nanoscience and Nanotechnology* **2003**, *3*, 171.

(4) Poncharal, P.; Berger, C.; Yi, Y.; Wang, Z. L.; de Heer, W. A. *J. Phys. Chem. B* **2002**, *106*, 12104.

(5) Ajayan, P. M. *Chem. Rev.* **1999**, *99*, 1787.

(6) Freitag, M.; Martin, Y.; Misewich, J. A.; Martel, R.; Avouris, P. H. *Nano Lett.* **2003**, *3*, 1067.

(7) Tans, S. J.; Verschueren, A. R. M.; Dekker, C. *Nature* **1998**, *393*, 49.

(8) Weitz, R. T.; Zschieschang, U.; Effenberger, F.; Klauk, H.; Burghard, M.; Kern, K. *Nano Lett.* **2007**, *7*, 22.

(9) Kong, J.; Franklin, N. R.; Zhou, C. W.; Chapline, M. G.; Peng, S.; Cho, K. J.; Dai, H. J. *Science* **2000**, *287*, 622.

(10) Li, J.; Hu, L.; Wang, L.; Zhou, Y.; Gruner, G.; Marks, T. J. *Nano Lett.* **2006**, *6*, 2472.

(11) Coleman, J. N.; Khan, U.; Blau, W. J.; Gun'ko, Y. K. *Carbon* **2006**, *44*, 1624.

(12) Dalton, A. B.; Collins, S.; Munoz, E.; Razal, J. M.; Ebron, V. H.; Ferraris, J. P.; Coleman, J. N.; Kim, B. G.; Baughman, R. H. *Nature* **2003**, *423*, 703.

(13) Lau, K. T.; Lu, M.; Liao, K. *Composites Part a-Applied Science and Manufacturing* **2006**, *37*, 1837.

(14) Choi, W. B.; Bae, E.; Kang, D.; Chae, S.; Cheong, B. H.; Ko, J. H.; Lee, E. M.; Park, W. *Nanotechnology* **2004**, *15*, S512.

(15) Ci, L. J.; Manikoth, S. M.; Li, X. S.; Vajtai, R.; Ajayan, P. M. *Adv. Mater.* **2007**, *19*, 3300.

(16) Jung, Y. J.; Kar, S.; Talapatra, S.; Soldano, C.; Viswanathan, G.; Li, X. S.; Yao, Z. L.; Ou, F. S.; Avadhanula, A.; Vajtai, R.; Curran, S.; Nalamasu, O.; Ajayan, P. M. *Nano Lett.* **2006**, *6*, 413.

(17) Li, B.; Cao, T. B.; Shi, Z. J.; Cao, W. X.; Gu, Z. N. *Acta Chim. Sinica* **2001**, *59*, 1536.

(18) Liu, H.; Li, S. H.; Zhai, J.; Li, H. J.; Zheng, Q. S.; Jiang, L.; Zhu, D. B. *Angewandte Chemie-International Edition* **2004**, *43*, 1146.

(19) Long, D. P.; Lazorcik, J. L.; Shashidhar, R. *Adv. Mater.* **2004**, *16*, 814.

(20) Paloniemi, H.; Lukkarinen, M.; Aaritalo, T.; Areva, S.; Leiro, J.; Heinonen, M.; Haapakka, K.; Lukkari, J. *Langmuir* **2006**, *22*, 74.

(21) Lin, Y.; Boker, A.; He, J. B.; Sill, K.; Xiang, H. Q.; Abetz, C.; Li, X. F.; Wang, J.; Emrick, T.; Long, S.; Wang, Q.; Balazs, A.; Russell, T. P. *Nature* **2005**, *434*, 55.

(22) Aizawa, M.; Buriak, J. M. *J. Am. Chem. Soc.* **2006**, *128*, 5877.

(23) Aizawa, M.; Buriak, J. M. *Chem. Mater.* **2007**, *19*, 5090.

(24) Harris, M.; Appel, G.; Ade, H. *Macromolecules* **2003**, *36*, 3307.

(25) Rui, X.; Song, Z. W.; Jing, S.; Tian, D. C. *Polym. J.* **2005**, *37*, 560.

(26) Ton-That, C.; Shard, A. G.; Bradley, R. H. *Polymer* **2002**, *43*, 4973.

(27) Ton-That, C.; Shard, A. G.; Daley, R.; Bradley, R. H. *Macromolecules* **2000**, *33*, 8453.

(28) Banerjee, S.; Kahn, M. G. C.; Wong, S. S. *Chemistry-a European Journal* **2003**, *9*, 1899.

(29) Chen, Y.; Haddon, R. C.; Fang, S.; Rao, A. M.; Lee, W. H.; Dickey, E. C.; Grulke, E. A.; Pendergrass, J. C.; Chavan, A.; Haley, B. E.; Smalley, R. E. *J. Mater. Res.* **1998**, *13*, 2423.

(30) Holzinger, M.; Vostrowsky, O.; Hirsch, A.; Hennrich, F.; Kappes, M.; Weiss, R.; Jellen, F. *Angewandte Chemie-International Edition* **2001**, *40*, 4002.

(31) Dyke, C. A.; Tour, J. M. *J. Phys. Chem. A* **2004**, *108*, 11151.

(32) Dyke, C. A.; Tour, J. M. *Chemistry-a European Journal* **2004**, *10*, 813.

(33) Li, S. P.; Qin, Y. J.; Shi, J. H.; Guo, Z. X.; Yongfang, L.; Zhu, D. B. *Chem. Mater.* **2005**, *17*, 130.

(34) Ramanathan, T.; Fisher, F. T.; Ruoff, R. S.; Brinson, L. C. *Chem. Mater.* **2005**, *17*, 1290.

(35) Tasis, D.; Tagmatarchis, N.; Bianco, A.; Prato, M. *Chem. Rev.* **2006**, *106*, 1105.

(36) Li, H. M.; Cheng, F. O.; Duft, A. M.; Adronov, A. *J. Am. Chem. Soc.* **2005**, *127*, 14518.

(37) Dillon, A. C.; Yudasaka, M.; Dresselhaus, M. S. *Journal of Nanoscience and Nanotechnology* **2004**, *4*, 691.

(38) Duan, X. J.; Son, H. B.; Gao, B.; Zhang, J.; Wu, T. J.; Samsonidze, G. G.; Dresselhaus, M. S.; Liu, Z. F.; Kong, J. *Nano Lett.* **2007**, *7*, 2116.

(39) Agag, T.; Takeichi, T. *Macromolecules* **2001**, *34*, 7257.

(40) Tsarevsky, N. V.; Sumerlin, B. S.; Matyjaszewski, K. *Macromolecules* **2005**, *38*, 3558.

(41) Mantovani, G.; Ladmiral, V.; Tao, L.; Haddleton, D. M. *Chem. Commun.* **2005**, 2089.

(42) Thurn-Albrecht, T.; Steiner, R.; DeRouchey, J.; Stafford, C. M.; Huang, E.; Bal, M.; Tuominen, M.; Hawker, C. J.; Russell, T. *Adv. Mater.* **2000**, *12*, 787.

Chapter 3

Effect of Spacer Chemistry on the Formation and Properties of Linear Reversible Polymers

3.1 Abstract

A series of four pairs of bismaleimide and bisfuran monomers were combined to make thermally reversible linear polymers. The monomers were prepared using diamines having different spacer chemistries: n-octyl, cyclohexyl, phenyl, and ethylenedioxy, such that a relatively constant spacer dimension among the four monomers was achieved. Heating of the bismaleimide/bisfuran couples resulted in low viscosity, easily processable liquids. Subsequent cooling to room temperature resulted in formation of hard films, with the rate of hardening varying significantly within the series of compounds. The rate and degree of polymerization were determined using ^{1}H NMR spectroscopy, and were both found to be dependent on the chemistry of the spacer group, as was the film rheology, which was measured using nanoindentation. Adhesion of the polymers was quantified by measurement of their tensile adhesive strength, and this was also found to be spacer dependent. Polymerization reversibility was verified using ^{1}H NMR spectroscopy.

3.2 Introduction

3.2.1 Reversible Polymers

Reversible polymers have been explored as a potential solution for thermal and mechanical breakdown of both structural and thin film polymers in a variety of applications.[1-5] Formation and propagation of micro-cracks within a polymer matrix ultimately lead to failure of the material. Reparation using traditional adhesive based methods only occurs on a macro scale, and does not treat the fracture at its onset. With reversible polymers, reparation can occur on a nano-scale within the crack, and can be implemented well before it has propagated to the point of material failure. The inherent low viscosity of the monomeric materials enables flow and realignment of the reactive sites across the damaged area, allowing formation of covalent bonds across the micro-crack without the use of healing agents or additives. This in turn enables much higher healing efficiencies than have been realized with traditional epoxies or surface treatments, and also allows the material to undergo multiple healing events.[6-10] The basic concept for reversible polymers, depicted in Figure 1, has been explored by numerous investigators using both covalent and non-covalent bonding motifs. In the molten state, reversible polymers can either consist of discrete, small molecule building blocks,[6-8] (Figure 3.1a) or of linear polymers that have been decorated with reversible functional groups (Figure 3.1b).[11-15] The reversible bonds can therefore be used either to intrinsically generate a polymer network, or to impart cross-linking to existing chains. In either case, the viscosity of the heated material would be expected to be significantly lower than would be realized by heating an analogous conventional polymer. These materials therefore not only lend themselves to the concept of self-healing, but also allow for much easier materials processing than their polymeric counterparts.

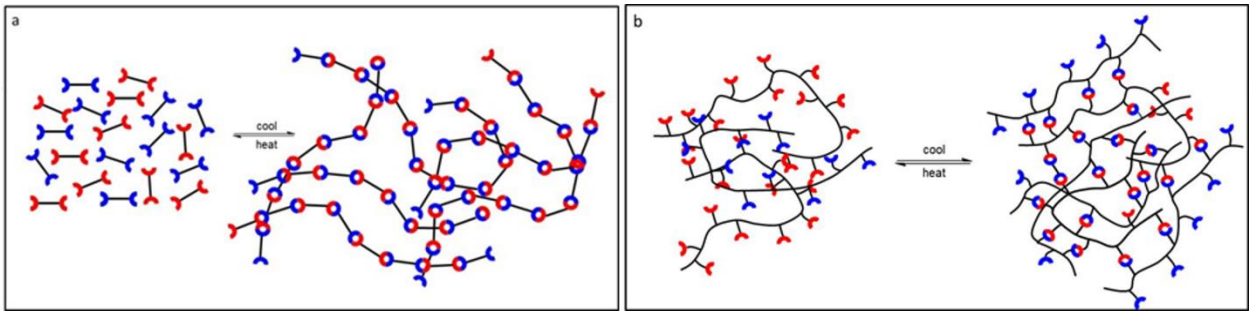

Figure 3.1. Schematic representation of reversible polymer formation: a) monomeric components; b) decorated polymer backbone.

3.2.2 Diels Alder Reaction for Reversible Polymers

Ideally, the linking chemistry in a reversible polymer is based on an addition rather than a condensation reaction, as the latter would result in liberation of small molecules that would render the reaction irreversible. The Diels-Alder (DA) reaction meets this requirement, and has been studied extensively as a reversible coupling method. In particular, the coupling of maleimides and furans has been the basis of much of the work in this field, as the electron deficient dienophile and s-cis configured diene are ideally suited for reversible DA chemistry.[6-10,16] Interest in this system was piqued by Wudl and co-workers in 2002,[6] who prepared reversible, cross-linked polymers using multi-valent maleimides and furans. In their work, a tetrapodal furan and tripodal maleimide were polymerized via DA cycloaddition to form tough, cross-linked polymers that could be reversibly melted and solidified. Tensile and compression strength and moduli were measured and compared favourably to typical epoxy resins. The practicality of this phenomenon was then demonstrated by repeated restoration of a fractured polymer via multiple heating and cooling cycles. A novel method of inducing and repairing cracks in the materials was used to quantify healing efficiency; by ensuring close alignment of the two newly exposed surfaces

during the repair, the polymers were found to recover more than 80% of their original strength. Further exploration by this group resulted in several remendable cross-linked polymeric materials that were also able to undergo multiple healing events.[7]

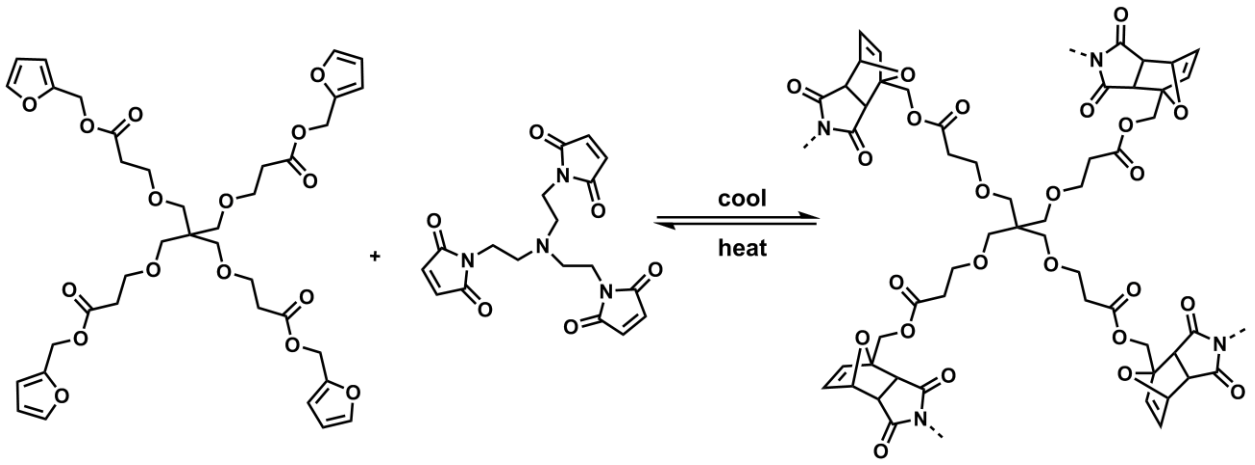

Figure 3.2. Preparation of cross-linked reversible polymer by Diels-Alder chemistry.

3.2.3 Alternative Methods for Preparation of Reversible Polymers

Along similar lines, decoration of existing polymer backbones with reactive furan groups was explored by Zhang et al. using readily available polyketones, which were converted to furan derivatives using mild conditions in a Paal-Knorr reaction with furfurylamine.[15] A bisphenyl based bismaleimide was then used as a cross-linking agent to afford a healable epoxy resin. Healing efficiencies of 100% were reported, although in this case healing was measured by grinding the entire sample of solidified resin into a powder and re-molding a fresh sample for a repeat mechanical analysis measurement.

Murphy et al. improved on the maleimide-furan coupling, as they prepared a single component re-mendable polymer using dicyclopentadiene as both diene and dienophile.[17] This linkage was used to form macrocyclic “mendomers”, which upon heating, would undergo ring opening via the retro-DA reaction. The resulting bis(cyclopentadiene) could then couple

intermolecularly to form linear reversible polymers. Indeed, this resulted in transparent, hard polymers that could be healed multiple times. A significant amount of additional work has been done to improve the DA reaction, including optimization of the temperature required to induce the retro-DA reaction,[18] and variation of the DA reaction rate by modifying the electronics of the diene and dienophile.[19] In addition to the DA reaction, other reversible polymerizations have been investigated for self-healing materials, including carbene dimerization,[20,21] photochemical cycloadditions,[22,23] hydrogen bonding,[24-26] and transesterification.[27]

Although cross-linking offers the opportunity for formation of structurally durable materials, and much of the research in the field of reversible polymers is based on multi-podal furans and maleimides that result in highly cross-linked networks, the resulting structures are complex and difficult to characterize. Linear polymers, comprised of bis-maleimides and bis-furans with different spacer compositions, have received less attention. Here, we study the effects of the spacer chemistries on the reaction kinetics and physical properties of the cured polymers. Initially, a relatively simple system, consisting of short chain bis-furans/bis-maleimides was chosen, in order to observe the effects of reversible polymerization on overall rheological characteristics, as well as the extent of the coupling reaction. To this end, four different spacer groups were used, including a straight chain alkyl (C_8), a cyclohexyl, a phenyl and an ethylenedioxy group.

3.3 Experimental

3.3.1 General

All reagents were obtained from Sigma-Aldrich and used as received. ^{1}H NMR spectra were obtained on a Bruker Avance 400 MHz Spectrometer using deuterated dimethyl sulfoxide

(d_6-DMSO) as solvent and TMS as internal reference. Viscosity measurements were made using an Ares 2000 viscometer from Rheometric Scientific, equipped with a 25 mm steel plate assembly set at a gap width of 200 µm. Nanoindentation measurements were made using a Hysitron Triboscan® nanoindenter equipped with a Berkovich diamond tip. Differential Scanning Calorimetry (DSC) analyses were performed on a DSC Q1000, from TA Instruments. X-Ray diffraction spectra were obtained on a Rigaku MiniFlex X-ray Diffractometer, fitted with a Cu target and variable slit interlocked with θ axis. High-resolution mass spectrometry using electrospray ionization (HRMS (EI+)) was conducted for the synthesized monomers on a Micromass Quattro Ultima triple quadrupole mass spectrometer using positive ion mode. Tensile strength measurements were made on an Instron 3367, using an extension rate of 100 µm per minute.

3.3.2 General procedure for synthesis of bismaleimides

In a 500 mL round-bottomed flask equipped with a magnetic stir bar was dissolved maleic anhydride (10.5 eq) in 75 mL DMF. The resulting solution was chilled on ice and the diamine (5 eq) dissolved in DMF (75 mL) was added dropwise over ~20 min. The ice bath was removed, and sodium acetate (1 eq) and acetic anhydride (11 eq) were added in one portion, and the mixture stirred overnight at 50°C. The mixture turned dark brown within 30 minutes of the addition of NaOAc and Ac_2O. DMF was removed by vacuum distillation (60°C), and DCM (150 mL) was added to the dark brown mixture. The organic layer was extracted with $NaHCO_3$ (5 x 100 mL), dried over $MgSO_4$, and the solvent removed under vacuum. The resulting compounds were purified by column chromatography.

1,1'-(octane-1,8-diyl)bis(1H-pyrrole-2,5-dione) (**M1**)

The general procedure was carried out using maleic anhydride (14.27 g, 146 mmol), 1,8-octanediamine (10.0 g, 69.3 mmol), sodium acetate (1.14 g, 13.9 mmol) and acetic anhydride (15.57 g, 153 mmol). The resulting compound was purified by column chromatography (98:2 DCM:EtOAc), and the product obtained as a white solid (5.2 g/25%): R_f (95:5 DCM:EtOAc) = 0.5; mp = 124.5°C; ^{1}H NMR (400 MHz, DMSO): δ (ppm) 6.99 (s, 4H), 3.37, (t, 4H, *J* = 6.7 Hz), 1.46 (m, 4H), 1.19 (m, 8H); ^{13}C NMR (400 MHz, DMSO): δ (ppm) 171.54, 134.90, 37.47, 28.77, 28.32, 26.46; Electrospray MS (positive ion mode): calcd. for $C_{16}H_{21}N_2O_4$ $[M + H]^+$: m/z = 305.15; found: 305.2 , calcd. for $C_{16}H_{20}N_2O_4Na$ $[M + Na]^+$: m/z = 327.14; found: 327.2.

1,1'-(cyclohexane-1,3-diylbis(methylene))bis(1H-pyrrole-2,5-dione) (**M2**)

The general procedure was carried out using maleic anhydride (20.59 g, 210 mmol), 1,3-cyclohexanebis(methylamine) (14.22 g, 100 mmol), sodium acetate (1.64 g, 20 mmol), and acetic anhydride (22.46 g, 220 mmol). The resulting compound was purified by column chromatography (98:2 DCM:EtOAc), and the product obtained as a white solid (3.55 g/12%): R_f (95:5 DCM:EtOAc) = 0.42; mp = 161.3°C; ^{1}H NMR (400 MHz, DMSO): δ (ppm) 6.97 (s, 4H), 3.19 (d, 4H, *J* = 6.7 Hz), 1.51 (m, 6H), 1.13 (m, 1H), 0.78 (m, 2H), 0.57 (m, 1H); ^{13}C NMR (400 MHz, DMSO): δ (ppm) 171.68, 134.81, 43.59, 36.75, 34.59, 30.35, 25.00; Electrospray MS (positive ion mode): calcd. for $C_{16}H_{20}N_2O_5$ $[M + H_2O]^+$: m/z = 320.15; found: 320.2, calcd. for $C_{16}H_{18}N_2O_4Na$ $[M + Na]^+$: m/z = 325.11; found: 325.2, calcd. for $C_{16}H_{18}N_2O_4K$ $[M + K]^+$: m/z = 341.23; found: 341.2.

1,1'-(1,3-phenylenebis(methylene))bis(1H-pyrrole-2,5-dione) (**M3**)

The general procedure was carried out using maleic anhydride (20.59 g, 210 mmol), m-xylylenediamine (13.62 g, 100 mmol), sodium acetate (1.64 g, 20 mmol), and acetic anhydride (22.46 g, 220 mmol). The resulting compound was purified by column chromatography (97:3 DCM:EtOAc), and the product obtained as a white solid (6.51 g/22%): R_f (95:5 DCM:EtOAc) = 0.35; mp = 129.8°C; ^{1}H NMR (400 MHz, DMSO): δ (ppm) 7.28 (t, 1H, *J* = 0.2 Hz), 7.11 (m, 3H), 7.09 (s, 4H), 4.56 (s, 4H); ^{13}C NMR (400 MHz, DMSO): δ (ppm) 171.25, 137.58, 135.16, 129.34, 126.69, 126.44; Electrospray MS (positive ion mode): calcd. for $C_{16}H_{12}N_2ONa$ $[M + Na]^+$: m/z = 319.27; found: 319.1.

1,1'-((ethane-1,2-diylbis(oxy))bis(ethane-2,1-diyl))bis(1H-pyrrole-2,5-dione) (**M4**)

The general procedure was carried out using maleic anhydride (13.23 g, 135 mmol), 2,2'-(ethylenedioxy)bis(ethylamine) (10.0 g, 67.5 mmol), sodium acetate (1.11 g, 13.5 mmol), and acetic anhydride (15.15 g, 148 mmol). The resulting compound was purified by column chromatography (95:5 DCM:EtOAc), and the product obtained as a white solid (4.5 g/22%): R_f (80:20 DCM:EtOAc) = 0.35; mp = 98.05°C; ^{1}H NMR (400 MHz, DMSO): δ (ppm) 7.01 (s, 4H), 3.53 (m, 4H), 3.47 (m, 4H), 3.42 (s, 4H); ^{13}C NMR (400 MHz, DMSO): δ (ppm) 171.5, 134.9, 69.76, 67.42, 37.24; Electrospray MS (positive ion mode): calcd. for $C_{14}H_{17}N_2O_6$ $[M + H]^+$: m/z = 309.11; found: 309.1, calcd. for $C_{16}H_{20}N_2O_4Na$ $[M + Na]^+$: m/z = 331.10; found: 331.0.

3.3.3 General procedure for synthesis of bisfurans

To a 500 mL RBF equipped with a magnetic stir bar was added the diamine (47.9 eq), triethylamine (95.7 eq), DMAP (1 eq) and DCM (200 mL). The solution was chilled on ice, then

furoyl chloride (100 eq) in DCM (50 mL) was added dropwise. The ice bath was removed, and the mixture stirred at room temperature overnight. The organic layer was extracted with $NaHCO_3$ (5 x 100 mL), dried over $MgSO_4$, and the solvent removed under vacuum. The resulting compounds were purified by column chromatography.

N,N'-(octane-1,8-diyl)bis(furan-2-carboxamide) (**F1**)

The general procedure was carried out using 1,8-octanediamine (10.0 g, 69.3 mmol), triethylamine (14.2 g, 141 mmol), DMAP (0.17 g, 1.35 mmol) and furoyl chloride (19.0 g, 146 mmol). The resulting compound was purified by column chromatography (98:2 DCM:EtOAc), and the product obtained as a white solid (21.5 g/92%): R_f (50:50 DCM:EtOAc) = 0.29; mp = 135.3°C; ^{1}H NMR (400 MHz, DMSO): δ (ppm) 8.30 (t, 2H, *J* = 5.7 Hz), 7.80 (d, 2H, *J* = 1.0 Hz), 7.05 (d, 2H, *J* = 3.4 Hz), 6.60 (dd, 2H, *J* = 1.7 Hz), 3.18 (q, 4H, *J* = 6.7 Hz), 1.48 (m, 4H), 1.27 (m, 8H); ^{13}C NMR (400 MHz, DMSO): δ (ppm) 158.09, 148.61, 145.17, 113.39, 112.18, 38.87, 29.62, 29.17, 26.16; Electrospray MS (positive ion mode): calcd. for $C_{18}H_{24}N_2O_4Na$ $[M + Na]^+$: m/z = 355.38; found: 355.16.

N,N'-(cyclohexane-1,3-diylbis(methylene))bis(furan-2-carboxamide) (**F2**)

The general procedure was carried out using 1,3-cyclohexanebis(methylamine) (10.0 g, 70.3 mmol), triethylamine (14.2 g, 141 mmol), dimethylaminopyridine (0.17 g, 1.41 mmol), and furoyl chloride (19.0 g, 146 mmol). The resulting compound was purified by column chromatography (95:5 DCM:EtOAc), and the product obtained as a white solid (3.5 g/15%): R_f (50:50 DCM:EtOAc) = 0.23; mp = 204.3°C; ^{1}H NMR (400 MHz, DMSO): δ (ppm) 8.30 (t, 2H, *J* = 5.3 Hz), 7.80 (d, 2H, *J* = 3.7 Hz), 7.05 (d, 2H, *J* = 3.4 Hz), 6.60 (dd, 2H, *J* = 1.7 Hz), 3.04 (t,

4H, *J* = 5.3 Hz), 1.70 (m, 4H), 1.51 (m, 2H), 1.18 (m, 1H), 0.80 (m, 2H), 0.55 (m, 1H); ^{13}C NMR (400 MHz, DMSO): δ (ppm) 158.23, 148.56, 145.18, 113.45, 112.17, 45.30, 37.83, 35.37, 30.95, 25.50; Electrospray MS (positive ion mode): calcd. for $C_{18}H_{23}N_2O_4$ $[M + H]^+$: m/z = 331.39; found: 331.2.

N,N'-(1,3-phenylenebis(methylene))bis(furan-2-carboxamide) (**F3**)

The general procedure was carried out using m-xylylenediamine (10.0 g, 73.4 mmol), triethylamine (14.9 g, 147 mmol), dimethylaminopyridine (0.17 g, 1.41 mmol), and furoyl chloride (20.13 g, 154 mmol). The resulting compound was purified by column chromatography (95:5 DCM:EtOAc), and the product obtained as a white solid (21.8 g/92%): R_f (50:50 DCM:EtOAc) = 0.27; mp = 181.8°C; ^{1}H NMR (400 MHz, DMSO): δ (ppm) 8.88 (t, 2H, *J* = 6.1 Hz), 7.82 (d, 2H, *J* = 1.2 Hz), 7.1 – 7.3 (m, 6H), 6.61 (dd, 2H, J = 1.7 Hz), 4.39 (d, 4H, *J* = 6.2 Hz); ^{13}C NMR (400 MHz, DMSO): δ (ppm) 158.20, 148.33, 145.47, 140.05, 128.72, 126.62, 126.28, 113.88, 112.27, 42.33; Electrospray MS (positive ion mode): calcd. for $C_{18}H_{16}N_2O_4$ $[M + H]^+$: m/z = 325.04; found: 325.1, calcd. for $C_{16}H_{20}N_2O_4Na$ $[M + Na]^+$: m/z = 347.32; found: 347.1.

N,N'-((ethane-1,2-diylbis(oxy))bis(ethane-2,1-diyl))bis(furan-2-carboxamide) (**F4**)

The general procedure was carried out using 2,2'-(ethylenedioxy)bis(ethylamine) (10.0 g, 67.5 mmol), triethylamine (13.66 g, 135 mmol), dimethylaminopyridine (0.17 g, 1.41 mmol), and furoyl chloride (18.5 g, 142 mmol). The resulting compound was purified by column chromatography (95:5 DCM:EtOAc), and the product obtained as a white solid (10.9 g/48%): R_f (95:5 DCM:MeOH) = 0.33; mp = 72.4°C; ^{1}H NMR (400 MHz, DMSO): δ (ppm) 8.30 (t, 2H, *J* =

5.5 Hz), 7.80 (d, 2H, *J* = 0.9 Hz), 7.08 (d, 2H, *J* = 3.3 Hz), 6.60 (dd, 2H, *J* = 1.7 Hz), 3.55 (s, 4H), 3.49 (m, 4H), 3.35 (m, 4H); ^{13}C NMR (400 MHz, DMSO): δ (ppm) 158.28, 148.36, 145.36, 113.71, 112.24, 69.97, 69.31, 38.81; Electrospray MS (positive ion mode): calcd. for $C_{16}H_{20}N_2O_4Na$ $[M + Na]^+$: m/z = 359.33; found: 359.1.

3.3.4 Mixture preparation

In a typical example, equimolar amounts of bismaleimide and bisfuran were combined in a vial. DCM/MeOH (95:5 v/v, 5 mL) was then added and the vial was shaken to ensure complete dissolution. The solvent was then removed under vacuum, and the resulting solid mixture ground into a uniform powder.

3.3.5 Nanoindentation

Samples were prepared by transferring the powder mixture (~ 50 mg) to a steel sample disc (15 mm diameter). The disc was placed on a hotplate that was pre-heated approximately 20°C above the melting point of the mixture. Air bubbles that appeared during melting were removed by agitation of the liquid with a clean spatula. The sample discs were removed from the heat source and stored at 60°C, resulting in smooth films with relatively flat surfaces. Samples were allowed to equilibrate at room temperature for 1 h before measurements were made. A 10-2-10 load function was used (10 second load time, 2 second hold, and 10 second unload time) with a maximum load of 1000 μN. Longer hold times have been claimed to be more effective for nanoindentation of viscoelastic materials.[28] A hold time of 30 seconds was also attempted, but results for modulus and hardness were largely similar, and this often resulted in adhesion of compliant material to the indenter tip, which significantly affected subsequent measurements.

Measurements were made in 3 x 3 grids, with a spacing of 15 μm between each indentation. Three separate locations spaced at least 1 mm apart were used on each sample stub. Values reported represent an average of these 27 measurements. Control samples (PMMA, quartz) were measured before and after each set of measurements to ensure that measurements were within 5% of their expected values.

3.3.6 ^{1}H NMR kinetics

Solid films were stored at 60°C for the specified period of time, and then dissolved in the NMR solvent. Reversion to furan/maleimide was accomplished by melting 10 mg of the neat sample in an NMR tube, and then immediately quenching in liquid nitrogen. The resulting solid was then dissolved in the NMR solvent.

3.3.7 DSC kinetics

Separate samples were prepared for each designated aging time. Samples were weighed and crimped in aluminum DSC pans, and subjected to a heat/cool/heat cycle. The pans were then stored at 60°C for the specified period of time, and then subjected to another heat/cool/heat cycle.

3.3.8 Adhesion testing

Two 3/8” diameter dowels made of stainless steel (grade 303) were pre-heated approximately 20°C above the melting point of the monomer mixture. The powdered mixture (5 ± 0.5 mg), which had been compressed into pellet form for easier handling, was then carefully placed on the polished surface of the dowel. The solid completely melted within seconds, and an alignment sleeve was then slipped over the first dowel, and a second dowel placed in the tube

onto the surface of the molten sample, applying minimal downward pressure. The sleeve was bored to allow 0.002" clearance, to ensure perfect alignment of the two dowels. The top dowel was turned gently for three complete revolutions to ensure complete surface area coverage at the interface of the two dowels. Only the weight of the upper dowel (30.38 ± 0.03g) was used to compress the liquid samples. The samples were incubated at 60°C for four days, and then equilibrated at room temperature for 1 h prior to testing for tensile strength. Eight samples were prepared for each test. Samples were tested on an Instron 3367 at an extension rate of 100 μm per minute until complete fracture had occurred. The highest and lowest values were eliminated, and the results for breaking strength reported as an average of the six remaining measurements.

3.4 Results and Discussion

3.4.1 Synthetic Procedures

Four pairs of bismaleimides and bisfurans, varying only in their linking chemistry, were prepared and characterized. Four different diamines, including n-octyl, 1,3-dimethylcyclohexyl, 1,3-dimethylphenyl, and 1,2-dimethoxyethane, were used as starting materials such that the spacer chain between the two functional groups contained approximately the same number of atoms (Scheme 3.1). The bismaleimides were prepared by condensation of two equivalents of maleic anhydride with the diamine using sodium acetate and acetic anhydride. The bisfurans were prepared using the same series of diamines coupled with two equivalents of furoyl chloride. The bisfurans therefore had amide linkages to the furan rings, thus their spacer groups were somewhat different from those of the bismaleimides. Nonetheless, the spacer chains within each of the bisfuran and bismaleimide series were consistent, and the resulting monomers therefore

represented a series having linear alkyl, dimethylcyclohexyl, dimethylphenyl and ethylenedioxy linkages (Scheme 3.1).

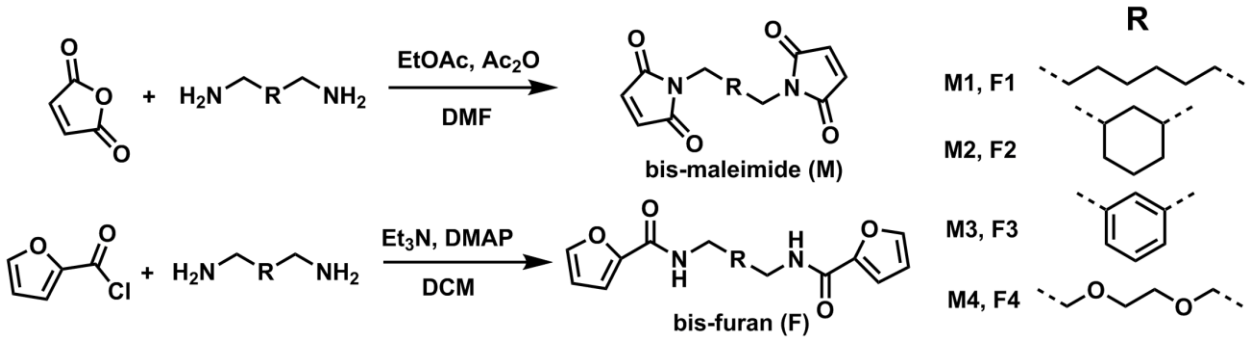

Scheme 3.1. Synthetic pathway to bismaleimides and bisfurans.

3.4.2 Monomer Characterization

Each of the eight compounds was characterized by DSC to determine their melting and crystallization transitions. For each compound, sharp melting peaks were observed that spanned a wide temperature range, commensurate with the substantial differences in chemistries of the four spacer groups (Table 3.1). Crystallization peaks were observed on the cooling cycle only for compounds **M1**, **F1** and **M2**, **F2**, consistent with the difference in crystallinity of the four spacer groups.

Table 3.1. Melting (mp) and crystallization points (Cp) of bismaleimides and bisfurans.

Bismaleimides			**Bisfurans**		
Compound	mp (°C)	Cp (°C)	Compound	mp (°C)	Cp (°C)
M1	124.5	91.8	**F1**	135.3	93.2
M2	161.3	144.3	**F2**	204.3	167.0
M3	129.8	-	**F3**	181.8	-
M4	98.1	-	**F4**	72.4	-

Complete dissolution of equimolar amounts of bismaleimide and bisfuran in DCM/MeOH (95:5 vol%) ensured intimate mixing of the two compounds. Solvent removal under reduced pressure resulted in white solids, which were then ground into powders. In all cases, ^{1}H NMR spectroscopy confirmed that the mixtures consisted of two discrete compounds, with no extraneous peaks indicative of DA coupling. Comparison of integration values of the signals corresponding to the α-vinyl protons of the furan and the two equivalent maleimide vinyl protons (at 7.8 and 7.0 ppm, respectively), confirmed that the two compounds were present in a 1:1 equimolar ratio.

The powdered mixtures were heated until complete melting had occurred. Viscosities of the molten mixtures were all below 100 cPs, making them easily manageable for all forms of material processing (Figure 3.3a).[29] The apparent dilatant behavior of the two mixtures **M2/F2** and **M3/F3** was attributed to the higher measurement temperature required for these compounds, which may have resulted in irreversible cross-linking of the maleimide resins **M2** and **M3** during the course of the measurement.[30] Fresh samples of **M2/F2** and **M4/F4** were then measured at 190°C, and this resulted in comparable thickening behavior for both compounds (Figure 3.3b). The new measurements were made at constant shear rate (100 s^{-1}), so as to eliminate dilatant behavior as a potential cause for the increase in viscosity. While the former compound did undergo a more rapid rise in viscosity, both polymers clearly experienced substantial thickening

when held at an elevated temperature, indicating that some degree of cross-linking had occurred. Further evidence for the temperature dependence of the viscosity increase was obtained with the mixture **M4/F4**, which was measured at several temperatures ranging from 90°C to 190°C (Figure 3.4). Initial viscosities were found to decrease with increasing temperature as might be expected. However, prolonged exposure to elevated temperatures led to substantial increases in viscosity, which became more pronounced as the measurement temperature was increased. In all cases, cooling and re-melting of the samples did not restore the low viscosities originally observed, confirming the irreversible nature of the reaction. To minimize the extent of this reaction, the molten samples were removed from the heat source within 5-10 seconds of melting and cooled to 60°C to enable solidification. Cooling of the molten mixtures resulted in the formation of clear tacky resins which, upon standing, turned to hard solid films. Interestingly, **M1/F1** and **M4/F4** remained tacky for several hours after cooling, while **M2/F2** and **M3/F3** turned to clear, hard solid films immediately upon removal of the heat source. Further, **M1/F1** became completely opaque upon cooling, while **M2/F2**, **M3/F3**, and **M4/F4** remained as clear films indefinitely (Figure 3.5). The opacity observed in **M1/F1** was attributed to the crystalline nature of the linear alkyl chains, and indeed X-Ray Diffraction (XRD) analysis revealed a significant degree of crystallinity in the **M1/F1** mixture, while the other three mixtures were found to be amorphous (Figure 3.6). Control experiments, in which the components **M1 – M4** and **F1 – F4** were melted individually, yielded either sticky films that did not harden with time, or crystalline solids with no film forming capacity.

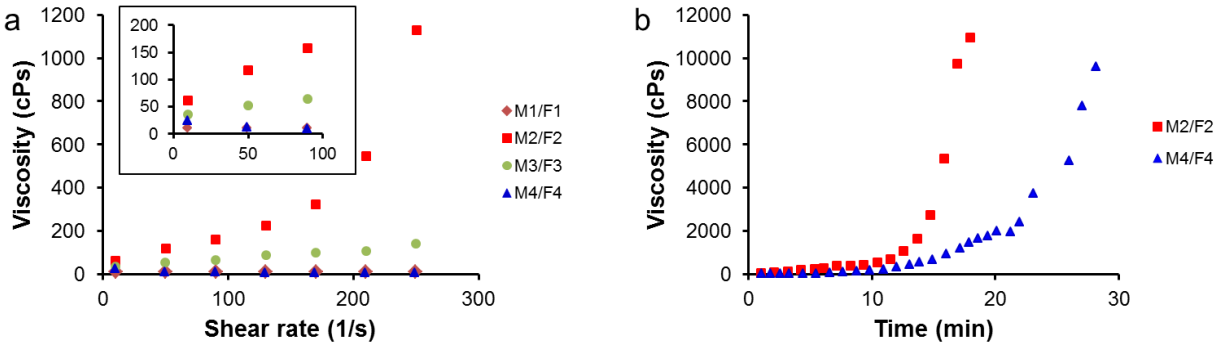

Figure 3.3. Viscosity of molten M/F mixtures measured under conditions of increasing shear rate:a) **M1/F1** measured at 120°C, **M2/F2** measured at 190°C, **M3/F3** measured at 150°C, **M4/F4** measured at 90°C. Inset shows magnified scale at low shear rates; b) viscosity of molten mixtures **M2/F2** and **M4/F4** measured at 190°C at constant shear rate (100 s^{-1}).

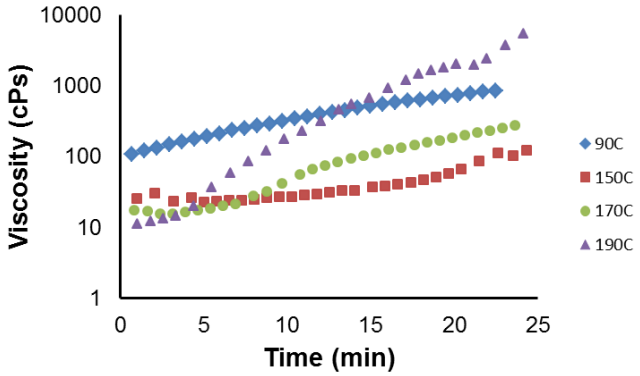

Figure 3.4. Viscosity of molten mixture **M4/F4** measured at varying temperatures under constant shear rate (100 s-1).

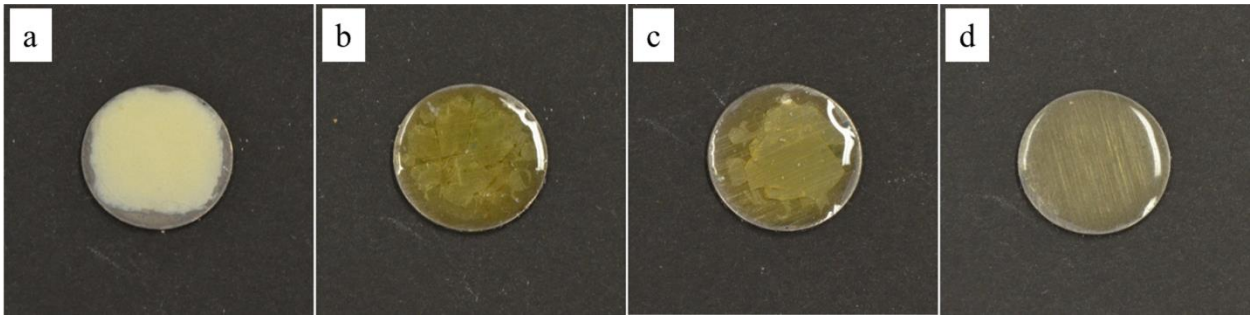

Figure 3.5. Polymer films cast from molten mixtures: a) **M1/F1**; b) **M2/F2**; c) **M3/F3**; d) **M4/F4**.

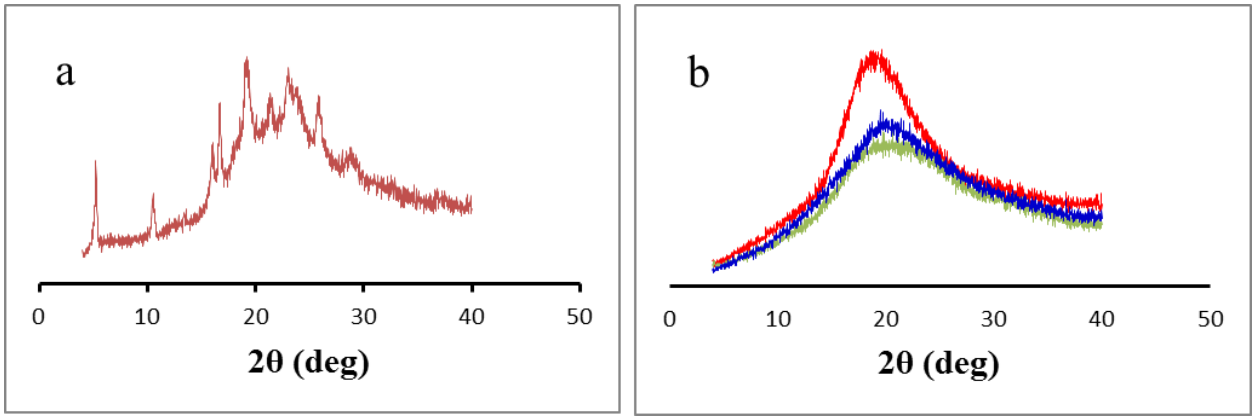

Figure 3.6. X-Ray Diffraction data for polymerized materials: a) data for the **M1/F1** mixture; b) data for **M2/F2** (brown), **M3/F3** (pink), and **M4/F4** (blue) mixtures.

3.4.3 ^{1}H NMR spectroscopy

^{1}H NMR spectroscopy confirmed that reversible Diels Alder coupling of the furan and maleimide moieties had occurred (Figures 3.7, 3.19 – 3.22). Figure 3.7a shows the spectrum for the unheated mixture of the two powdered components **M4** and **F4** in an equimolar ratio. All peak assignments and integrations corresponded to the peaks observed in the spectra of the individual components, confirming that coupling had not occurred between the two compounds

prior to heating. After a single melt/cool cycle, the resulting solid film was stored for 7 days at 60°C. The spectrum of the resulting material was consistent with the formation of a DA adduct (Figure 3.7b). Specifically, a new peak, attributed to the bridgehead proton on the newly formed fused ring system, emerged at 5.2 ppm. Further, the appearance of a doublet of doublets centred at 6.6 ppm could be attributed to the new norbornyl double bond. These new signals increased in intensity in a 2:1 ratio, consistent with the number of protons generating the signals. Two additional signals would be expected from the protons at the junction of the two fused rings, but these peaks were obscured in the aliphatic region of the spectrum. Melting of the solid film, followed by a rapid quench in liquid nitrogen, almost completely restored the original spectrum (Figure 3.7c), thus confirming the reversibility of the reaction. It should be noted that the signal at 7.8 ppm did not quantitatively disappear during the incubation period, indicating that the DA polymerization did not go to completion. Kinetic studies were therefore undertaken for each of the four mixtures to quantify the degree of polymerization in each case.

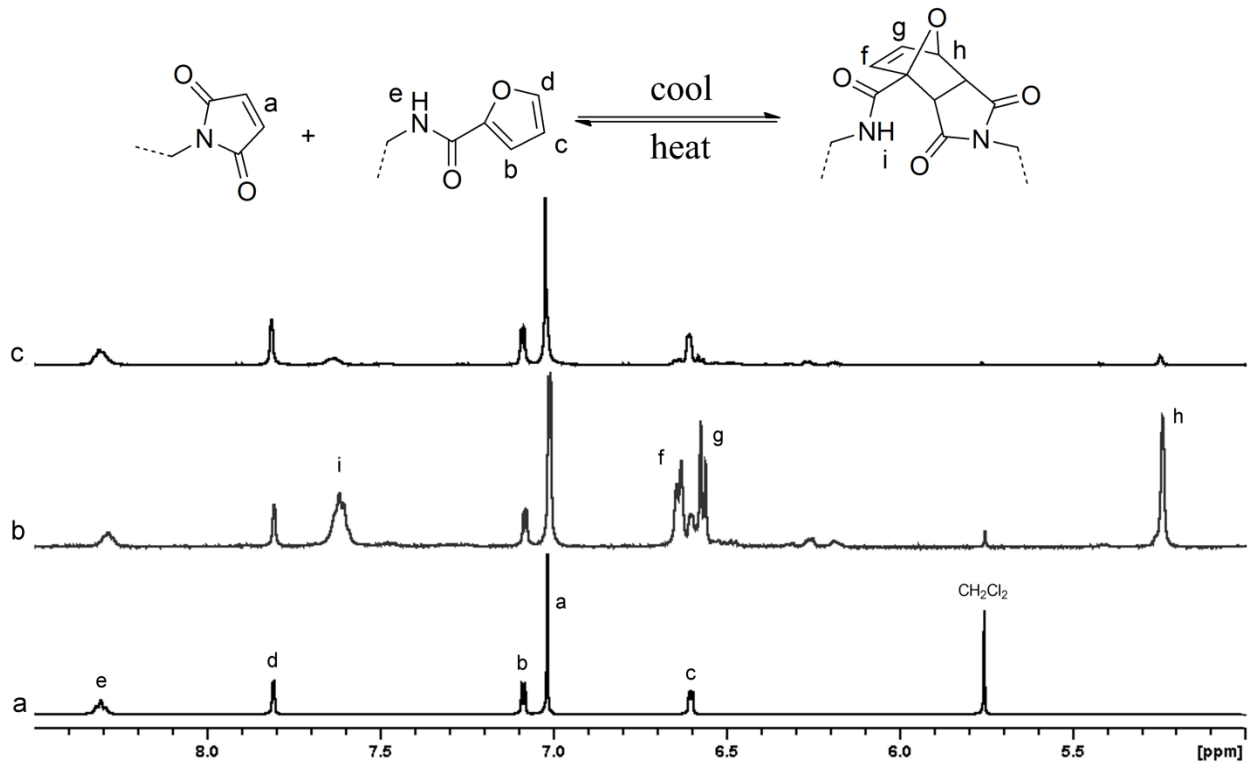

Figure 3.7. ^{1}H NMR showing the reversible polymerization of **M4/F4**: Spectra were recorded: a) prior to melting; b) after melting and incubation at 60°C for 7 days; c) after re-melting and rapid quenching in liquid nitrogen. Similar data for the other mixtures can be found in Supporting Information, Figures 3.19 – 3.22.

3.4.4 DA Reaction Kinetics

Molten mixtures were cooled and aged at 60°C as described above, and ^{1}H NMR spectra were acquired at specific time intervals. The ratio of the newly formed product peak at 5.2 ppm to the original vinyl furan peak at 7.8 ppm served as an indicator of polymer conversion, which was calculated using the formula $i_{5.2}/(i_{5.2} + i_{7.8})\times100\%$, where i_x is the integral of the NMR peak at x ppm. Mixtures **M1/F1** and **M4/F4**, while having similarly slow hardening times, had significantly different polymer conversion percentages, the former having a much lower value

(Figure 3.8). It is believed that the inherent crystallinity in **M1/F1** restricted mobility of the maleimide and furan moieties in the cooled film, thus suppressing more extensive DA coupling. Despite its slow hardening rate, the **M4/F4** mixture exhibited the fastest and most extensive polymerization, presumably enabled by the flexibility of the diether linkers.

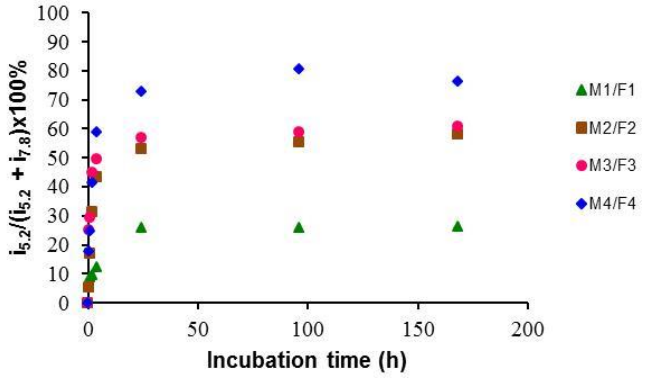

Figure 3.8. Polymer conversion percentages over time, determined by ^{1}H NMR spectroscopy.

3.4.5 Thermal Analysis of DA Polymers

Thermal analysis was performed on both the monomeric powder mixtures and the solidified polymers and provided further evidence for polymerization. Initial heating of the maleimide and furan powders produced a sharp melting peak. A second heating of the mixture immediately following the cooling cycle resulted in the disappearance of this peak, and the appearance of two weaker endothermic transitions at ca. 100°C and 135°C representing, respectively, the collapse of the endo and exo stereoisomers of the DA polymer via the retro-DA reaction. Thermal analysis was performed on both the monomeric powder mixtures and the solidified polymers and provided further evidence for polymerization (Figure 8). Initial heating of the maleimide and furan powders produced a sharp melting peak. A second heating of the

mixture immediately following the cooling cycle resulted in the disappearance of this peak, and the appearance of a very weak, broad, endothermic peak corresponding to the cleavage (retro-DA reaction) of a small number of DA linkages that were formed in the short duration of sample cooling. After the initial heat-cool-heat cycle was completed, samples were cooled and stored at 60°C and the heat-cool-heat cycle was repeated after 1, 4 and 7 days. Upon first heating of the incubated samples, two endothermic transitions were observed at ca. 100°C and 135°C representing, respectively, the collapse of the endo and exo stereoisomers of the DA linkages within the polymer via the retro-DA reaction. After 24 hours of incubation, the size of the two new peaks was significant, commensurate with the growth of the polymer during that time. In each case, a second heating (dashed line) resulted in the single broad endothermic peak observed in the initial heat/cool/heat cycle, corresponding to the formation and cleavage of only the exo DA linkages. Peak intensities did not change substantially after 24 hours of aging, confirming that polymer conversion was maximized after 24 hours, which is consistent with the observed NMR data (above). Interestingly, the peak at lower temperature diminished in size after 7 days of incubation. It is believed that this is due to a slow isomerization of the endo form of the DA adduct to the more thermodynamically stable exo form. The appearance of only a single peak at ca. 135°C for the polymer **M4/F4,** regardless of incubation time, is attributed to the long solidification times of the resulting polymer, which led to the formation of only the more thermodynamically stable isomer.[31] A glass transition would also be expected to appear in each trace, although this was only observed for the polymer **M4/F4** at ca. 65°C. It is believed that the glass transitions for the polymers having more rigid spacers occurred at higher temperatures, and were thus obscured by the two broad peaks arising from the retro-DA reaction.[31] A glass transition would also be expected to appear in each trace, although this was only observed for the

polymer **M4/F4** at ca. 65°C. It is believed that the glass transitions for the polymers having more rigid spacers occurred at higher temperatures, and were thus obscured by the two broad peaks arising from the retro-DA reaction. After the initial heat-cool-heat cycle was completed, samples were cooled and stored at 60°C and the heat-cool-heat cycle repeated after 1, 4 and 7 days. After 24 hours of incubation, the size of the two new peaks had grown significantly, commensurate with the growth of the polymer during that time. In each case, a second heating (dashed line) resulted in the two weaker transitions seen in the initial heat/cool/heat cycle. Peak intensities did not change substantially after 24 hours of aging, confirming that polymer conversion was maximized after 24 hours, which is consistent with the observed NMR data (above). Interestingly, the peak at lower temperature diminished in size after 7 days of incubation. It is believed that this is due to a slow isomerization of the endo form of the DA adduct to the more thermodynamically stable exo form.[31]

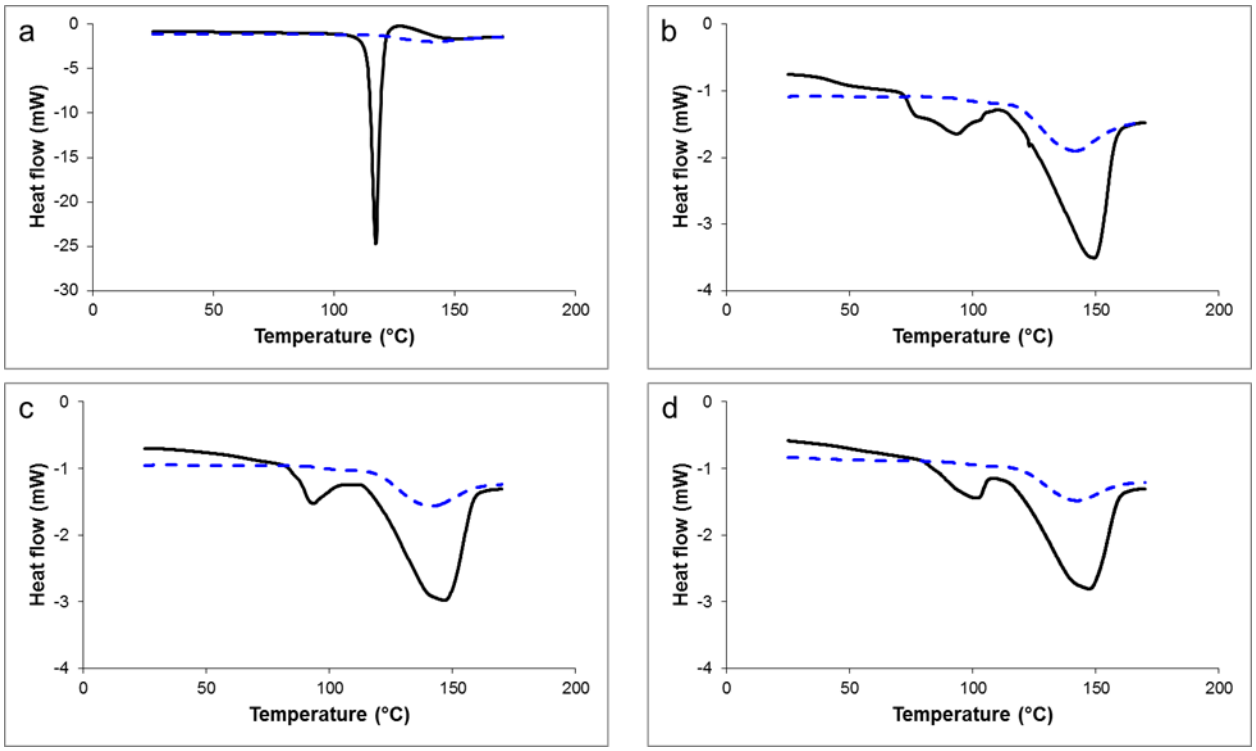

Figure 3.9. DSC cycling of the **M1/F1** mixture: Initial heating (solid line), second heating, immediately following first (dashed line). a) Dry blended mixture of the monomers; b) 24 hours after initial heat/cool/heat cycle; c) 4 days after initial heat/cool/heat cycle; d) 7 days after initial heat/cool/heat cycle. Exothermic transitions point upward. DSC traces for all mixtures can be found in Supporting Information, Figures 3.16 – 3.18.

3.4.6 Nanoindentation

Rheology of the films was measured using a Hysitron® nanoindenter. The inherent brittleness of the polymers precluded sample preparation for conventional DMA analysis, thus rheology of the films was determined using nanoindentation. This technique is commonly used to determine rheological characteristics of a wide variety of materials.[32-34] An indenter tip with well-known geometry is used to penetrate a sample film under load controlled conditions. The depth of penetration can be used to calculate the exact area of indentation, which in turn allows

for calculation of the hardness (H) of the material, as the maximum load over the area of penetration. A plot of the load vs displacement of the tip during indentation can be recorded, and the stiffness and reduced modulus (E_r) of the material calculated from the unloading curve. This allows for rheological measurements of samples in their working state; measurements can be made on thin films cast by simple melting and cooling of the small molecule mixtures. Samples were prepared by melting the powdered mixtures on a 15 mm diameter metal disc. Measurements were made directly on the films after aging for four days at 60°C on three remote spots on each disc in 3x3 grids with a spacing of 15 µm between each indent. A load of 1000 µN with a 10 second loading time, 2 second hold and 10 second unloading time (10-2-10 load function) was used. Modulus and hardness data for the four sets of compounds, averaged from the 27 separate indentation measurements made for each compound, are provided in Figure 3.10.

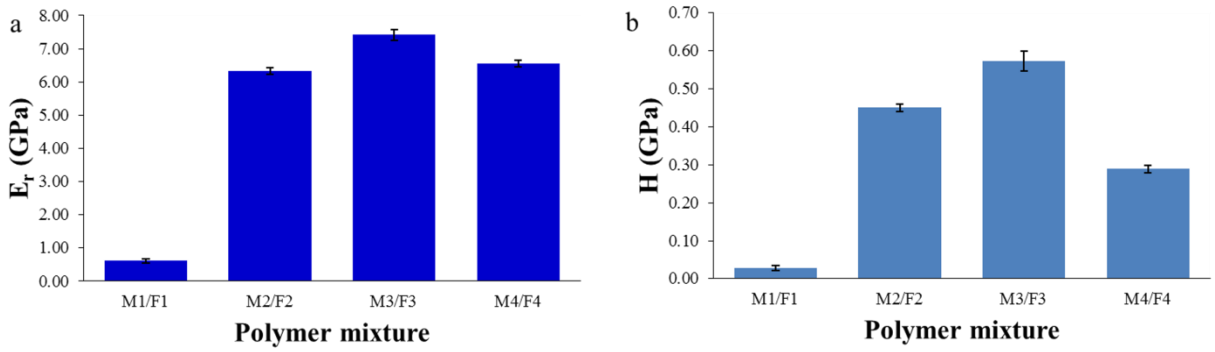

Figure 3.10. Rheological data of polymer films measured by nanoindentation: a) reduced modulus; b) hardness.

Hardness data indicated that **M1/F1** was dramatically softer than the other three mixtures although this did not seem to be the case macroscopically. The **M1/F1** samples exhibited a much higher degree of macro roughness on the crystalline surface, making them difficult to measure by

nanoindentation. Furthermore, they were significantly more brittle than the other three polymers, and had a decidedly lower level of adhesion to metal, often resulting in complete delamination of the films from the metal support stubs. It is therefore conceivable that some degree of delamination had occurred on the samples being measured, which would profoundly influence the nanoindentation measurement. This is supported by the images in Figure 3.11, which depict micrographs of the indents made in each sample. The nine indents made in the **M1/F1** sample are not observed, while they are clearly visible in the other samples. This could be attributed to elastic response of the material to the indents or to micro-delamination, resulting in a lack of compression of the film by the nanoindenter tip. Attempts to bond the film to the metal support stub using epoxy resins did not influence the data.

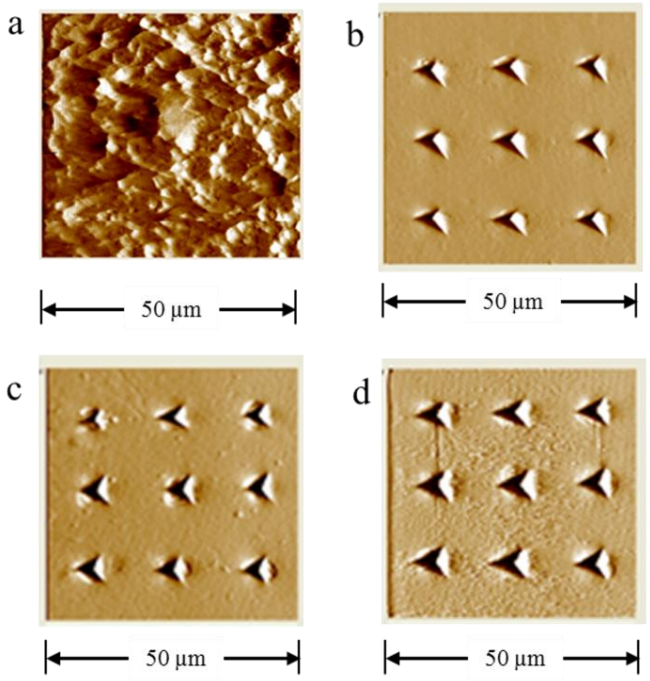

Figure 3.11. Micrographs showing typical 3x3 nanoindentation grids for: a) **M1/F1**; b) **M2/F2**; c) **M3/F3**; d) **M4/F4**.

Hardness and modulus of the polymer films could not be directly correlated to the rate or conversion data reported in Figure 3.8. While **M4/F4** produced the highest polymer conversion rate, it was not the hardest of the films measured. Thus it appears that both the rigidity of the spacer chain and % polymer conversion play a role in the hardness of the polymer film. Kinetic data of the rheology of the films could not be determined for the first 24 hours of curing as the initial samples were too soft for measurement by nanoindentation.

The mixture **M4/F4** afforded polymers having excellent film forming characteristics, but required a long time to harden, and was ultimately found to be softer than either of the other film formers **M2/F2** and **M3/F3**. We therefore decided to explore the effects of combining the **M4/F4** monomer mixture with **M1/F1**, **M2/F2**, and **M3/F3** to potentially capture the advantages of both materials in each combination. Mixtures containing the maleimide/furan couples in 4:1, 1:1, and 1:4 ratios were prepared, and polymer films were cast for rheological evaluation. The mixture **M4/F4** + **M1/F1** in a 4:1 ratio afforded a film that remained smooth and transparent after several weeks, thus demonstrating that the crystalline and amorphous materials could be combined to provide clear, hard films (Figure 3.12). Higher loadings of the crystalline **M1/F1** resulted in rough, opaque films, similar to the **M1/F1** mixture itself. Nevertheless, a clear trend in hardness and modulus data could be observed for a series of mixtures of the two monomer pairs (Figure 3.13). Combination of **M4/F4** with the cyclohexyl spaced monomers **M2/F2** yielded smooth, transparent films also having a clear trend in rheological characteristics. Hardness values were found to increase with increasing loading of the harder **M2/F2** monomers, while solidification times, noted by an audible click when the polymer films were tapped with a spatula, decreased with an increased loading of **M2/F2**. Similar observations were made with the combination of **M4/F4** and **M3/F3** (Figure 3.13). Combination of the two mixtures therefore resulted in harder

films while retaining the film forming characteristics of the softer material, which was the intended result.

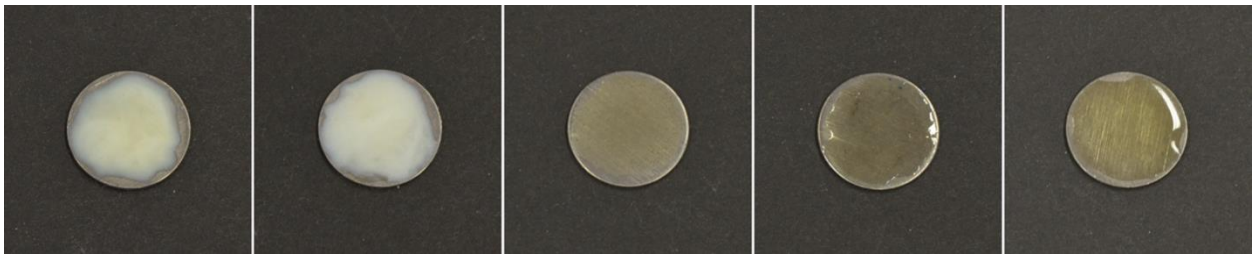

Figure 3.12. Polymer films cast from molten mixtures of **M4/F4** and **M1/F1** in ratios of: a) 0:100; b) 20:80; c) 50:50; d) 80:20; e) 100:0.

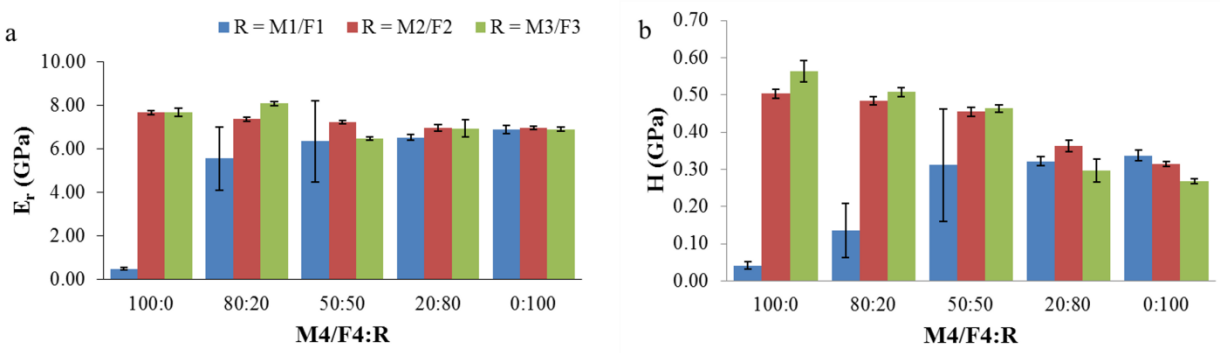

Figure 3.13. Rheological data of polymer films measured by nanoindentation: a) reduced modulus; b) hardness.

3.4.7 Polymer Adhesive Strength

While the polymers prepared in this study were found to be brittle, they also demonstrated a very high level of adhesion to the steel nanoindentation support stubs. We attempted to quantify the adhesion using a technique based on the American Society for Testing and Materials (ASTM)

Method D2095,[35] used for measuring the tensile strength of adhesives. A controlled amount of each mixture was melted between two pre-heated stainless steel dowels, and, after cooling, tested for tensile adhesive strength (for images of the test apparatus, see Supporting Information Figure 3.25). The brittleness and lack of adhesion to the nanoindentation sample stubs was in evidence here as the **M1/F1** mixtures completely failed upon handling of the dowels after they had cooled to room temperature. Furthermore, the brittle polymers **M2/F2** and **M3/F3** had lower adhesive strength than the more flexible **M4/F4**. It is significant that all three of these materials showed considerably higher adhesion than a typical film forming polymer such as polyethylene glycol (PEG, M_n = 14,000) (Figure 3.14). While brittleness and wettability would be expected to play a key role in adhesion, the adhesion data for the reversible polymers also correlated well to the degree of polymerization discussed earlier (Figure 3.8). It is therefore difficult to determine the most significant factor affecting adhesive strength, although we have demonstrated that adhesive strength is strongly influenced by spacer chemistry.

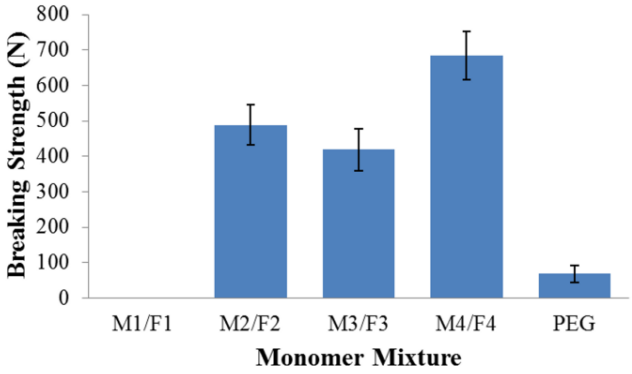

Figure 3.14. Breaking strength of polymer mixtures.

In keeping with our experiments combining the most elastic with the hardest materials for rheological evaluation (Figure 3.13), we tested the adhesive strength of the combination **M4/F4**

and **M3/F3**. Mixtures comprised of 50:50 and 80:20 **M4/F4:M3/F3** were prepared and characterized using the same tensile test described above. As was found with the rheological properties of the polymer mixtures (Figure 3.13), a trend could be observed from the stronger (**M4/F4**) to the weaker (**M3/F3**) adhesive. Interestingly, we did not find that the adhesion strength of the polymer was improved by any mixture of of **M4/F4:M3/F3**, with the best adhesion coming from the **M4/F4** sample alone (Figure 3.15).

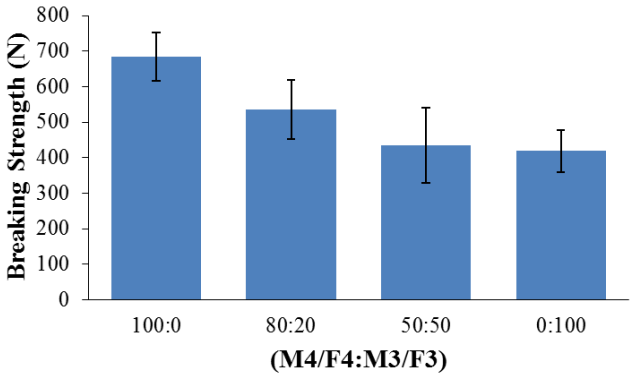

Figure 3.15. Breaking strength of polymer mixtures comprised of **M4/F4** and **M3/F3**.

3.5 Conclusions

Linear reversible polymers, based on maleimide-furan DA linkages, have been prepared and characterized in monomeric and polymeric form. Melting and cooling of equimolar amounts of a bismaleimide and bisfuran resulted in hard films with moduli and hardness ranging from 0.6-8 GPa and 0.1-0.6 GPa respectively, as measured by nanoindentation. Solidification times of these films varied greatly, from seconds to hours. Differences in morphology were also observed, as the films ranged from opaque, crystalline solids to clear hard solids. Mixtures of the polymers having different spacer chemistries leveraged the advantages of both materials, resulting in rapidly solidified, hard materials with excellent film forming characteristics. Adhesive strength

was measured and found to be higher than a conventional film forming polymer (PEG). Reversibility of the polymerization was verified by ^{1}H NMR spectroscopy and DSC. Degree and rate of polymerization, as well as rheological properties and adhesion, were found to be dependent on the chemistry of the spacer molecule joining the functional endgroups. Practically speaking, this would provide a wide range of properties and working temperatures for polymer formation and processing.

3.5.1 Acknowledgements

The authors wish to acknowledge Sonja Hadzidedic for completing numerous DSC analyses and for providing useful discussion. This work was financially supported by Xerox Research Centre of Canada (XRCC).

3.6 Supporting Information

Effect of spacer chemistry on the formation and properties of linear reversible polymers

James D. Mayo, Alex Adronov

Prof. A. Adronov

McMaster University

1280 Main Street West

Hamilton, ON

L8S 4L8

J.D. Mayo

Xerox Research Centre of Canada

2660 Speakman Drive

Mississauga, ON

L5K 2L1

e-mail: adronov@mcmaster.ca

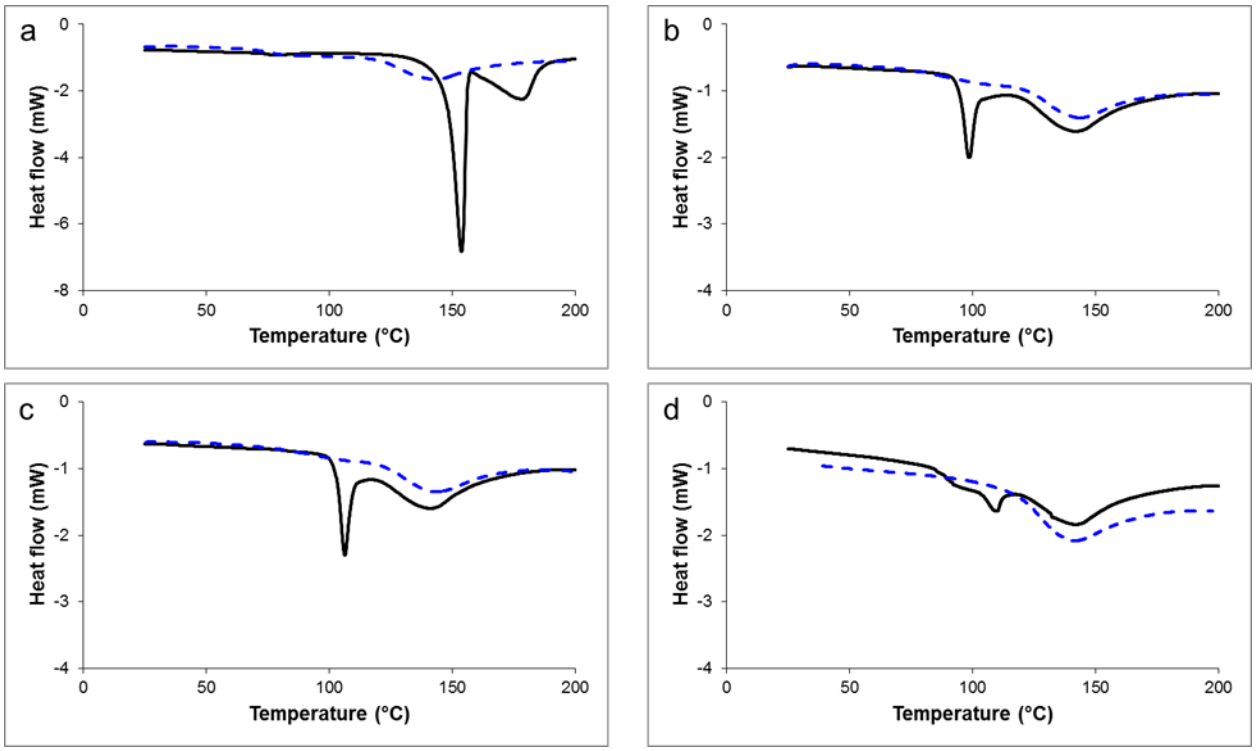

Figure 3.16. DSC cycling of **M2/F2**: a) dry blended mixture; b) 24 hours after initial heat/cool/heat cycle; c) 4 days after initial heat/cool/heat cycle; d) 7 days after initial heat/cool/heat cycle. Initial heating (solid line), second heating, immediately following first (dashed line). Exothermic transitions point upward.

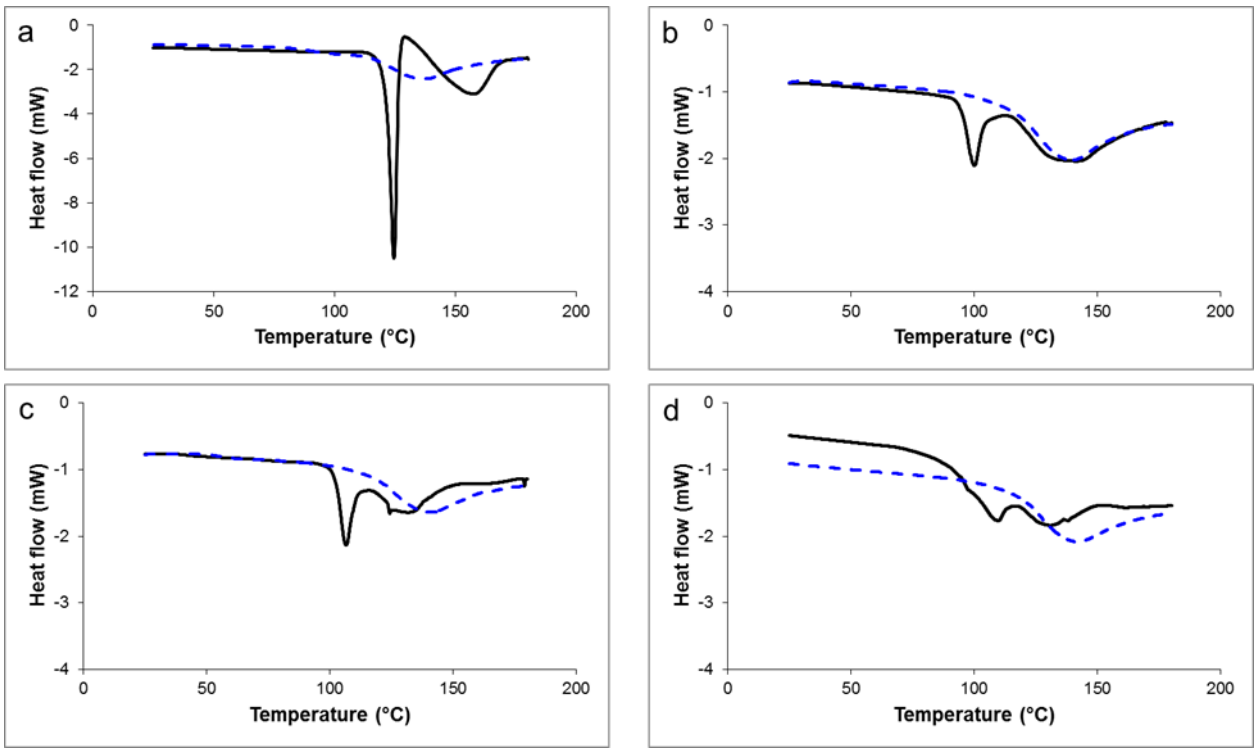

Figure 3.17. DSC cycling of **M3/F3**: a) dry blended mixture: b) 24 hours after initial heat/cool/heat cycle; c) 4 days after initial heat/cool/heat cycle; d) 7 days after initial heat/cool/heat cycle. Initial heating (solid line), second heating, immediately following first (dashed line). Exothermic transitions point upward.

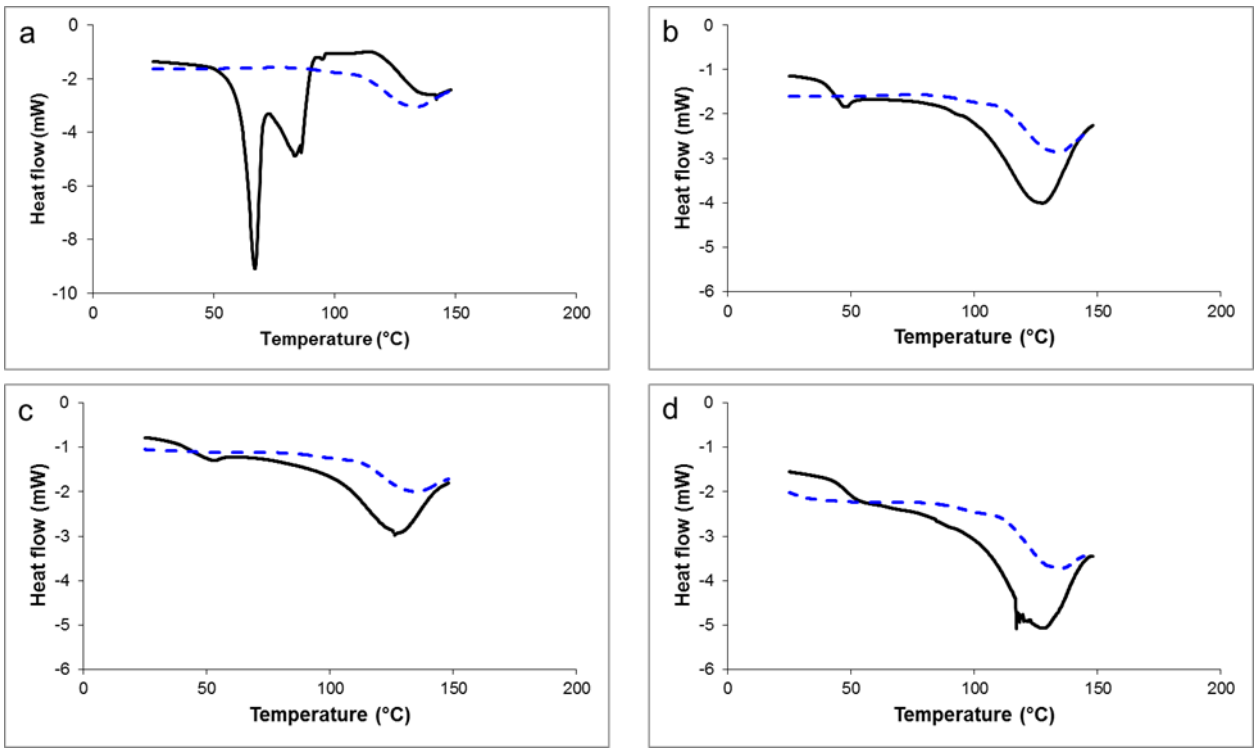

Figure 3.18. DSC cycling of **M4/F4**:a) dry blended mixture; b) 24 hours after initial heat/cool/heat cycle; c) 4 days after initial heat/cool/heat cycle; d) 7 days after initial heat/cool/heat cycle. Initial heating (solid line), second heating, immediately following first (dashed line). Exothermic transitions point upward.

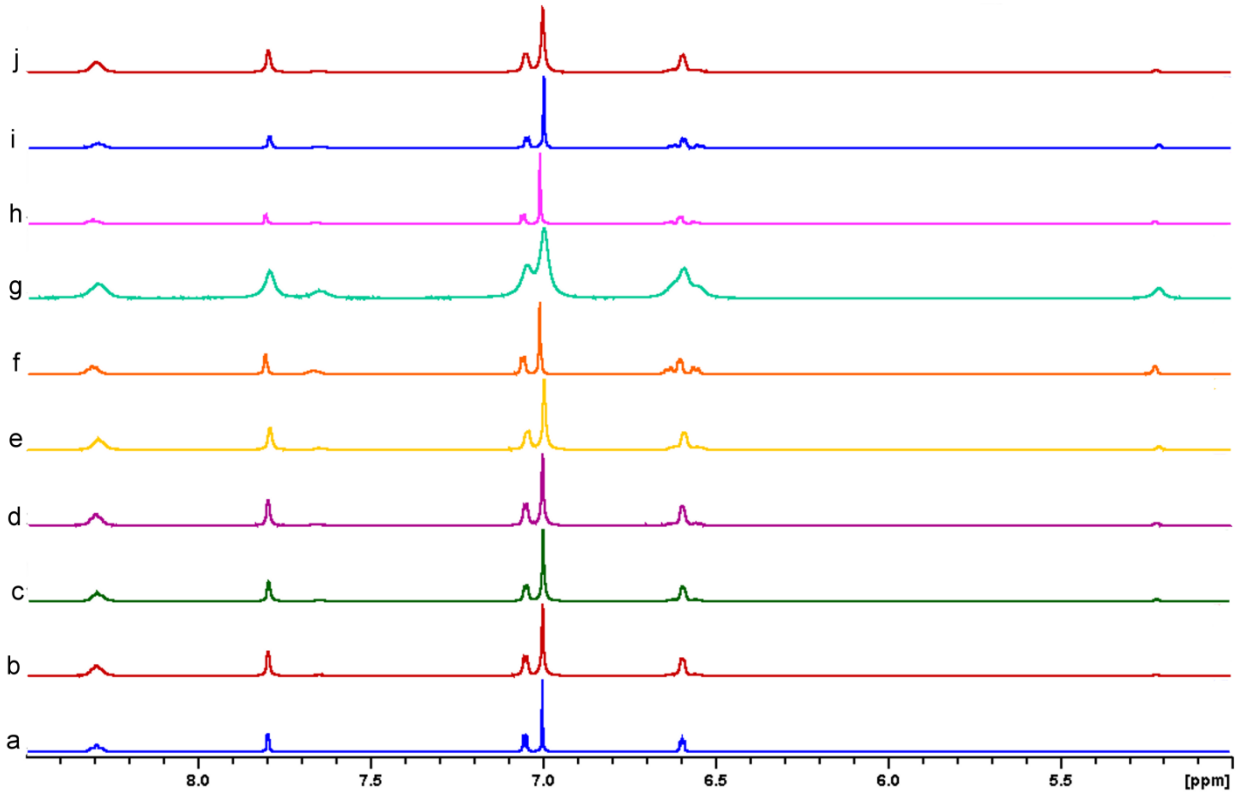

Figure 3.19. ^{1}H NMR kinetic study of polymerization of **M1/F1**: a) dry blended mixture. Sample was melted and then stored at 60°C for: b) 30 minutes; c) 1 h; d) 2 h; e) 4 h; f) 8 h; g) 24 h; h) 4 days; i) 7 days; j) sample was re-melted and quenched in liquid nitrogen.

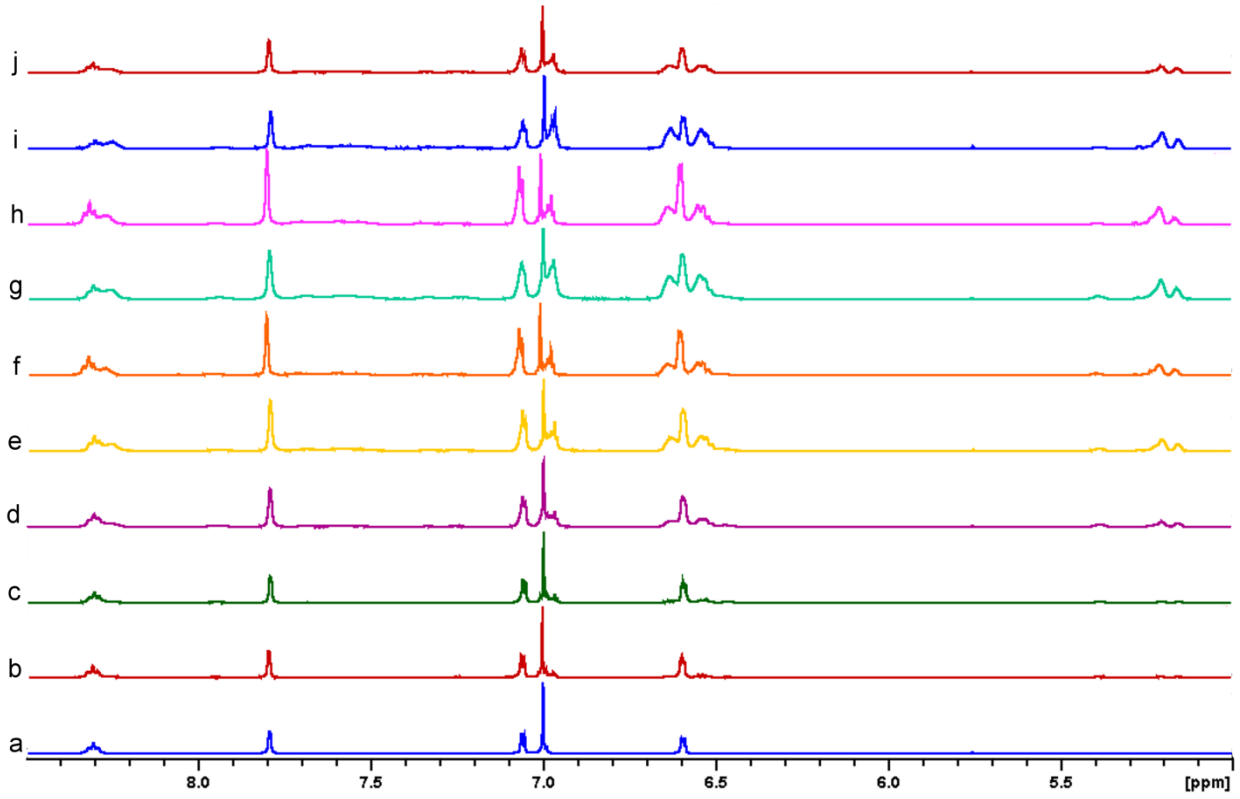

Figure 3.20. ^{1}H NMR kinetic study of polymerization of **M2/F2**: a) dry blended mixture. Sample was melted and then stored at 60°C for: b) 30 minutes; c) 1 h; d) 2 h; e) 4 h; f) 8 h; g) 24 h; h) 4 days; i) 7 days; j) sample was re-melted and quenched in liquid nitrogen.

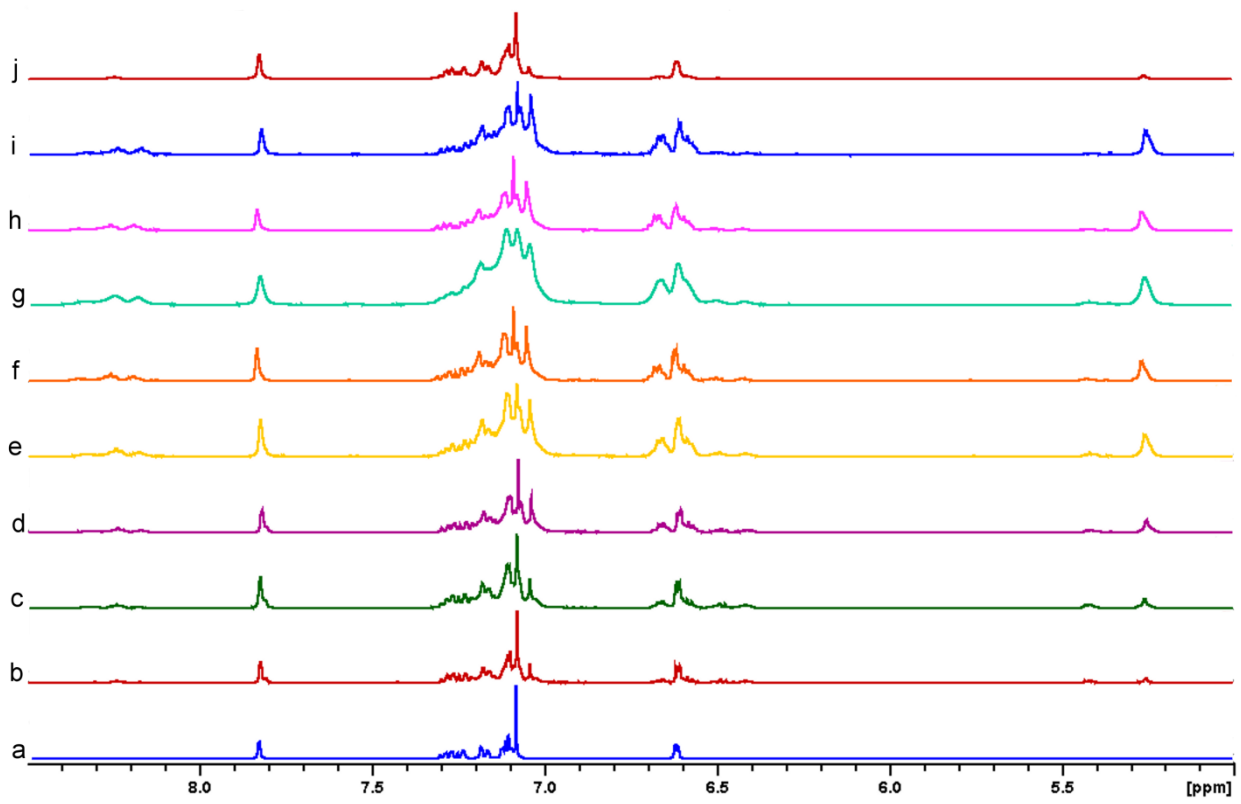

Figure 3.21. ^{1}H NMR kinetic study of polymerization of **M3/F3**: a) dry blended mixture. Sample was melted and then stored at 60°C for: b) 30 minutes; c) 1 h; d) 2 h; e) 4 h; f) 8 h; g) 24 h; h) 4 days; i) 7 days; j) sample was re-melted and quenched in liquid nitrogen.

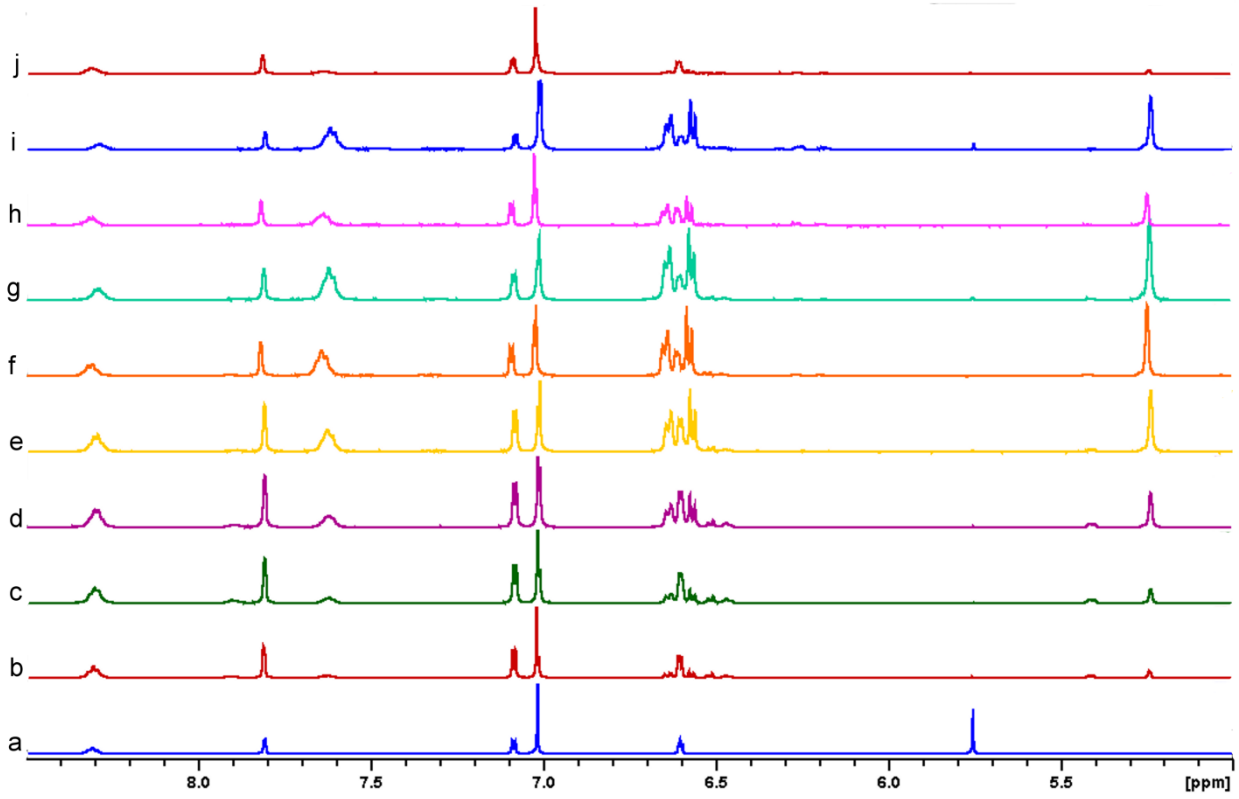

Figure 3.22. ^{1}H NMR kinetic study of polymerization of **M4/F4**: a) dry blended mixture. Sample was melted and then stored at 60°C for: b) 30 minutes; c) 1 h; d) 2 h; e) 4 h; f) 8 h; g) 24 h; h) 4 days; i) 7 days; j) sample was re-melted and quenched in liquid nitrogen.

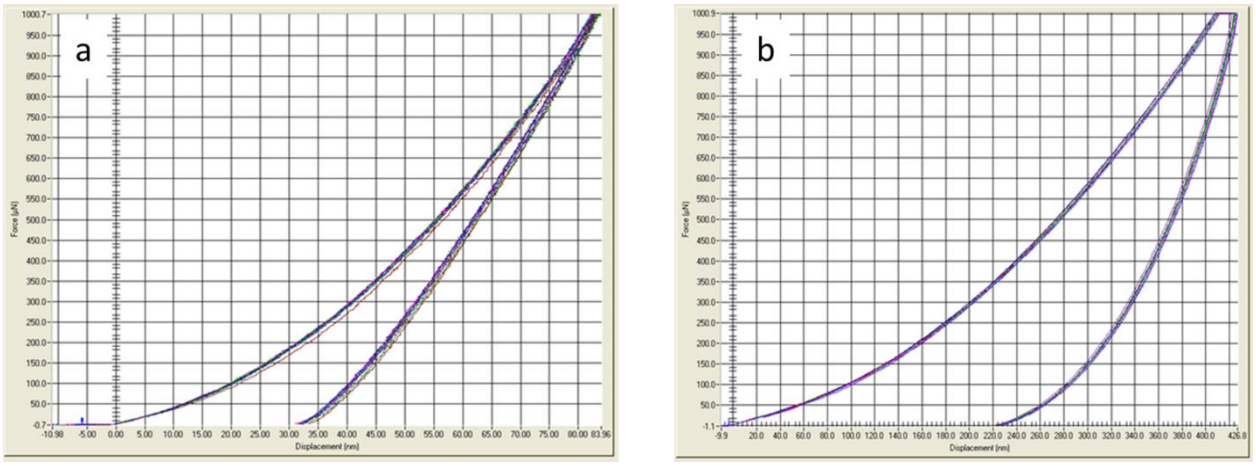

Figure 3.23. Typical load/unload curves for calibration standards: a) quartz; b) PMMA.

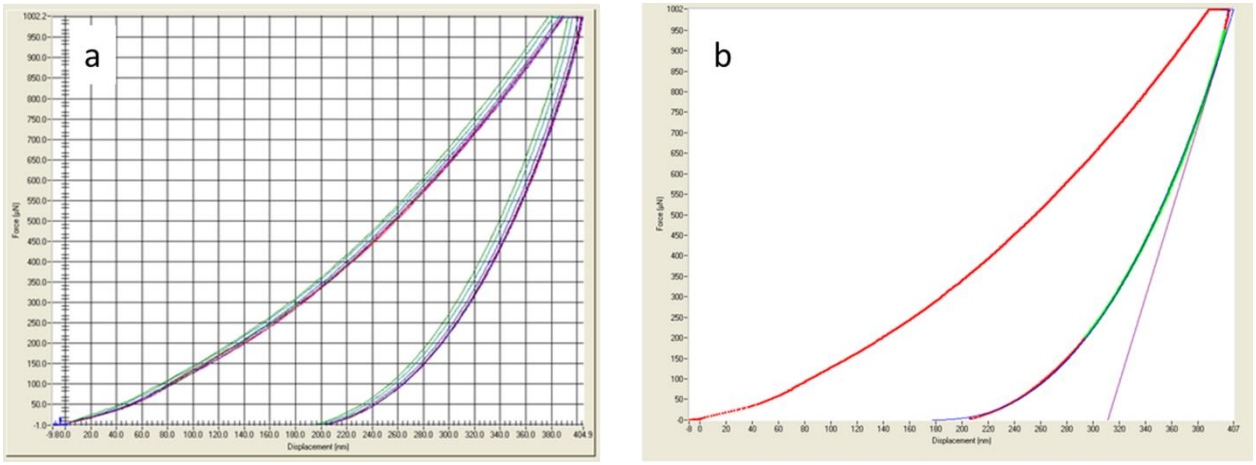

Figure 3.24. Nanoindentation data: a) typical load/unload curves for 3x3 indentation pattern on **M4/F4**. b) slope determination based on average of nine curves.

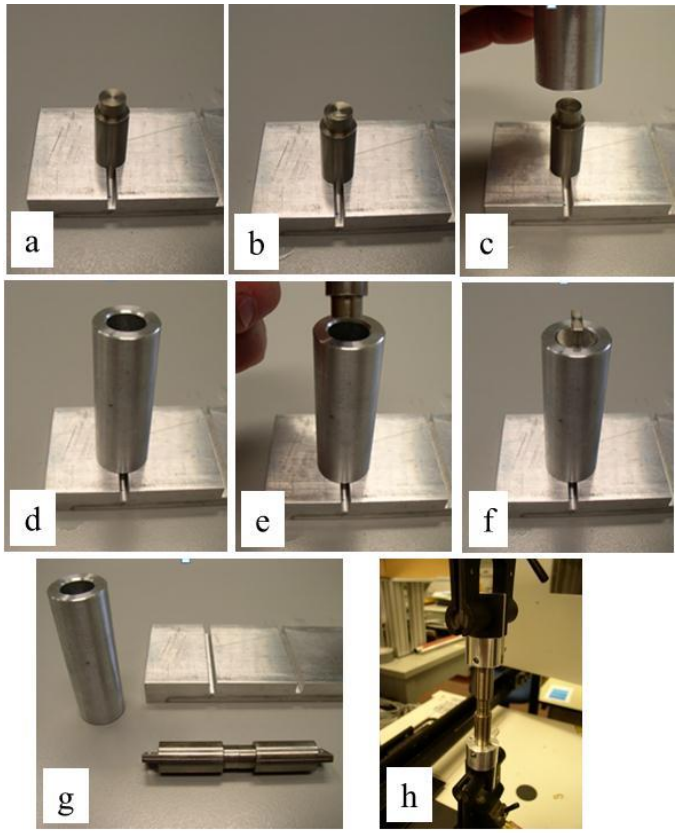

Figure 3.25. Sample preparation method for tensile testing of adhesive strength: a) pre-heated sample rod; b) powdered sample melted on polished surface of heated rod; c,d) application of alignment sleeve; e,f) placement of top pre-heated rod to form butt joint; g) final cooled sample; h) sample setup in Instron for tensile testing.

3.7 References

(1) Bergman, S. D.; Wudl, F. *J. Mater. Chem.* **2008**, *18*, 41.

(2) Murphy, E. B.; Wudl, F. *Prog. Polym. Sci.*, *35*, 223.

(3) Wool, R. P. *Soft Matter* **2008**, *4*, 400.

(4) Wu, D. Y.; Meure, S.; Solomon, D. *Prog. Polym. Sci.* **2008**, *33*, 479.

(5) Yuan, Y. C.; Yin, T.; Rong, M. Z.; Zhang, M. Q. *Express Polym. Lett.* **2008**, *2*, 238.

(6) Chen, X. X.; Dam, M. A.; Ono, K.; Mal, A.; Shen, H. B.; Nutt, S. R.; Sheran, K.; Wudl, F. *Science* **2002**, *295*, 1698.

(7) Chen, X. X.; Wudl, F.; Mal, A. K.; Shen, H. B.; Nutt, S. R. *Macromolecules* **2003**, *36*, 1802.

(8) Liu, Y. L.; Hsieh, C. Y. *Journal of Polymer Science Part a-Polymer Chemistry* **2006**, *44*, 905.

(9) Plaisted, T. A.; Nemat-Nasser, S. *Acta Mater.* **2007**, *55*, 5684.

(10) Tian, Q.; Yuan, Y. C.; Rong, M. Z.; Zhang, M. Q. *J. Mater. Chem.* **2009**, *19*, 1289.

(11) Adachi, K.; Achimuthu, A. K.; Chujo, Y. *Macromolecules* **2004**, *37*, 9793.

(12) Gousse, C.; Gandini, A.; Hodge, P. *Macromolecules* **1998**, *31*, 314.

(13) Imai, Y.; Itoh, H.; Naka, K.; Chujo, Y. *Macromolecules* **2000**, *33*, 4343.

(14) Laita, H.; Boufi, S.; Gandini, A. *Eur. Polym. J.* **1997**, *33*, 1203.

(15) Zhang, Y.; Broekhuis, A. A.; Picchioni, F. *Macromolecules* **2009**, *42*, 1906.

(16) Kwart, H., King, K. *Chem. Rev.* **1968**, *68*, 415.

(17) Murphy, E. B.; Bolanos, E.; Schaffner-Hamann, C.; Wudl, F.; Nutt, S. R.; Auad, M. L. *Macromolecules* **2008**, *41*, 5203.

(18) Boul, P. J.; Reutenauer, P.; Lehn, J. M. *Org. Lett.* **2005**, *7*, 15.

(19) Boutelle, R. C.; Northrop, B. H. *J. Org. Chem.***2011**, *76*, 7994.

(20) Coady, D. J.; Bielawski, C. W. *Macromolecules* **2006**, *39*, 8895.

(21) Kamplain, J. W.; Bielawski, C. W. *Chem. Commun.* **2006**, 1727.

(22) Decker, C.; Bianchi, C. *Polym. Int.* **2003**, *52*, 722.

(23) Decker, C.; Bianchi, C.; Jonsson, S. *Polymer* **2004**, *45*, 5803.

(24) Beijer, F. H.; Sijbesma, R. P.; Kooijman, H.; Spek, A. L.; Meijer, E. W. *J. Am. Chem. Soc.* **1998**, *120*, 6761.

(25) Lange, R. F. M.; Van Gurp, M.; Meijer, E. W. *Journal of Polymer Science Part a-Polymer Chemistry* **1999**, *37*, 3657.

(26) Sijbesma, R. P.; Beijer, F. H.; Brunsveld, L.; Folmer, B. J. B.; Hirschberg, J.; Lange, R. F. M.; Lowe, J. K. L.; Meijer, E. W. *Science* **1997**, *278*, 1601.

(27) Montarnal, D.; Capelot, M.; Tournilhac, F.; Leibler, L. *Science*, *334*, 965.

(28) Nai, M. H.; Lim, C. T.; Zeng, K. Y.; Tan, V. B. C., *J. Metastab. Nanocryst.* **2005**, *23*, 363.

(29) Rochman, A.; Frick, A.; Martin, P. *Polym. Eng. Sci.* **2012**, *52*, 2114.

(30) Rozenberg, B. A.; Dzhavadyan, E. A.; Morgan, R.; Shin, E. *Polym. Adv. Technol.* **2002**, *13*, 837.

(31) Canadell, J.; Fischer, H.; De With, G.; Van Benthem, R. *Journal of Polymer Science Part a-Polymer Chemistry* **2010**, *48*, 3456.

(32) Naimi-Jamal, M. R.; Kaupp, G. *Macromolecular Symposia* **2008**, *274*, 72.

(33) Oliver, W. C.; Pharr, G. M. *MRS Bull.*, **2010**, *35*, 897.

(34) Pharr, G. M.; Oliver, W. C. *MRS Bull.* **1992**, *17*, 28.

(35) ASTM-D2095; Materials, A. S. f. T. a., Ed.; American Society for Testing and Materials: 1996, p 1.

Chapter 4
Preparation and Properties of Cross-linked Reversible Polymers

4.1 Abstract

Previously, we prepared and characterized a series of four bismaleimide and bisfuran monomers that were used to make linear reversible polymers (see Chapter 3). Melt blending and cooling of the monomers resulted in polymer films having a wide range of physical properties that were dependent on the chemistry of the spacer used in the disubstituted monomers. Here we report the preparation of a tripodal maleimide and furan, with an aim to exploring the effects of cross-linking on these useful materials. Mixtures of the tripodal monomers alone, as well in combination with the disubstituted systems, were prepared and characterized in both the molten and solid states. Interestingly, the melt viscosity rose to much higher values than had been observed with any of the linear systems, which was attributed to a greater degree of irreversible cross-linking of the maleimide. Hardness and reduced modulus of the solidified films was measured using nanoindentation. While we expected the cross-linked polymer to have greater mechanical integrity than the linear polymers, we found some of the linear polymers to be harder. Adhesion of the cross-linked system, as a function of tensile adhesive strength, was found to be significantly weaker than most of the linear systems. This was attributed to the high melt viscosity, which hindered wetting of the surfaces that were being fastened together. Reversibility of the Diels Alder (DA) reaction was demonstrated using both ^{1}H NMR spectroscopy and differential scanning calorimetry (DSC).

4.2 Introduction

4.2.1 Reversible Polymers

The study of reversible polymers has received considerable attention in the past two decades. Much of the work in this field has been focussed on the concept of self-healing, wherein the application of heat to a fractured polymer results in restoration of the rupture and the mechanical integrity of the device.[1-5] The inherent low melt viscosity of the monomers enables rapid material flow and subsequent covalent bonding across the damage site. However, this low viscosity also allows for excellent materials processing characteristics, as the molten monomer viscosity can be significantly lower than what would be realized with heating of a conventional polymer. This enables the design of materials having the mechanical advantages of thermosets and the ability to revert to low viscosity liquids under the influence of applied heat. Diels Alder (DA) chemistry is ideally suited for this purpose, as it requires only a thermal stimulus for reversibility, and is an addition reaction, thus does not generate small molecule by-products that would render the reaction irreversible. A cis-configured, electron deficient diene and an electron rich dienophile can undergo a reversible cycloaddition reaction so as to generate a fused cyclic system. Application of heat to this system then restores the small molecule starting materials (Figure 4.1).[6] Wudl and co-workers exploited this concept using multi-podal maleimides and furans to generate cross-linked polymers that were subjected to controlled fracture, and then re-mended using gentle heating. This resulted in healing efficiencies of greater than 80% of the original strength of the material. Reversibility was confirmed by ^{13}C NMR spectroscopy, and demonstrated in practical terms by repeating the healing process multiple times.

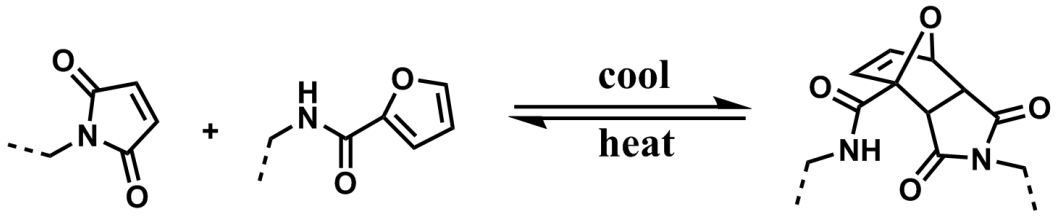

Figure 4.1. Thermally induced DA and retro-DA reaction.

4.2.2 Linear Reversible Polymers

Recently, we investigated the preparation and characterization of a series of linear reversible polymers based on DA chemistry (Figure 4.2a) (see Chapter 3). Bisfurans and bismaleimides were combined to afford hard, film forming polymers that readily reverted to low viscosity monomeric liquids with the application of heat. The spacer groups between the two reactive endgroups were comprised of a linear n-octyl chain, a 1,3-dimethylenecyclohexyl, 1,3-dimethylenephenyl, and an ethylenedioxy group, such that each of the monomers contained approximately the same number of atoms. Equimolar amounts of the furan and maleimide were melted together and then allowed to cool, so as to enable polymerization via the DA reaction. Despite having a common linking group that enabled polymer formation, the compounds exhibited profoundly different material properties. Solidification times of the films varied greatly, from seconds to hours, while their physical appearance ranged from opaque, crystalline solids to clear hard, amorphous films. Hardness and modulus values of the films were measured by nanoindentation, and ranged from 0.6-8 GPa and 0.1-0.6 GPa respectively. Reversibility of the polymerization was confirmed using both ^{1}H NMR spectroscopy and DSC. Degree of polymerization (DP), as well as rheological properties, was found to be dependent on the chemistry of the spacer molecule joining the functional endgroups. Finally, the adhesive strength of these polymers was found to be surprisingly high, and was measured using a standardized

tensile strength test method.[7] Indeed, adhesive strength was significantly greater than the conventional film forming polymer polyethylene glycol (PEG). As with many other properties of these materials, adhesion was found to vary with spacer chemistry.

The mechanical integrity of the linear polymers exceeded our expectations. While some of the polymer films were too brittle for practical applications, they did form very hard solids when cooled from the molten state. Importantly, we found that mixtures of the polymers having different spacer chemistries leveraged the advantages of both materials, resulting in rapidly solidified, hard materials with excellent film forming characteristics. We anticipate that cross-linked networks would further improve the mechanical performance of these materials, thus we have now prepared a tri-podal maleimide and furan (Figure 4.2b).

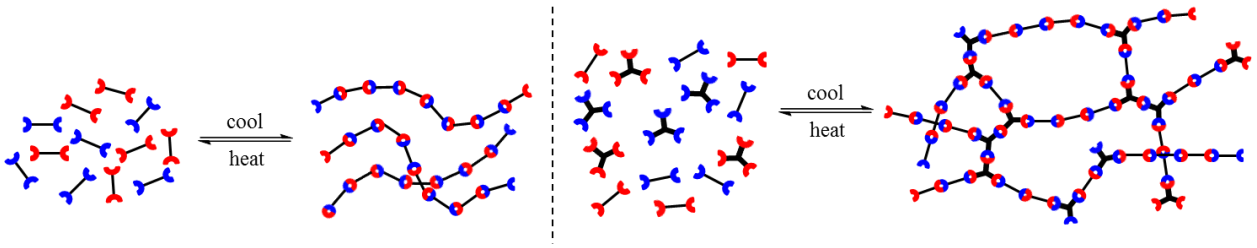

Figure 4.2. Schematic representation of reversible polymers. a) linear; b) cross-linked.

4.3 Experimental

4.3.1 General

All reagents were obtained from Sigma-Aldrich and used as received. ^{1}H NMR spectra were obtained on a Bruker Avance 400 MHz Spectrometer using deuterated dimethyl sulfoxide (d_6-DMSO) as solvent and TMS as internal reference. Viscosity measurements were made using an Ares 2000 viscometer from Rheometric Scientific, equipped with a 25 mm steel plate assembly set at a gap width of 200 µm. Nanoindentation measurements were made using a Hysitron

Triboscan® nanoindenter equipped with a Berkovich diamond tip. Differential Scanning Calorimetry (DSC) analyses were performed on a DSC Q1000, from TA Instruments. X-Ray diffraction spectra were obtained on a Rigaku MiniFlex X-ray Diffractometer, fitted with a Cu target and variable slit interlocked with θ axis. High-resolution mass spectrometry using electrospray ionization (HRMS (EI+)) was conducted for the synthesized monomers on a Micromass Quattro Ultima triple quadrupole mass spectrometer using positive ion mode. Tensile strength measurements were made on an Instron 3367, using an extension rate of 100 μm per minute.

4.3.2 Synthesis

1,1',1''-(nitrilotris(ethane-2,1-diyl))tris(1H-pyrrole-2,5-dione) ***(M5)***

In a 500 mL round-bottomed flask under argon was dissolved maleic anhydride (20.1 g, 205 eq) in 75 mL DMF. The resulting solution was chilled on ice and then tris(2-aminoethyl)amine (10.0 g, 68.4 mmol) dissolved in DMF (75 mL) was added dropwise over ~20 min. The ice bath was removed, and sodium acetate (1.68 g, 20.52 mmol) and acetic anhydride (23.04 g, 226 mmol) were added in one portion, and the mixture stirred overnight at 50°C. The mixture turned dark brown within 30 minutes of the addition of NaOAc and Ac_2O. DMF was removed by vacuum distillation (60°C), and DCM (150 mL) was added to the dark brown mixture. The organic layer was extracted with $NaHCO_3$ (5 x 100 mL), dried over $MgSO_4$, and the solvent removed under vacuum. The resulting compound was purified by column chromatography (95:5 DCM:EtOAc), to yield a light yellow solid (8.0 g, 30%): R_f (EtOAc) = 0.5; mp = 123.7°C; ^{1}H NMR (400 MHz, DMSO): δ (ppm) 6.97 (s, 6H), 3.37 (t, 6H, *J* = 6.6 Hz), 2.60 (t, 6H, *J* = 6.6 Hz); ^{13}C NMR (400 MHz, DMSO) δ (ppm) 171.35, 134.93, 51.31, 35.48;

Electrospray MS (positive ion mode): calcd. for $C_{18}H_{19}N_4O_6$ $[M + H]^+$: m/z = 387.36; found: 387.3.

N,N',N''-(nitrilotris(ethane-2,1-diyl))tris(furan-2-carboxamide) ***(F5)***

In a 500 mL RBF under argon was added the 1,8-octanediamine (10.0 g, 68.4 mmol), triethylamine (20.76 g, 205 mmol), DMAP (0.68 g, 20.5 mmol) and DCM (350 mL). The solution was chilled on ice, then furoyl chloride (27.7 g, 212 mmol) in DCM (150 mL) was added dropwise. The ice bath was removed, and the mixture stirred at room temperature overnight. The organic layer was extracted with $NaHCO_3$ (5 x 100 mL), dried over $MgSO_4$, and the solvent removed under vacuum. The resulting compound was purified by column chromatography (99:1 DCM:EtOAc) to yield a white solid (16.1 g, 82%):

R_f (95:5 EtOAc:MeOH) = 0.18; mp = 143.5°C; ^{1}H NMR (400 MHz, DMSO): δ (ppm) 8.16 (t, 3H, *J* = 5.5 Hz), 7.74 (d, 3H, *J* = 0.8 Hz), 7.06 (d, 3H, *J* = 3.1 Hz), 6.57 (dd, 3H, *J* = 1.7 Hz), 3.29 (t, 6H, *J* = 6.3 Hz), 2.65 (t, 6H, *J* = 6.7 Hz); ^{13}C NMR (400 MHz, DMSO) δ (ppm) 158.26, 148.41, 145.27, 113.57, 112.18, 53.49, 37.22; Electrospray MS (positive ion mode): calcd. for $C_{21}H_{25}N_4O_6$ $[M + H]^+$: m/z = 429.44; found: 429.3.

4.3.3 Mixture preparation

In a typical example, equimolar amounts of bismaleimide and bisfuran were combined in a vial. DCM/MeOH (95:5 v/v, 5 mL) was then added and the vial was shaken to ensure complete dissolution. The solvent was then removed under vacuum, and the resulting solid mixture ground into a uniform powder.

4.3.4 Nanoindentation

Samples were prepared by transferring the powder mixture (~ 50 mg) to a steel sample disc (15 mm diameter). The disc was placed on a hotplate that was pre-heated approximately 20°C above the melting point of the mixture. Air bubbles that appeared during melting were removed by agitation of the liquid with a clean spatula. This resulted in smooth films with relatively flat surfaces. The sample discs were removed from the heat source and stored at 60°C. Samples were allowed to equilibrate at room temperature for at least 24 h before measurements were made. A 10-2-10 load function was used (10 second load time, 2 second hold, and 10 second unload time) with a maximum load of 1000 μN. Longer hold times have been claimed to be more effective for nanoindentation of viscoelastic materials.[8] A hold time of 30 seconds was also attempted, but results for modulus and hardness were largely similar, and this often resulted in adhesion of compliant material to the indenter tip, which significantly affected subsequent measurements. Measurements were made in 3 x 3 grids, with a spacing of 15 μm between each indentation. Three separate locations spaced at least 1 mm apart were used on each sample stub. Values reported represent an average of these 27 measurements. Control samples (PMMA, quartz) were measured before and after each set of measurements and found to be within 5% of their expected values.

4.3.5 ^{1}H NMR kinetics

Solid films were stored at 60°C for the specified period of time, and then dissolved in the NMR solvent. Reversion to furan/maleimide was accomplished by melting 10 mg of the neat sample in an NMR tube, and then immediately quenching in liquid nitrogen. The resulting solid was then dissolved in the NMR solvent.

4.3.6 DSC kinetics

Separate samples were prepared for each designated aging time. Samples were weighed and crimped in aluminum DSC pans, and subjected to a heat/cool/heat cycle. The pans were then stored at 60°C for the specified period of time, and then subjected to another heat/cool/heat cycle.

4.3.7 Adhesion testing

Two 3/8" diameter dowels made of 303 stainless steel were pre-heated approximately 20C° above the melting point of the monomer mixture. The powdered mixture (5 ± 0.5 mg), which had been compressed into pellet form for easier handling, was then carefully placed on the polished surface of the dowel. The solid completely melted within seconds, and an alignment sleeve was then slipped over the first dowel, and a second dowel placed in the tube onto the surface of the molten sample, applying minimal downward pressure. The sleeve was bored to allow 0.002" clearance, to ensure perfect alignment of the two dowels. The top dowel was turned gently for three complete revolutions to ensure complete surface area coverage at the interface of the two dowels. Only the weight of the upper dowel (30.38 ± 0.03g) was used to compress the liquid samples. The samples were incubated at 60°C for four days, and then equilibrated at room temperature for 1 h prior to testing for tensile strength. Eight samples were prepared for each test. Samples were tested on an Instron 3367 at an extension rate of 100 µm per minute until complete fracture had occurred. The highest and lowest values were eliminated, and the results for breaking strength reported as an average of the six remaining measurements.

4.4 Results and discussion

4.4.1 Synthesis

A tripodal maleimide and furan were prepared and characterized, using synthetic methods based on our earlier work (see Chapter 3). The maleimide was prepared by condensation of three equivalents of maleic anhydride with tris(2-aminoethyl)amine (TAEA) using sodium acetate and acetic anhydride, while the furan was prepared using TAEA coupled with three equivalents of furoyl chloride (Scheme 4.1).

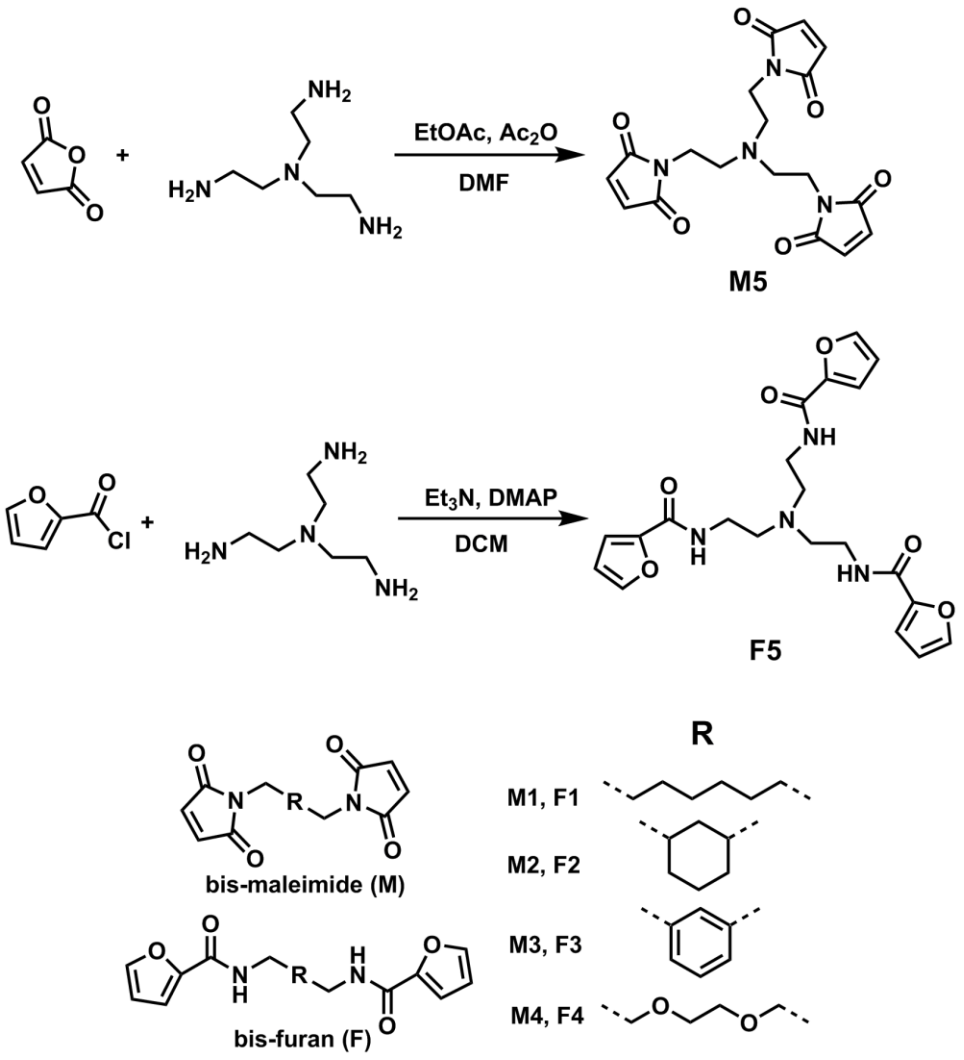

Scheme 4.1. Synthetic pathway to maleimides and furans.

Polymer samples were prepared in neat form by melting equimolar quantities of the two monomers, and allowing them to cool to 60°C. Incubation at this temperature resulted in polymer formation via the DA reaction. The physical appearance of the linear polymers varied widely, from an opaque, highly brittle material (**M1/F1**), to a clear, hard, robust polymer film (**M4/F4**). The cross-linked polymer prepared in this study (**M5/F5**) was found to be similar to the linear **M4/F4**, in that it afforded an amorphous, glassy polymer that was not highly brittle. (X-ray powder diffraction (XRD) traces for all of the polymers can be found in the Supporting Information.) Among the linear reversible polymers, we found that **M4/F4** showed the most promising properties, in that it possessed excellent film forming characteristics while providing a durable, relatively non-brittle material. We therefore focused on this system as a reference to compare the linear and cross-linked polymers.

4.4.2 Polymerization Reversibility

4.4.2.1 ^{1}H NMR Spectroscopy

Reversibility of the polymerization was confirmed using ^{1}H NMR spectroscopy. An initial spectrum of the maleimide and furan powders gave no indication of DA coupling (Figure 4.3a). Complete melting of the mixture, followed by cooling and incubation at 60°C, allowed polymerization to occur. As was the case with the linear polymers, a new peak at ca. 5.2 ppm, assigned to the newly formed bridgehead proton, and a doublet of doublets centered at 6.6 ppm, due to the norbornyl double bond, were clear indicators of DA polymerization (Figure 4.3b). The diagnostic peak at 5.2 ppm also provided an indication of the extent of conversion to the polymeric form. Comparison of the integral of this growing peak with that of the α-proton on the furan ring allowed for calculation of the degree of polymerization, according to the formula

$i_{5.2}/(i_{5.2} + i_{7.8})\times100\%$, where i_x is the integral of the NMR peak at x ppm. Melting of the polymer, followed by a rapid liquid nitrogen quench, restored the original spectrum (Figure 4.3c). ^{1}H NMR spectra were acquired at several intervals during the 7 day incubation period, revealing that polymer conversion was maximized after 24 hours (All of the ^{1}H NMR spectra can be seen in the Supporting Information, Figure 4.10). Polymer conversion did not reflect the hardness of the incubated film, as the linear polymer **M4/F4** reached a significantly higher DP than did the cross-linked polymer **M5/F5**, but was actually softer. Conversion rates for both the linear (**M(1-4)/F(1-4)**) and cross-linked (**M5/F5**) polymers can be seen in Figure 4.4.

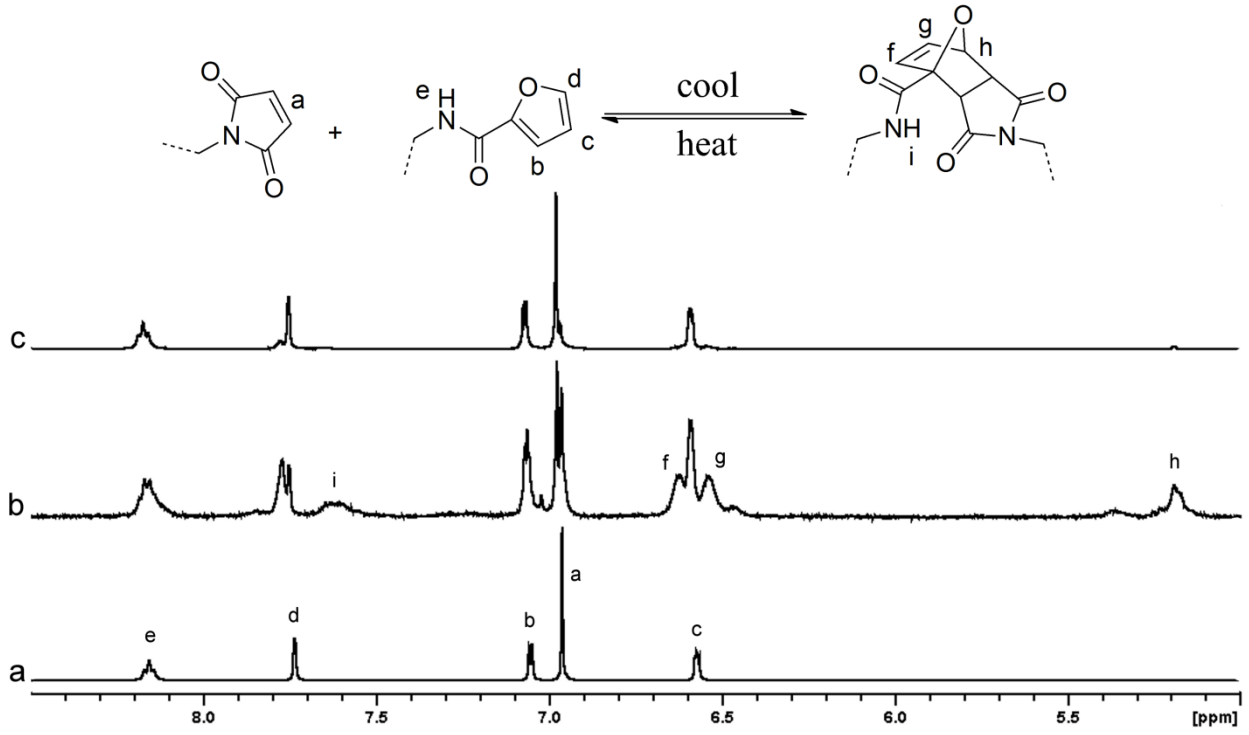

Figure 4.3. ^{1}H NMR showing the reversible polymerization of **M5/F5**: Spectra were recorded: a) prior to melting; b) after melting and incubation at 60°C for 7 days; and c) after re-melting and rapid quenching in liquid nitrogen.

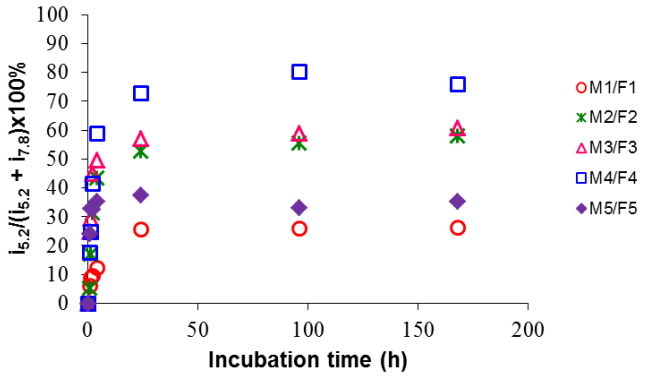

Figure 4.4. Polymer conversion percentages over time, determined by ^{1}H NMR spectroscopy.

4.4.2.2 DSC

Reversibility was also demonstrated using differential scanning calorimetry (DSC). An equimolar mixture of **M5** and **F5** was subjected to a heat-cool-heat cycle, such that the mixture was heated to the molten state prior to the cooling step. The mixture was then re-heated immediately after cooling, and in this second heating pass, only a single broad melting peak was observed, indicating that some polymer formation had occurred during the cooling period (Figure 4.5). Upon heating a second time, two melting peaks were observed at ca. 100°C and 150°C that were attributed to the breakdown of the polymer structure via the retro-DA reaction.[9] Samples were then stored at 60°C after the initial heat-cool cycles had been completed, and re-processed by DSC after designated periods of time. In each case, two peaks were observed at ca. 100°C and 150°C after the cooling period, but were replaced by a single broad melting peak when the polymer was subjected to a second heating immediately following the first. Canadell et al have used ^{1}H NMR spectroscopy and DSC analysis to assign these two peaks to the collapse of the endo and exo stereoisomers of the DA polymer, respectively.[9] In our study of linear DA polymers, we found that the lower temperature peak diminished in size over time, contrary to what was observed here (see Chapter 3, Figures 3.9, 3.16 – 3.18). This was rationalized as an

increase in formation of the more thermodynamically stable exo isomer at the expense of the endo conformer. Since the increased sharpness of the peak in Figure 4.5 cannot be attributed to crystallization of the polymer (Figure 4.11, Supporting Information), it appears that in this case, the endo conformation is the more stable of the two. It is not clear whether this is a result of an inherent difference between linear and cross-linked polymers, or if it is due to the particular spacer used in the two tripodal monomers.

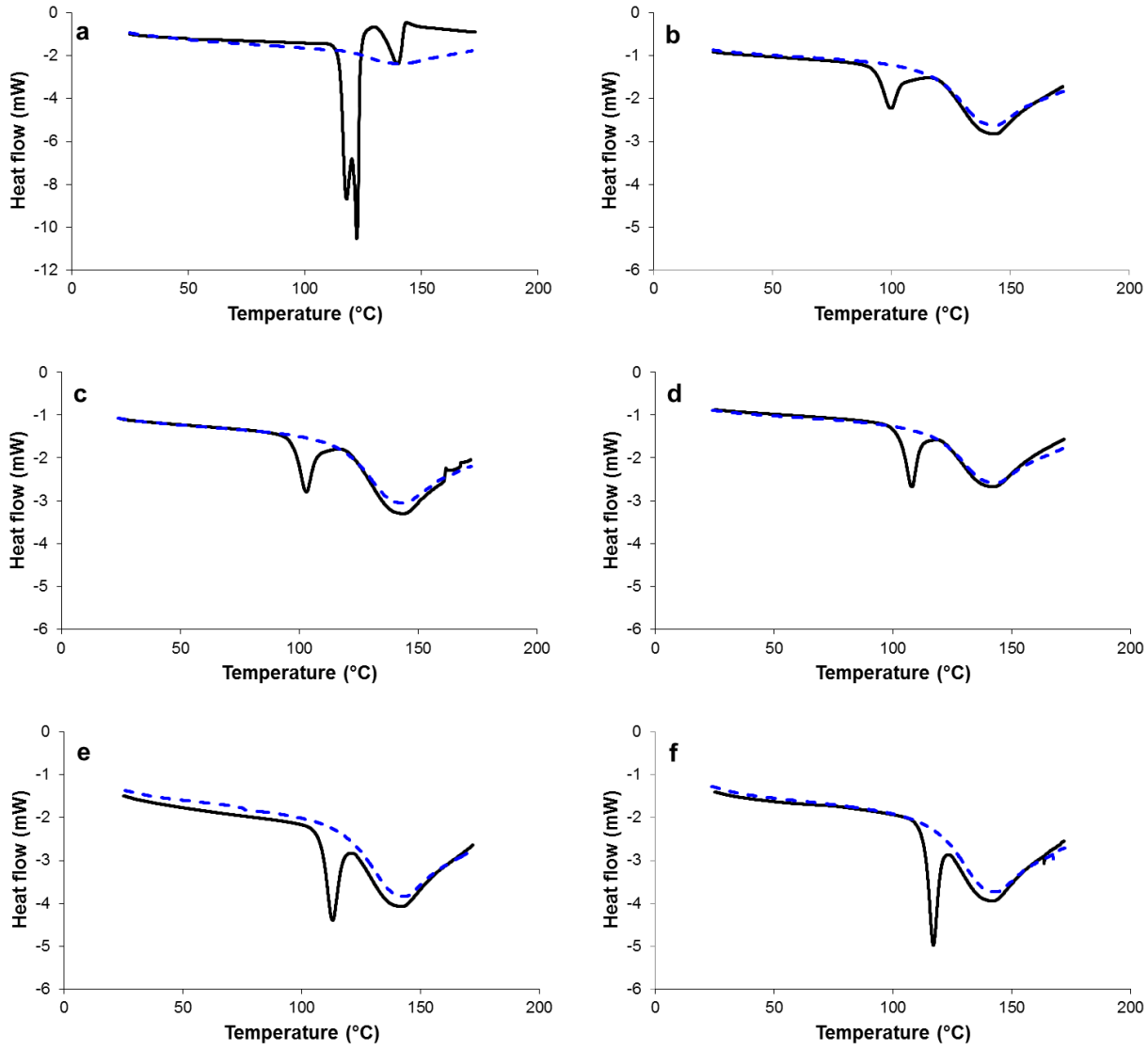

Figure 4.5. DSC cycling of the **M5/F5** mixture: Initial heating (solid line), second heating, immediately following first (dashed line). a) dry blended mixture of the monomers; b) 4 hours after initial heat/cool/heat cycle; c) 8 hours after initial heat/cool/heat cycle; d) 24 hours after initial heat/cool/heat cycle; e) 4 days after initial heat/cool/heat cycle; f) 7 days after initial heat/cool/heat cycle. Exothermic transitions point upward.

4.4.3 Nanoindentation

Nanoindentation was used for the determination of the rheological properties of the solidified polymer films. A Berkovich indenter tip was used to penetrate samples using a controlled loading force. Since the geometry of the tip is very well known, the penetration depth can be used to calculate the exact area of indentation. According to the method of Oliver and Pharr, the hardness (H) of the material can be determined as a function of the maximum load over the area of penetration.[10] A plot of the load vs displacement of the tip during indentation can then be used to calculate the stiffness and reduced modulus (E_r) of the sample. This technique allows for rheological measurements to be made on materials in their working state, and in this case, measurements were made directly on thin polymer films cast onto a 15 mm diameter metal disc. Samples were aged four days at 60°C, and measurements made on three remote spots on each disc in 3x3 grids with a spacing of 15 µm between each indent. A 10-2-10 load function (10 second loading time, 2 second hold and 10 second unloading time), with a loading force of 1000 µN was used. Modulus and hardness data, averaged from the 27 separate indentation measurements made for each compound, are provided in Figure 4.6. Modulus for the cross-linked film was approximately the same as was found for the linear film forming polymers **M2/F2**, **M3/F3** and **M4/F4**. Interestingly, this cross-linked material was not as hard as some of the linear polymers, although it was harder than the linear **M4/F4**. One might expect that a highly cross-linked network would lead to a very hard, brittle material, but this was not the case here as the cross-linked **M5/F5** displayed similar toughness and flexibility to **M4/F4**. The solid **M5/F5** retained solubility in d6-DMSO and DCM after prolonged incubation times, suggesting that cross-linking was not extensive in the product polymer. Nevertheless, solubility did decrease as the polymer was incubated, and was lower than what was observed with the linear systems, thus we concluded

that some cross-linking had occurred (see Chapter 3). Unfortunately, ^{1}H NMR spectroscopy, while providing confirmation of the occurrence of the DA reaction, could not distinguish between linear and cross-linked connectivities, thus we were unable to quantify the degree of cross-linking in this polymer.

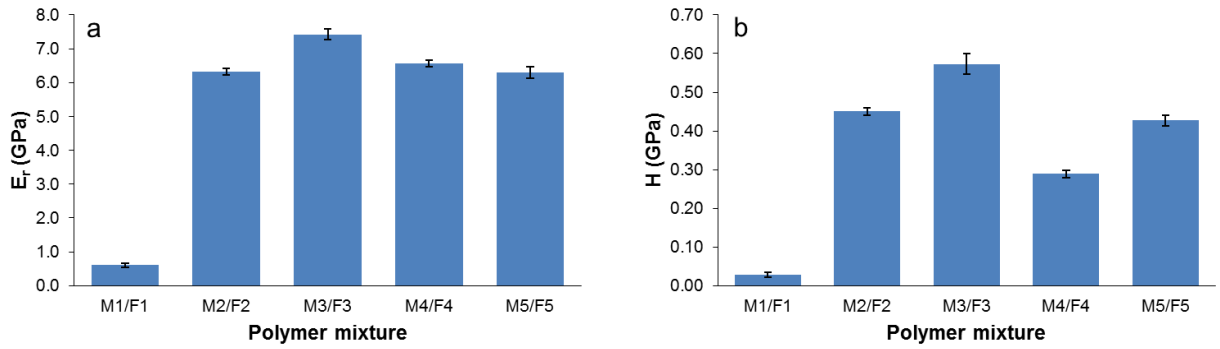

Figure 4.6. Rheological data of polymer films measured by nanoindentation: a) reduced modulus; b) hardness.

4.4.4 Polymer Mixtures

We then attempted to improve the durability of the linear polymer by imparting cross-linking to the linear **M4/F4** backbone. Mixtures of the two sets of monomers (**M4/F4** + **M5/F5**) were prepared and cast into solid films and then characterized by nanoindentation as described above. No discernible phase separation was observed in the molten or solidified mixtures, as all the films appeared homogeneous after incubation at 60°C. Hardness and modulus values did not change appreciably upon incorporation of the cross-linking agent, indicating that cross-linking had limited impact on the rheology of the resulting films (Figure 4.7). While an increase in hardness of the linear polymer **M4/F4** was achieved with the addition of the cross-linking agent, the resulting value did not exceed the level obtained for the cross-linked system itself, thus only a

minor improvement was realized. Nevertheless, the incorporation of cross-linking did ultimately result in an increase in the hardness of the linear polymer, which was the intended result. It is notable that the hardness and modulus values obtained for the 50:50 mixture were higher than those obtained for either of the two component polymers **M4/F4** and **M5/F5**. We believe this result to be aberrant, as mixtures of the softer **M4/F4** with each of the harder linear polymers **M1/F1**, **M2/F2** and **M3/F3** each showed steady trends in both the hardness and modulus data, with no such maximum observed for the 50:50 mixtures (see Chapter 3).

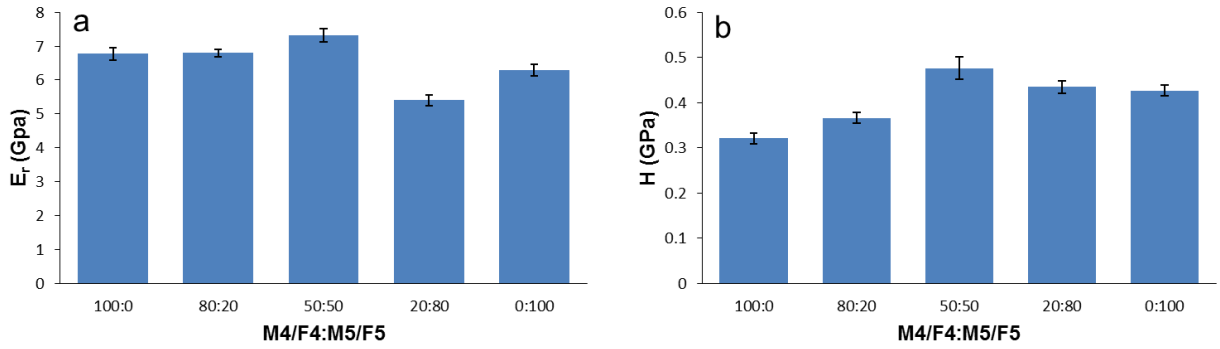

Figure 4.7. Rheological data of polymer films prepared from mixtures of **M4/F4** + **M5/F5**, measured by nanoindentation: a) reduced modulus; b) hardness.

4.4.5 Melt Viscosities

While the rheology of the hardened cross-linked polymer was not substantially different from the linear polymers, the characteristics of the molten liquid exhibited a marked difference. Viscosities were measured at a temperature approximately 20°C above the melt temperature of each monomer mixture. Measurements were made continually over a period of 30 minutes under a constant applied shear rate of 100 s^{-1}. (Figure 4.8) The four bis-maleimide/bis-furan systems displayed excellent flow and processability at their respective measurement temperatures, as their

initial viscosities were all below 100 cPs. However, the trigonal monomer mixture was considerably more viscous at time zero. Furthermore, the increase in viscosity experienced by each of the polymers over the course of the measurement was substantially greater for the cross-linked system **M5/F5**. It is believed that this viscosity increase is due to the radical based 2 + 2 cycloaddition reaction occurring within the maleimides that result in highly cross-linked networks.[11] As the monomer mixtures remained in the molten phase, the viscosity steadily increased, and eventually formed a hard intractable solid, at which point the low viscosity liquid phase could not be restored. This side reaction was avoided by minimizing the time that the materials were held in the molten phase during the polymer preparation process. In terms of materials processing, this provides an advantage to the lower melting systems such as **M4/F4**, in that they can be processed at lower temperatures. Small amounts of the radical inhibitor IrgaStab UV-10® were also found to substantially reduce in viscosity increase, although this approach was not pursued further (data not shown).

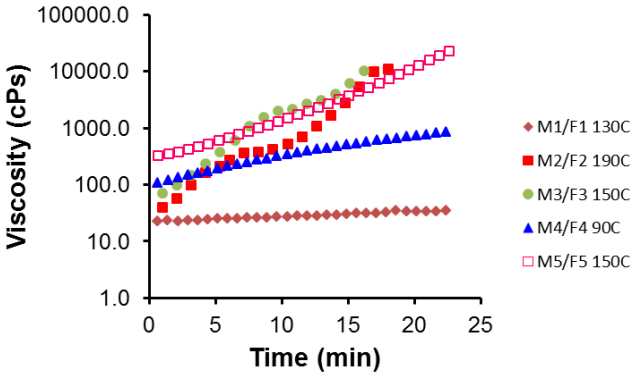

Figure 4.8. Melt viscosities of polymer mixtures measured at constant shear rate (100 s^{-1}).

4.4.6 Adhesive Strength

We have also quantified the adhesive strength of these polymers, using a method based on American Society for Testing and Materials (ASTM) Method D2095.[7] Tensile strength was measured as the breaking strength of a polymer joint made between two aligned stainless steel dowels. We again combined the two polymers **M5/F5** and **M4/F4** in varying ratios to observe the characteristics of the cross-linked polymer by itself and as a cross-linking additive in a linear system. Surprisingly, the breaking strength was highest for the linear **M4/F4** system, and steadily decreased as **M5/F5** was added. (Figure 4.9) This could be attributed to the higher viscosity of the molten **M5/F5**, which inhibited wetting of the steel substrate during sample preparation. The adhesion of the native cross-linked polymer **M5/F5** was significantly inferior to the linear system **M4/F4**, thus the addition of cross-linking did not afford any improvement to the linear polymer.

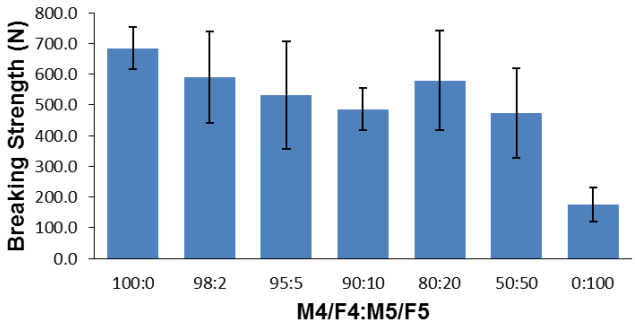

Figure 4.9. Breaking strength of mixtures of the **M4/F4** and **M5/F5** systems.

4.5 Summary

We have observed a dramatic influence made by the spacer chemistry within linear reversible polymers (see Chapter 3). While we expected an equally large effect with the incorporation of cross-linking into these reversible systems, our findings did not substantiate this. Addition of varying amounts of the tripodal maleimide and furan **M5/F5** to the linear **M4/F4** did not lead to significant changes in the rheology of the polymer film. Similar results were observed when two linear systems were combined, thus the incorporation of cross-linking did not prove to be as beneficial as anticipated. While we were able to determine the degree of polymerization in these polymers, the extent of cross-linking that occurs within the tripodal system is unclear. The solubility of the hardened polymer in common solvents leads us to believe that the degree of cross-linking is not high. While one might expect a higher DP with the increased number of bonding sites available for the tripodal monomers, the rigidity of the branches may have hindered the required alignment of the maleimide and furan for coupling.

4.6 Supporting Information

The formation and properties of cross-linked reversible polymers

James D. Mayo, Alex Adronov

Prof. A. Adronov

McMaster University

1280 Main Street West

Hamilton, ON

L8S 4L8

J.D. Mayo

Xerox Research Centre of Canada

2660 Speakman Drive

Mississauga, ON

L5K 2L1

e-mail: adronov@mcmaster.ca

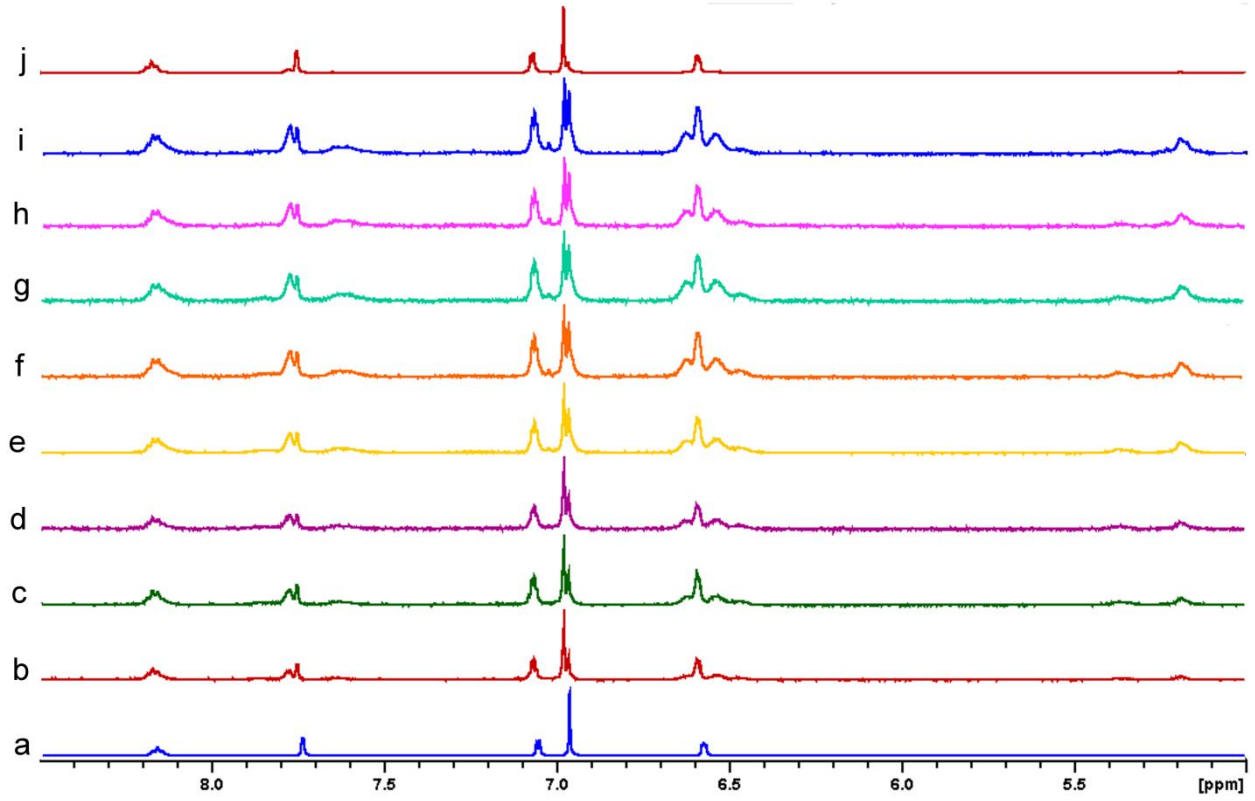

Figure 4.10. ^{1}H NMR showing the reversible polymerization of **M5/F5**: Spectra were recorded: (a) prior to melting, and then after melting and incubation at 60°C for: (b) 30 m; (c) 1 h; (d) 2 h; (e) 4 h; (f) 24 h; (g) 48 h; (h) 4 days; (i) 7 days; and (j) after re-melting and rapid quenching in liquid nitrogen.

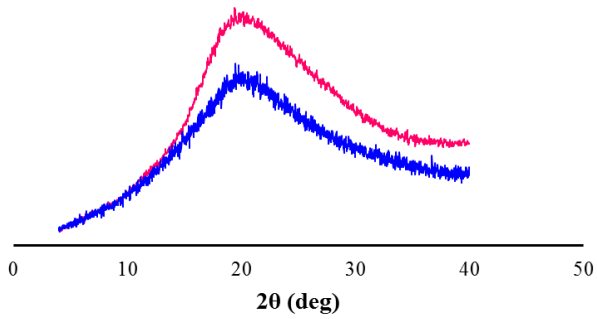

Figure 4.11. X-Ray Powder Diffraction (XRD) traces of polymers after incubation period of 4 days at 60°C. (**M4/F4** - lower/blue curve; **M5/F5** - upper/fuschia curve)

4.7 References

(1) Bergman, S. D.; Wudl, F. *J. Mater. Chem.* **2008**, *18*, 41.

(2) Murphy, E. B.; Wudl, F. *Prog. Polym. Sci.*, *35*, 223.

(3) Wool, R. P. *Soft Matter* **2008**, *4*, 400.

(4) Wu, D. Y.; Meure, S.; Solomon, D. *Prog. Polym. Sci.* **2008**, *33*, 479.

(5) Yuan, Y. C.; Yin, T.; Rong, M. Z.; Zhang, M. Q. *Express Polym. Lett.* **2008**, *2*, 238.

(6) Kwart, H., King, K. *Chem. Rev.* **1968**, *68*, 415.

(7) ASTM-D2095; Materials, A. S. f. T. a., Ed.; American Society for Testing and Materials: 1996, p 1.

(8) Nai, M. H.; Lim, C. T.; Zeng, K. Y.; Tan, V. B. C. In *Science and Technology of Nanomaterials - ICMAT 2003* 2005; Vol. 23, p 363.

(9) Canadell, J.; Fischer, H.; De With, G.; Van Benthem, R. *Journal of Polymer Science Part a-Polymer Chemistry* **2010**, *48*, 3456.

(10) Oliver, W. C.; Pharr, G. M. *MRS Bull.*,**2010**, *35*, 897.

(11) Rozenberg, B. A.; Dzhavadyan, E. A.; Morgan, R.; Shin, E. *Polym. Adv. Technol.* **2002**, *13*, 837.

Chapter 5
Dissolution of Carbon Nanotubes Using Reversible Diels Alder Polymers

5.1 Introduction

5.1.1 Functionalization of Carbon Nanotubes

Since the 1990's, carbon nanotubes have garnered a great deal of scientific interest as a result of their exceptional electrical, mechanical and thermal properties. A wide range of applications were envisioned in both electrical and mechanical devices, generating tremendous volumes of scientific literature in the fields of transistors,[1-3] chemical sensors,[4] and light emitting diodes (LED),[5] as well as in the study of nanocomposites.[6-8] For many of these applications, the complete lack of solubility of nanotubes in common organic solvents was a significant obstacle. Ironically, the strong intermolecular forces that make up the cylindrical graphene network also generate very strong interactions between nanotubes, resulting in the formation of bundles that are exceedingly difficult to solubilize or disperse. Surface functionalization of particles or nanotubes is a common means to impart solubility or dispersability. Amphiphilic polymers are often used in this capacity as they can at once bind themselves to the nanotube surface and extend into the surrounding solvent environment, creating compatibility of the insoluble nanotube with the solvent medium. Attachment of dispersants to the surface of the particle can be achieved in four ways, as shown in Figure 5.1.

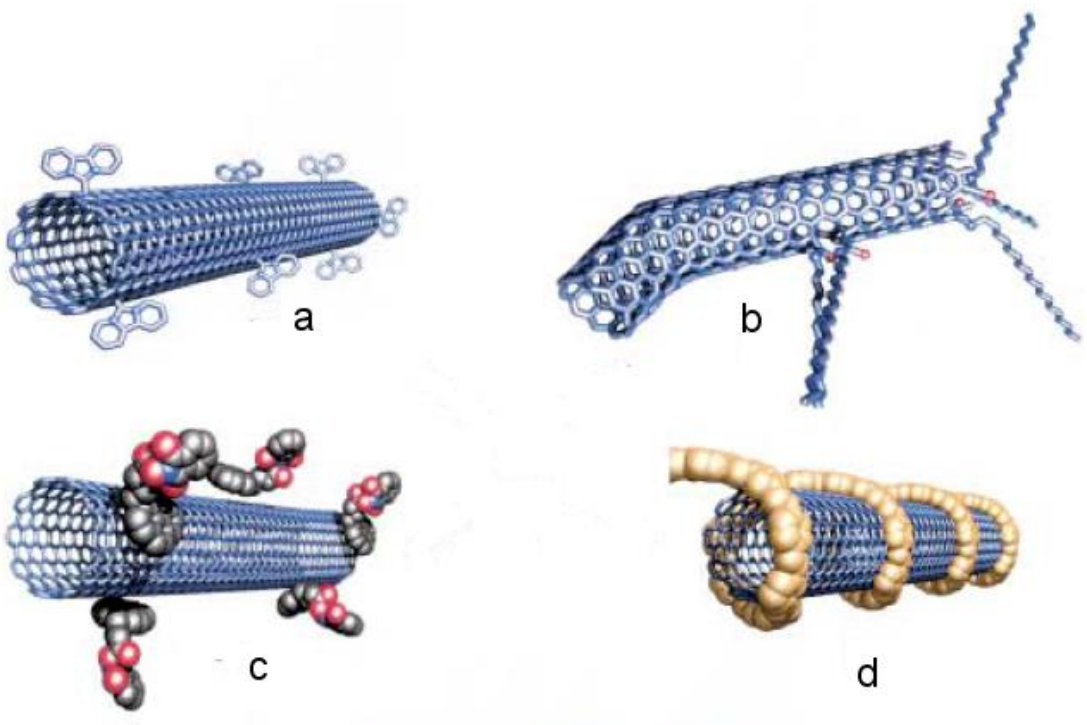

Figure 5.1. Functionalization of carbon nanotubes: a) covalent sidewall functionalization; b) defect site functionalization; c) exohedral non-covalent functionalization with surfactants; d) non-covalent exohedral functionalization with polymers. (Copyright 2002 Wiley. Used with permission from Hirsch, A., Functionalization of Single-walled Carbon Nanotubes, Angewandte Chemie - International Edition, 2002, 41, 1853.)

Each of these approaches, while having its own advantages and disadvantages, has been studied extensively, with successful solubilization of single and multi-walled nanotubes reported in many cases.[9-17] We have successfully used the [3 + 2] Huisgen cycloaddition as a synthetic route to covalent sidewall functionalization of carbon nanotubes (Figure 5.2).[18]

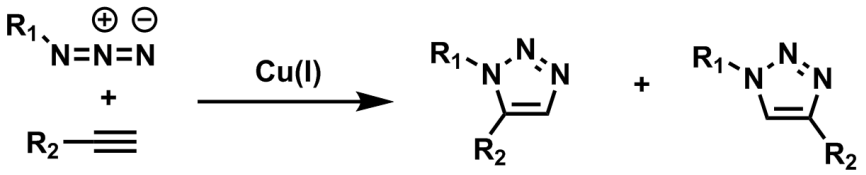

Figure 5.2. [3+2] Huisgen cycloaddition.

Reactive alkyne groups were introduced to the nanotube surface by means of a highly reactive diazonium salt intermediate. Using the 'grafting to' methodology, azide terminated polymers were then coupled to the pendant alkynes by formation of highly stable 1,2,3-triazoles. Both polystyrene (PS) and poly(methyl methacrylate) (PMMA) were thus covalently bound to virgin single-walled carbon nanotubes, and used to examine the migration of functionalized carbon nanotubes in polymer solutions. Solutions containing equimolar amounts of PS/PMMA were spin cast and annealed to form the distinctive self-assembled patterns seen in Figure 1.1, caused by the phase separation of PS into domains within the PMMA continuous phase. Films were then prepared in the same manner, except that functionalized carbon nanotubes were incorporated into the PS-PMMA blend solutions prior to spin casting and annealing. The unique Raman fingerprint of carbon nanotubes was then leveraged as a means to illustrate selective migration of carbon nanotubes within the thin films.[18-20] Both PS- and PMMA-functionalized nanotubes were incorporated into the films, and were found to spontaneously migrate to their respective polymer domains.

These findings prompted us to investigate the functionalization of carbon nanotubes using reversible polymers. It is well known that carbon nanotubes can provide tremendous reinforcement to polymeric structures, with the resulting nanocomposites exhibiting strengths far exceeding that of the native polymer.[21-23] While many different synthetic strategies have been employed to achieve functionalization, very little has been reported on the use of reversible

systems in this capacity.[24] The ability to self-heal or to disconnect the polymer after processing would provide a unique attribute to the stabilized nanotube dispersions.

5.2 Experimental

5.2.1 General

All reagents were obtained from Sigma-Aldrich and used as received. ^{1}H NMR spectra were obtained on a Bruker Avance 400 MHz Spectrometer using deuterated dimethyl sulfoxide (d_6-DMSO) as solvent and TMS as internal reference. Differential Scanning Calorimetry (DSC) analyses were performed on a DSC Q1000, from TA Instruments. High-resolution mass spectrometry using electrospray ionization (HRMS (EI+)) was conducted for the synthesized monomers on a Micromass Quattro Ultima triple quadrupole mass spectrometer using positive ion mode. Centrifugation was performed using a Clinical 50 centrifuge, available from VWR Scientific. Samples were centrifuged for 10 minutes at a speed of 4000 RPM (2000 g).

1,1'-((ethane-1,2-diylbis(oxy))bis(ethane-2,1-diyl))bis(1H-pyrrole-2,5-dione) (**M4**)

In a 500 mL round-bottomed flask equipped with a magnetic stir bar was dissolved maleic anhydride (13.23 g, 135 mmol) in 75 mL DMF. The resulting solution was chilled on ice and the 2,2'-(ethylenedioxy)bis(ethylamine) (10.0 g, 67.5 mmol) dissolved in DMF (75 mL) was added dropwise over ~20 min. The ice bath was removed, and sodium acetate (1.11 g, 13.5 mmol) and acetic anhydride (15.15 g, 148 mmol) were added in one portion, and the mixture stirred overnight at 50°C. The mixture turned dark brown within 30 minutes of the addition of NaOAc and Ac_2O. DMF was removed by vacuum distillation (60°C), and DCM (150 mL) was added to the dark brown mixture. The organic layer was extracted with $NaHCO_3$ (5 x 100 mL), dried over

$MgSO_4$, and the solvent removed under vacuum. The resulting compound was purified by column chromatography (95:5 DCM:EtOAc), and the product obtained as a white solid (4.5 g/22%): R_f (80:20 DCM:EtOAc) = 0.35; mp = 98.05°C; ^{1}H NMR (400 MHz, DMSO): δ (ppm) 7.01 (s, 4H), 3.53 (m, 4H), 3.47 (m, 4H), 3.42 (s, 4H); ^{13}C NMR (400 MHz, DMSO): δ (ppm) 171.5, 134.9, 69.76, 67.42, 37.24; Electrospray MS (positive ion mode): calcd. for $C_{14}H_{17}N_2O_6$ $[M + H]^+$: m/z = 309.11; found: 309.1, calcd. for $C_{16}H_{20}N_2O_4Na$ $[M + Na]^+$: m/z = 331.10; found: 331.0.

N,N'-((ethane-1,2-diylbis(oxy))bis(ethane-2,1-diyl))bis(furan-2-carboxamide) (**F4**)

To a 500 mL RBF equipped with a magnetic stir bar was added 2,2'-(ethylenedioxy)bis(ethylamine) (10.0 g, 67.5 mmol), triethylamine (13.66 g, 135 mmol), dimethylaminopyridine (0.17 g, 1.41 mmol) and DCM (200 mL). The solution was chilled on ice, then and furoyl chloride (18.5 g, 142 mmol) in DCM (50 mL) was added dropwise. The ice bath was removed, and the mixture stirred at room temperature overnight. The organic layer was extracted with $NaHCO_3$ (5 x 100 mL), dried over $MgSO_4$, and the solvent removed under vacuum. The resulting compound was purified by column chromatography (95:5 DCM:EtOAc), and the product obtained as a white solid (10.9 g/48%): R_f (95:5 DCM:MeOH) = 0.33; mp = 72.4°C; ^{1}H NMR (400 MHz, DMSO): δ (ppm) 8.30 (t, 2H, *J* = 5.5 Hz), 7.80 (d, 2H, *J* = 0.9 Hz), 7.08 (d, 2H, *J* = 3.3 Hz), 6.60 (dd, 2H, *J* = 1.7 Hz), 3.55 (s, 4H), 3.49 (m, 4H), 3.35 (m, 4H); ^{13}C NMR (400 MHz, DMSO): δ (ppm) 158.28, 148.36, 145.36, 113.71, 112.24, 69.97, 69.31, 38.81; Electrospray MS (positive ion mode): calcd. for $C_{16}H_{20}N_2O_4Na$ $[M + Na]^+$: m/z = 359.33; found: 359.1.

5.2.2 Preparation of benzoic acid functionalized SWNTs

To a 250 mL round bottomed flask equipped with a reflux condenser was added 150 mg of pristine SWNTs and 75 mL distilled water. The nanotubes were dispersed by sonication (45 min) and then 6.00 g of 4-aminobenzoic acid (58 mmol, 3.5 equiv per mol carbon) was added, followed by 3.00 mL of isoamylnitrite (22.5 mmol, 1.9 equiv per mol carbon). The flask was then heated to 80°C for 24 h. After cooling to room temperature, the nanotubes were isolated by filtration through a 200 nm Teflon membrane and washed with DMF until the filtrate became colorless. DMF was then removed by washing with DCM (250 mL).

5.2.3 Preparation of Furan functionalized SWNTs

Benzoic acid functionalized SWNTs, as prepared above, were dispersed by bath sonication (20 min) in 100 mL anhydrous DMF and stirred at 0°C under a constant flow of nitrogen. $SOCl_2$ (5 mL) was added slowly and the reaction temperature was raised to room temperature and allowed to stir for 4 h. The resulting acyl chloride functionalized SWNTs were isolated by filtration through a Teflon membrane (200 nm pore size) and washed with anhydrous DCM (250 mL) to remove excess $SOCl_2$. The substituted nanotubes were immediately dispersed by bath sonication in ca. 150 mL anhydrous DCM under N_2 and furfurylamine (3 mL) added slowly at 0°C. The reaction was warmed and stirred for 12h at room temperature (with one 10 minute period of sonication at t = 8 hours). The resulting nanotubes were isolated by filtration through a Teflon membrane (200 nm pore size) and washed sequentially with DMF (250 mL), water (250 mL), DMF (250 mL) and DCM (250 mL). In an effort to prevent complete drying of the SWNTs, no yield was obtained.

5.2.4 Dissolution of Furan-functionalized SWNTs

In a 10 mL vial was dissolved **M4** (43.8 mg/0.142 mmol) and **F4** (47.75 mg/0.142 mmol) in $CHCl_3$ (5 mL). A dispersion consisting of 17.2 wt% furan substituted carbon nanotubes in DCM (5 mg) was then added, and the contents sonified for one minute at room temperature. This represented a 5-fold molar excess relative to the furan content on the nanotubes, which was established by thermogravimetric analysis (TGA). The vial was then placed on a wrist shaker and agitated for a period of 7 days. The tube was sonified for one minute periods in the morning and evening of each day. After seven days, the contents of the vials were centrifuged at 4000 rpm for 10 minutes. The liquid was then filtered through a cotton plug placed in a glass pipette. The resulting clear liquid was placed in a sealed heavy wall pressure tube, which was submerged in an oil bath at 120°C for approximately 15 minutes, at which time a substantial amount of black precipitate was observed in the tube. The internal temperature of the $CHCl_3$ solution was not measured.

The process was repeated using a 10-fold molar excess of **M4** (87.6 mg/0.284 mmol) and **F4** (95.5 mg /0.284 mmol), and then with a 25-fold molar excess of **M4** (219.0 mg/0.71 mmol) and **F4** (238.8 mg/0.71 mmol).

A sample of polymer **M4/F4** was prepared by dissolving **M4** (616.6 mg/2.0 mmol) and **F4** (672.7 mg/2.0 mmol) in DCM (10 mL). After removing the solvent under reduced pressure, the white solid was heated in a petri dish at 120°C, until complete melting had occurred. The dish was then stored in an oven at 60°C for four days, yielding a clear, hard solid polymer **M4/F4**.

The process described above was repeated using a 5-fold molar excess (91.55 mg), a 10-fold molar excess (183.1 mg), and a 25-fold molar excess (457.8mg) of **M4/F4**.

5.3 Results and Discussion

Carbon nanotubes were decorated with furan-bearing moieties using a three-step process (Scheme 1). Benzoic acid groups were first installed on the surface of pristine single-walled carbon nanotubes via a diazonium salt intermediate formed using isoamyl nitrite. Transformation of the benzoic acid groups to acid chlorides led to the final step, an amidation of the acid chlorides using furfurylamine. To ensure dispersability, the furan functionalized nanotubes were not dried, but isolated as a suspension in DCM (22.9 wt%). Thermogravimetric analysis (TGA) of this suspension established that the nanotubes consisted of 25 wt% of the furan substituent.

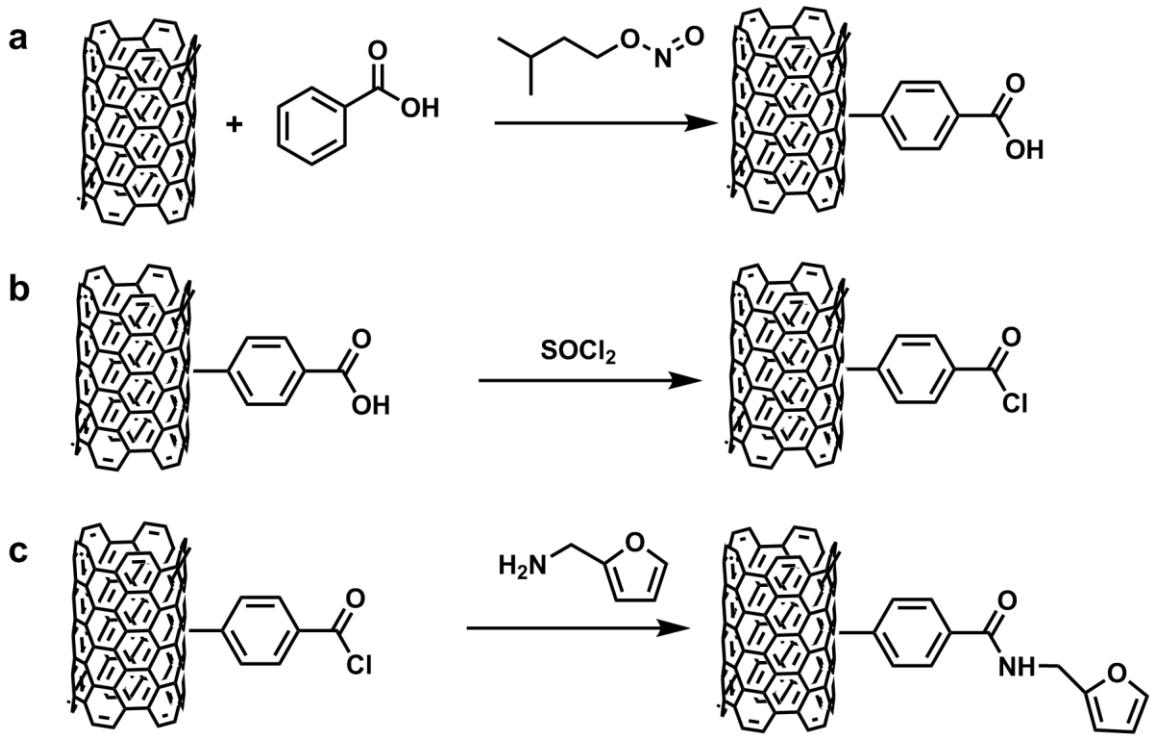

Scheme 5.1. Preparation of furan-substituted carbon nanotubes: a) benzoic acid substitution via diazonium salt of aminobenzoic acid; b) conversion to benzoyl chloride; c) amidation of benzoyl chloride.

The suspension containing furan-substituted nanotubes in DCM was dispersed in $CHCl_3$ so as to afford solutions containing 10 mg/mL of CNTs. Grafting of the reversible polymers was attempted in two different ways, based on the 'grafting from' and 'grafting to' methodologies. In the former case, the furan-substituted nanotubes were added to a solution containing equimolar amounts of the monomers **M4** and **F4**. Polymer formation from the surface of the tubes would be expected to occur by a step-growth mechanism, as the monomeric units would sequentially add to the furan group bound to the nanotube surface. For the latter method, the substituted nanotubes were added to a solution containing pre-fabricated **M4/F4** polymer. In this case, only maleimide terminated polymer chains would bind to the nanotube surface, thus one might expect that only half of the polymer chains would be available for bonding. However, in the grafting from approach, numerous DA linkages would need to be formed to produce a polymer, and since the solution concentrations were all very low, we anticipated that the grafting to approach might be more effective. Based on the calculated content of furan groups on the surface of the nanotubes, three different concentrations of DA adduct were used. The monomers **M4** and **F4**, or the polymer **M4/F4** was added in a 5, 10 and 25 times molar excess of the furan moieties. A control sample containing only the surface treated nanotubes in $CHCl_3$ was also prepared. The vials were continually mixed using an orbital wrist shaker to ensure intimate mixing of the nanotubes and monomer/polymer solutions. Periodic sonification was used to disperse the multi-tube bundles, so as to expose as much fresh surface area as possible for potential grafting. After seven days, the contents of the vials were centrifuged at 4000 rpm for 10 minutes, and the contents decanted and filtered. A significant difference could be observed between the monomer and polymer containing solutions. In the former case, the supernatant fluid was slightly yellow in color, but

did not have any dissolved nanotubes (Figure 5.3a). On the other hand, each of the solutions containing polymer was dark in color after filtration, indicating a significant degree of nanotube solubilization. While the concentration was not quantified, the gradation in color in the 5X, 10X and 25X solutions was a clear indication of increased solubility (Figure 5.3b). The control sample, in which no polymer was added, was light yellow (Figure 5.3c). These results are in agreement with our initial speculation that the pre-formed polymer would offer superior dispersion efficiency.

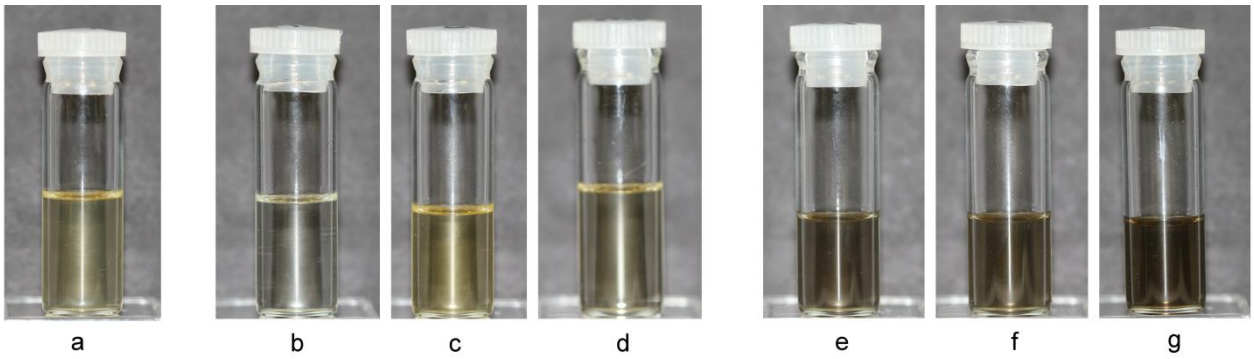

Figure 5.3. Solubility of furan-functionalized SWNTs in $CHCl_3$: a) mixture of monomers **M4** + **F4** in $CHCl_3$. Monomers **M4** + **F4** combined with furan-functionalized SWNTs at: b) 5:1; c) 10:1; d) 25:1 monomer to furan ratio. Polymer **M4/F4** combined with furan-functionalized SWNTs at: e) 5:1; f) 10:1; g) 25:1 polymer to furan ratio.

After centrifugation and filtration of the excess carbon nanotubes, the darkened solutions were placed in a heavy walled pressure tube and submerged in an oil bath at 120°C. After approximately 15 minutes, a dark precipitate could be easily observed in all three solutions (Figure 5.4). This was considered as clear evidence for the collapse of the stabilizing polymer **M4/F4** via the retro-DA reaction, as the unsubstituted nanotubes were rendered insoluble in the

monomer solution. Shaking of the cooled solution for seven days at room temperature did not re-solubilize the precipitated nanotubes. It is therefore expected that the heating caused collapse of the polymer **M4/F4** into its component parts **M4** and **F4**, which, as we described earlier, did not afford solubility to the nanotubes.

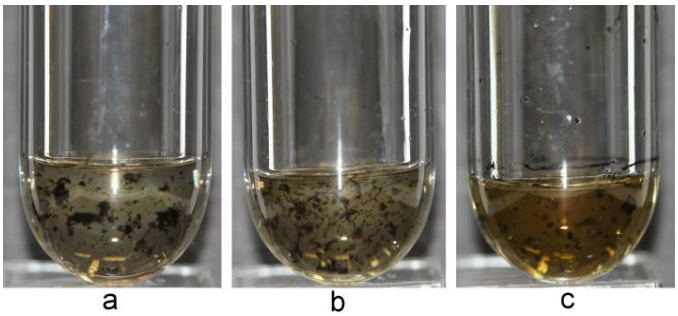

Figure 5.4. Furan-functionalized SWNTs dissolved in $CHCl_3$ solution of polymer **M4/F4** at: a) 5:1; b) 10:1; c) 25:1 polymer to furan ratio, after heating at 120°C for 1 hour.

5.4 Conclusion

Functionalization of carbon nanotubes has been explored extensively, using a wide variety of approaches.[9,11,25,26] Typically, polymers or oligomers have been bound to the nanotube surface so as to impart steric stability to the macro structures, which in turn affords solubility in a solvent system of choice. Dispersibility or solubilization enables processing and manipulation of the aggregated nanotubes, and opens up a wide array of possible applications for these extraordinary materials. We have investigated a novel aspect to the concept of nanotube functionalization, as we have successfully grafted a reversible polymer to the surface of pristine SWNTs. Using a small molecule furan as an anchoring point, pre-fabricated DA polymers were grafted to the surface of CNTs, resulting in solubilization of the nanotubes in DCM. Subsequent heating of the

darkened solution resulted in the collapse of the polymer, and precipitation of the nanotubes from solution. The element of reversibility offers an opportunity for removal of the solubilizing polymer after processing. This would be of interest in applications such as carbon nanotube purification and separation, where the presence of the polymer is no longer required after separation of the nanotubes had occurred.

5.5 References

(1) Freitag, M.; Martin, Y.; Misewich, J. A.; Martel, R.; Avouris, P. H. *Nano Lett.* **2003**, *3*, 1067.

(2) Tans, S. J.; Verschueren, A. R. M.; Dekker, C. *Nature* **1998**, *393*, 49.

(3) Weitz, R. T.; Zschieschang, U.; Effenberger, F.; Klauk, H.; Burghard, M.; Kern, K. *Nano Lett.* **2007**, *7*, 22.

(4) Kong, J.; Franklin, N. R.; Zhou, C. W.; Chapline, M. G.; Peng, S.; Cho, K. J.; Dai, H. J. *Science* **2000**, *287*, 622.

(5) Li, J.; Hu, L.; Wang, L.; Zhou, Y.; Gruner, G.; Marks, T. J. *Nano Lett.* **2006**, *6*, 2472.

(6) Coleman, J. N.; Khan, U.; Blau, W. J.; Gun'ko, Y. K. *Carbon* **2006**, *44*, 1624.

(7) Dalton, A. B.; Collins, S.; Munoz, E.; Razal, J. M.; Ebron, V. H.; Ferraris, J. P.; Coleman, J. N.; Kim, B. G.; Baughman, R. H. *Nature* **2003**, *423*, 703.

(8) Lau, K. T.; Lu, M.; Liao, K. *Composites Part a-Applied Science and Manufacturing* **2006**, *37*, 1837.

(9) Bahun, G. J.; Wang, C.; Adronov, A. *Journal of Polymer Science Part a-Polymer Chemistry* **2006**, *44*, 1941.

(10) Dyke, C. A.; Tour, J. M. *J. Am. Chem. Soc.* **2003**, *125*, 1156.

(11) Dyke, C. A.; Tour, J. M. *J. Phys. Chem. A* **2004**, *108*, 11151.

(12) Dyke, C. A.; Tour, J. M. *Chemistry-a European Journal* **2004**, *10*, 813.

(13) Hirsch, A. *Angewandte Chemie-International Edition* **2002**, *41*, 1853.

(14) Holzinger, M.; Vostrowsky, O.; Hirsch, A.; Hennrich, F.; Kappes, M.; Weiss, R.; Jellen, F. *Angewandte Chemie-International Edition* **2001**, *40*, 4002.

(15) Homenick, C. M.; Lawson, G.; Adronov, A. *Polymer Reviews* **2007**, *47*, 265.

(16) Hu, C. Y.; Xu, Y. J.; Duo, S. W.; Zhang, R. F.; Li, M. S. *J. Chin. Chem. Soc.* **2009**, *56*, 234.

(17) Ma, P. C.; Siddiqui, N. A.; Marom, G.; Kim, J. K. *Composites Part a-Applied Science and Manufacturing* **2010**, *41*, 1345.

(18) Mayo, J. D.; Behal, S.; Adronov, A. *Journal of Polymer Science Part a-Polymer Chemistry* **2009**, *47*, 450.

(19) Costa, S.; Borowiak-Palen, E.; Kruszynska, M.; Bachmatiuk, A.; Kalenczuk, R. J. *Materials Science-Poland* **2008**, *26*, 433.

(20) Keszler, A. M.; Nemes, L.; Ahmad, S. R.; Fang, X. *Journal of Optoelectronics and Advanced Materials* **2004**, *6*, 1269.

(21) Faulkner, S. D.; Kwon, Y. W. *Journal of Pressure Vessel Technology-Transactions of the Asme* **2011**, *133*.

(22) Wang, W.; Ciselli, P.; Kuznetsov, E.; Peijs, T.; Barber, A. H. *Philosophical Transactions of the Royal Society a-Mathematical Physical and Engineering Sciences* **2008**, *366*, 1613.

(23) Yesil, S.; Koysuren, O.; Bayram, G. *Polym. Eng. Sci.* **2010**, *50*, 2093.

(24) Llanes-Pallas, A.; Yoosaf, K.; Traboulsi, H.; Mohanraj, J.; Seldrum, T.; Dumont, J.; Minoia, A.; Lazzaroni, R.; Armaroli, N.; Bonifazi, D. *J. Am. Chem. Soc.* **2011**, *133*, 15412.

(25) Banerjee, S.; Kahn, M. G. C.; Wong, S. S. *Chemistry-a European Journal* **2003**, *9*, 1899.

(26) Clave, G.; Campidelli, S. *Chemical Science* **2011**, *2*, 1887.

Chapter 6
Summary

6.1 Self-assembly of Carbon Nanotubes

In the initial phase of our research, we exploited the phenomenon of phase separation of polystyrene (PS) and poly(methyl methacrylate) (PMMA) blends as a means to pattern PS- or PMMA-functionalized single-walled carbon nanotubes (SWNTs) in thin films. The PF-SWNTs were incorporated into PS-PMMA solutions, which were then cast as thin films and annealed at high temperature to induce phase separation of the two immiscible polymers. Scanning Raman Spectroscopy enabled accurate mapping of the functionalized SWNTs within the films relative to the two phase-separated polymers. In each case, the majority of the nanotube-rich spots were found predominately at the interface between the two phase-separated polymers, which constituted evidence for nanotube self-assembly. We then turned our attention to the preparation and characteristics of reversible polymers.

6.2 Reversible Polymers

The potential for formation of dimensionally stable materials has steered much of the research in the field of reversible polymers toward multi-podal furans and maleimides that offer the potential for highly cross-linked reversible networks. This has led to significant advances in the field of reversible polymers, encompassing several different classes of materials, such as gels, foams, and adhesives.[1-10] Less attention has been paid to linear reversible polymers, made by combination of bis-maleimides and bis-furans. The formation of very durable solids arising from a series of these monomers prompted us to study the effects of the spacer chemistries joining

these functional endgroups. Initially, a relatively simple system, consisting of short chain bis-furans/bis-maleimides was chosen, in order to observe the effects of the spacer group on the formation and overall physical characteristics of the resulting materials. To this end, a straight chain alkyl group (C-8) (**M1/F1)**, a cyclohexyl (**M2/F2)**, a phenyl group (**M3/F3)** and an ethylene glycol group (**M4/F4)** were used as spacers (Scheme 3). Equimolar amounts of the maleimide-furan couples were mixed and cast as neat films, and then characterized in both the solid and molten state. Dependance on spacer chemistry was clearly evident, as a wide range of molten viscosities and solid state rheological properties were observed. While the degree of crystallinity and brittleness varied widely within this set of compounds, very hard films were formed in all cases.

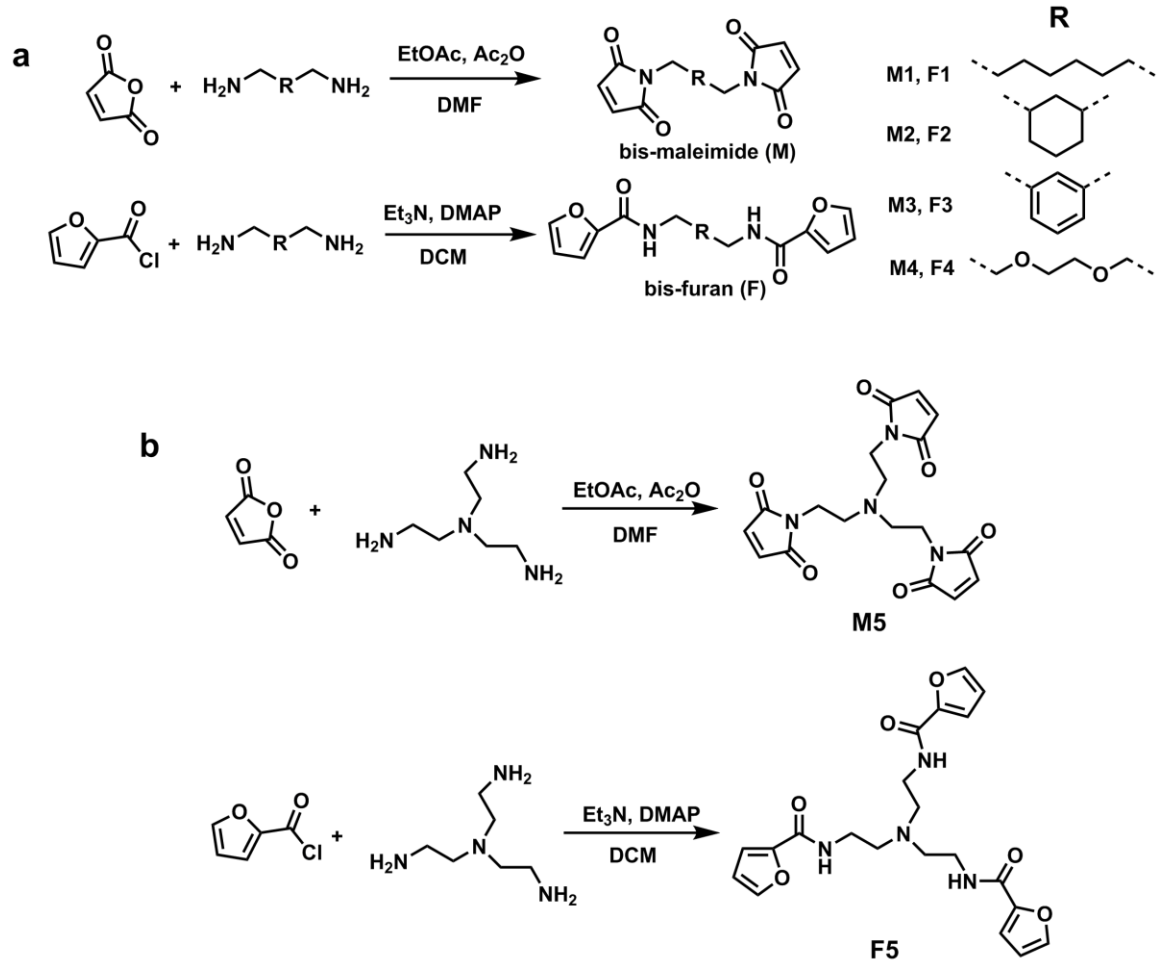

Scheme 6.1. Maleimide and furan compounds prepared and characterized: a) dimers; b) trimers.

6.2.1 Irreversible Cross-linking of Maleimides

Two additional phenomena were observed over the course of our investigation. Heating of the maleimide-furan monomer mixtures beyond their melting points generated low viscosity liquids in all cases. However, prolonged exposure to these temperatures resulted in a dramatic increase in viscosity, ultimately leading to the formation of hard solids. This was attributed to the non-reversible cross-linking of the bis-maleimides, which are known to undergo a thermal or radical induced [2+2] cyclodimerization (Figure 6.1).[11,12] This represents one of the shortcomings of these systems, as the low viscosity polymers can quickly become intractable solids when

exposed extensively to UV light or elevated temperatures. Interestingly, this phenomenon was found to be dependent on spacer chemistry, as the series of monomer pairs showed varying degrees of stability at a given temperature. Fortunately, the kinetics of the irreversible coupling was such that the issue could largely be avoided by simply exercising control of the heating times. We found that the addition of a small amount of a TEMPO-based radical inhibitor also served to repress the coupling, although we did not explore this avenue extensively. Instead, we opted to avoid this additional level of complexity by simply limiting heating times of the molten monomer mixtures. It is believed that this is common practice in studies involving maleimide-furan systems, as the phenomenon is rarely mentioned in the literature. Nevertheless, irreversible cross-linking of maleimides is a significant issue that must be taken into consideration when studying these materials.

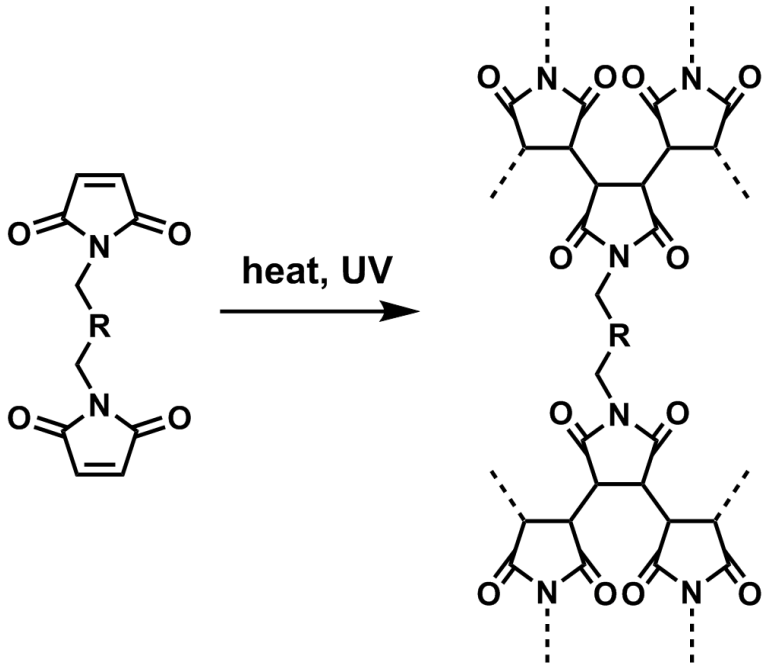

Figure 6.1. Irreversible cross-linking of bis-maleimides.

6.2.2 Adhesive Strength of DA Polymers

The second finding that captured our attention was the surprising adhesive strength of the DA polymers. While preparing samples for characterization, it was discovered that the solidified polymers were exceedingly difficult to remove from virtually all substrates being used, including aluminum, glass, and stainless steel. Polymer adhesives are of course well known and understood,[13,14] but relatively little attention has been given to reversible adhesives.[1,2,4,6] The advantages of a reversible adhesive are fairly obvious, as the ability to decouple an existing bond between two substances without causing irreversible damage would allow for repair and possible re-use of the materials. The use of DA polymers as adhesives has in fact been reported by Aubert, who incorporated reversibility into conventional epoxy adhesives.[1,2] Furfuryl glycidyl ether and a commercially available diamine curing agent were coupled with a bismaleimide to afford a thermally removable elastomeric epoxy adhesive. Dynamic mechanical analysis was used to quantify the modulus of a series of lap-shear samples as a function of temperature, and indeed, the initial adhesive strength compared favorably to a commercial epoxy adhesive. As expected, heating of the bonded samples triggered the retro-DA reaction, resulting in a dramatic decrease in adhesive strength, allowing easy removal of the adhesive. True reversibility was then confirmed by cycling three times between liquid and solid. However, it is important to note that adhesion was achieved using conventional epoxy chemistry, with the DA moieties only imparting the feature of reversibility. In keeping with the exploratory nature of our study of the physical properties of these materials, we decided to quantify the adhesive strengths of each of the polymers we had prepared. Tensile strengths of the solidified polymers were measured as the breaking strength of two stainless steel dowels that were carefully aligned and then fastened using

only the reversible polymers. As with many of the other properties of these materials, adhesive strength was found to be dependent on spacer chemistry.

6.2.3 Tripodal Furan-maleimide Systems

The impressive characteristics of the linear polymers prepared in our initial study led us to investigate the effects of cross-linking on these systems. A tri-podal maleimide and furan were prepared and coupled using the same methodology as used with the linear systems. Rheological characterization revealed relatively little change in the mechanical properties of the resulting cross-linked polymers. Attempts to use the trigonal monomers as cross-linking agents in the linear system also did not afford improved robustness of the final polymers. A dramatic difference was observed in the molten viscosity of the trigonal monomer mixture as compared with the ditopic derivatives, as it thickened much more quickly than the latter mixtures. It appears that the irreversible cross-linking reaction described earlier becomes more prevalent with the multi-podal monomers, although this was not pursued further. Confirmation of this hypothesis using alternative multi-podal systems is warranted.

6.3 References

(1) Aubert, J. H. *Materials Technology* **2002**, *17*, 74.

(2) Aubert, J. H. *J. Adhes.* **2003**, *79*, 609.

(3) Cordier, P.; Tournilhac, F.; Soulie-Ziakovic, C.; Leibler, L. *Nature* **2008**, *451*, 977.

(4) Loy, D. A., Wheeler, D.R., Russick, E.M., Saunders, R.S., Sandia Corporation, 6,337,384, January 8, 2002.

(5) Loy, D. A., Wheeler, D.R., McElhanon, J.R., Saunders, R.S., Sandia Corporation, 6,403,753, June 11, 2002.

(6) Luo, X. F.; Lauber, K. E.; Mather, P. T. *Polymer* **2010**, *51*, 1169.

(7) McElhanon, J. R.; Russick, E. M.; Wheeler, D. R.; Loy, D. A.; Aubert, J. H. *J. Appl. Polym. Sci.* **2002**, *85*, 1496.

(8) Small, J. H., Loy, D.A., Wheeler, D.R., McElhanon, J.R., Saunders, R.S., Sandia Corporation, 6,271,335, August 7, 2001.

(9) Tian, Q.; Yuan, Y. C.; Rong, M. Z.; Zhang, M. Q. *J. Mater. Chem.* **2009**, *19*, 1289.

(10) Wietor, J.-L.; Sijbesma, R. P. *Angewandte Chemie-International Edition* **2008**, *47*, 8161.

(11) Rozenberg, B. A.; Dzhavadyan, E. A.; Morgan, R.; Shin, E. *Polym. Adv. Technol.* **2002**, *13*, 837.

(12) Sunitha, M.; Nair, C. P. R.; Krishnan, K.; Ninan, K. N. *Thermochim. Acta* **2001**, *374*, 159.

(13) Brown, H. R. *Macromolecules* **1989**, *22*, 2859.

(14) Brown, H. R. *Macromolecules* **1993**, *26*, 1666.

Chapter 7
Future Work

While we have clearly demonstrated the influence of the spacer group in reversible polymer systems, we have only considered a small subset of compounds. Further exploration of the spacer chemistry in these polymers is warranted. A systematic study of a library of compounds, examining the effects of branching, spacer size/length, and functionality would be very revealing in terms of material properties. Although we did not observe any significant improvements in mechanical integrity with cross-linked systems as opposed to the linear polymers, our study only included a single multi-podal monomer M/F pair. Clearly, the inclusion of these compounds in the study would offer a wider array of compounds, and illustrate the effects of cross-linking on the material properties. A reduction in the brittleness of the materials developed would allow sample preparation for full DMA analysis, which would provide a more thorough rheological profile, including detailed information about their storage and loss moduli as a function of temperature. To this end, incorporation of ethylenedioxy, or other more flexible segments would offer a greater breadth of practical material properties. Optimal characteristics could ultimately require a mixture of different monomers, and this would need to be given consideration.

One of the major shortcomings of the maleimide-furan system is the irreversible coupling of the maleimides, which undermines the thermal stability of the polymers. This also affects their self-healing characteristics, as repeated heating and cooling cycles would ultimately lead to a permanently cross-linked system. The use of these materials in industrial applications would necessitate a more comprehensive solution to this problem. We found that radical inhibitors, such

as TEMPO-based molecules, suppressed the cross-linking of the maleimides, although the effect was limited. At this time, the influence of different types of inhibitor, and their concentrations in the monomer mixtures, is not clearly understood. A more fundamental understanding of the mechanism of the irreversible coupling of maleimides would enable a more comprehensive study of material solutions to this problem.

In any industrial application, cost is a parameter that must always be considered. Based on the chemistry described here, successful implementation of DA polymers into a working device would require at least two monomer adducts, a diene and dienophile. While these could potentially be purchased as commodity chemicals, the highly specific rheological specifications that would be required for application in coatings or structural elements would force the need for a custom, multi-step synthesis of the two monomers, making them prohibitively expensive. The use of DCPD as a single monomer acting as both diene and dienophile represents a significant opportunity to reduce the cost and complexity of a working reversible polymer.[1] This system also offers the possibility for formation of linear or cross-linked polymers within the same system, as the cyclopentene double bond could potentially act as a dienophile (Figure 7.1). A further advantage to this approach would be found in the thermal stability of the DCPD monomers, as they are not prone to the thermally induced irreversible coupling experienced by maleimides. One might expect that the effects of spacer chemistry would be similar to what we have observed in our research using maleimide/furan systems, thus a systematic examination of the effects of a variety of spacer chemistries would be of great interest.

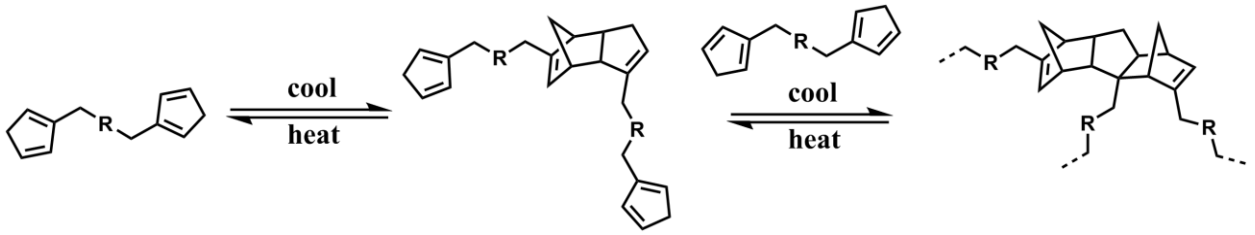

Figure 7.1. Reversible coupling of DCPD.

The use of carbon nanotubes in the preparation of composite materials has been reported extensively.[2-7] Their exceptional mechanical strength, coupled with extremely high aspect ratios, make them ideally suited for reinforcement of polymer networks. As described earlier, functionalization of CNTs has been demonstrated with a wide variety of polymers, with much of this work directed toward polymer composites. However, to our knowledge, this concept has not been reduced to practice using a reversible polymer. To this end, we have recently solubilized pristine single-walled carbon nanotubes using a linear, reversible DA polymer. Solutions containing furan-functionalized nanotubes and an excess of a DA polymer were agitated for several days, resulting in the solubilization of the nanotubes. Heating of the solutions to induce the retro-DA reaction then resulted in the complete loss of solubility of the nanotubes due to the collapse of the polymer. Subsequent cooling did not restore the solubility of the nanotubes, thus we were unable to demonstrate true reversibility in this system. Furthermore, due to the very small amounts of material used, we did not isolate the functionalized nanotubes, and did not determine the mechanical properties of the solid composite. Nevertheless, the association of these two unique materials offers the potential for a highly reinforced, self-healing composite material, and measurement of the rheological characteristics of such a material would be of great interest. Initially, isolation of a sample of solubilized nanotubes would allow for a comparison of the mechanical integrity of this material and the pure reversible polymer. A study of the effects of

spacer chemistry could then be undertaken to determine the influence of this important parameter on mechanical properties.

7.1 References

(1) Murphy, E. B.; Bolanos, E.; Schaffner-Hamann, C.; Wudl, F.; Nutt, S. R.; Auad, M. L. *Macromolecules* **2008**, *41*, 5203.

(2) Breuer, O.; Sundararaj, U. *Polym. Compos.* **2004**, *25*, 630.

(3) Coleman, J. N.; Khan, U.; Blau, W. J.; Gun'ko, Y. K. *Carbon* **2006**, *44*, 1624.

(4) Eken, A. E.; Tozzi, E. J.; Klingenberg, D. J.; Bauhofer, W. *Polymer* **2012**, *53*, 4493.

(5) Harris, P. J. F. *Int. Mater. Rev.* **2004**, *49*, 31.

(6) Khan, M. U.; Gomes, V. G.; Altarawneh, I. S. *Carbon* **2010**, *48*, 2925.

(7) Kordkheili, H. Y.; Farsi, M.; Rezazadeh, Z. *Composites Part B-Engineering* **2013**, *44*, 750.